EXPLORING THE MECHANISMS BEHIND CIGARETTE SMOKE-INDUCED INTERNALIZATION OF CFTR

Abigail Jane Marklew

Submitted for the degree of Doctor of Philosophy

Date of submission: 27th May 2016

Institute for Cell and Molecular Biosciences, Faculty of Medical Sciences, Newcastle University

Marsico Lung Institute/Cystic Fibrosis Center, The University of North Carolina at Chapel Hill

Abstract

Chronic obstructive pulmonary disease (COPD) the third leading cause of death, with an estimated 65 million cases worldwide. Despite this, most research to date has focused on treating the symptoms of COPD rather than the underlying mechanisms. Recently, we have shown that exposure to cigarette smoke (CS), the leading cause of COPD, results in an increase in cytosolic calcium and the rapid internalization and insolublization of the cystic fibrosis transmembrane conductance regulator (CFTR). Normal ion transport is imperative for mucus hydration and clearance, and its dysfunction after CS exposure may be responsible for the mucus dehydration and accumulation seen in COPD patients. Thus, the primary aim of this thesis was to establish the mechanism(s) behind the CS-induced internalization of CFTR.

Confocal imaging and Förster resonance energy transfer demonstrated that CFTR-CFTR interactions were reduced upon internalization of CFTR, and that CFTR was internalized with a $T_{1/2}$ of 27.7 min. U0126, an inhibitor of MEK1 and MEK2, abolished the internalization of CFTR by CS. Furthermore, U0126 had no effect on CS-induced Ca^{2+} release. These data implicate the necessity of MAPK/ERK kinases in CS-induced internalization, and suggest that this kinase activity is downstream of Ca^{2+} release. Furthermore, CS caused dephosphorylation of plasma membrane CFTR, and CS-induced internalization of CFTR was prevented by forskolin, suggesting that dephosphorylation of CFTR by CS may lead to its internalization.

CS-induced CFTR internalization was ablated by inhibitors of endocytosis, hypertonic sucrose and dynasore. Consistent with results demonstrating that CS-internalized colocalization CFTR with clathrin light chain, these data suggest that CS-induced internalization of CFTR is both clathrin- and dynamin-dependent. CS-internalized CFTR colocalized substantially with markers of the endoplasmic reticulum. Partial colocalization of CS-internalized CFTR with markers of the early endosomes, late endosomes, and the Golgi apparatus but not recycling endosomes, suggest that CFTR is trafficked in a retrograde pathway from the plasma membrane to the endoplasmic reticulum.

This thesis provides new insights into the mechanism of CS-induced CFTR internalization, and may help in the development of new therapies for CFTR correction and airway surface liquid rehydration in patients with COPD.

Acknowledgements

Firstly, I would like to thank my supervisors, Dr. Rob Tarran and Dr. Mike Gray for their unwavering support and motivation. I have been extremely lucky to have two supervisors throughout my PhD. Through their mentorship, not only have both Dr Tarran and Dr Gray been a constant source of guidance and patience, they have also provided countless opportunities for me to interact with the scientific community, and to better myself professionally. For all of this, I am very grateful.

Next, I would like to thank all members of the Tarran Lab, past and present, for their encouragement and support throughout my time here. At this point, there are too many to name, but my experience at Chapel Hill would not have been the same without each and every one of them. I would like to give special thanks to Dr. Chong Da Tan, Waseema Patel, and Dr. Megan Webster for their advice and assistance in the lab. I would also like to acknowledge Rodney Gilmore for his time and patience in teaching me molecular biology techniques.

I would like to thank my Mum, Dad, and brother, for their endless love and support. I have received nothing but encouragement from them, even when I told them I was moving 3000 miles away. They are my biggest fans, and I cannot thank them enough for their dedication. I would also like to thank my friends, who welcomed me to Chapel Hill with open arms, and have made me feel at home here.

Finally, I would like to thank my boyfriend, Chris. I truly appreciate the time and effort he has put forth to not only to keep me healthy, happy, and motivated during my PhD, but also for every time he drove me to the lab after hours.

Table of Contents

Figures

Tables

Abbreviations

ABC transporter	ATP-binding cassette transporter
AMPK	5’ AMP-activated protein kinase
AP	Adaptor protein
ANOVA	Analysis of variance
Ano1	Anoctamin 1
ASL	Airway surface liquid
ATP	Adenosine-5’-triphosphate
AUC	Area under the curve
AQP	Aquaporin
BCA	Bicinchoninic acid
BHK	Baby hamster kidney
BK	Large conductance potassium channel
CaCC	Calcium-activated chloride channel
CAL	CFTR-associated ligand
cAMP	Cyclic adenosine monophosphate
CB	Chronic bronchitis
CF	Cystic fibrosis
CFTR	Cystic fibrosis transmembrane conductance regulator
COP	Coat protein complex
COPD	Chronic obstructive pulmonary disease
CS	Cigarette smoke
DMEM	Dulbecco’s modified Eagle’s medium
DMSO	Dimethyl sulphoxide
EDTA	Ethylenediaminetetraacetic acid
EGF	Epidermal growth factor
EGFR	Epidermal growth factor receptor
ENaC	Epithelial sodium channel
ER	Endoplasmic reticulum
ERK	Extracellular signal-regulated kinase

FBS	Foetal bovine serum
FEV_1	Forced expiratory volume in 1 second
FVC	Forced expiratory volume in 1 second/Forced vital capacity
FRET	Förster resonance energy transfer
GFP	Green fluorescent protein
GTP	Guanosine-triphosphate
HBEC	Human bronchial epithelial cell
HEK	Human embryonic kidney
IK	Intermediate conductance potassium channel
LDS	Lithium dodecyl sulphate
mRNA	Messenger ribonucleic acid
MAPK	Mitogen-activated protein kinase
MEK	Mitogen-activated protein kinase kinase
MSD	Membrane spanning domain
NA	Numerical Aperture
NBD	Nucleotide binding domain
NHERF1	Sodium-hydrogen exchange regulatory factor
PBS	Phosphate-buffered saline
PCR	Polymerase chain reaction
PCD	Pericilliary dyskinesia
PCL	Pericilliary layer
PD	Potential difference
PDE	Phosphodiesterase
PVDF	Polyvinylidene fluoride
PDZ	Post synaptic density protein (PSD95), drosophila disc large tumor suppressor (Dlg1), and zonula occludens-1 protein (zo-1)
PKA	Protein kinase A
PKC	Protein kinase C
PM	Plasma membrane
PP	Protein phosphatase
R domain	Regulatory domain

ROI	Region of interest
SEM	Standard error of the mean
SK	Small conductance potassium channel
SOS	Sons of sevenless
SOCE	Store-operated calcium entry
SNARE	Soluble N-ethylmalemide-sensitive fusion protein attachment protein receptor
Stim1	Stromal interacting molecule 1
TGF	Transforming growth factor
WT	Wild-type
YFP	Yellow fluorescence protein

1.0 Introduction

1.1 Anatomy and physiology of the airways

The primary purpose of the lungs is to facilitate oxygen intake and carbon dioxide output between the outside world and the circulatory system. The lungs inspire approximately 10,000 – 20,000 L each day during normal breathing (Tamashiro et al., 2009). The structural design of the lungs is therefore functionally important and allows for efficient respiration. The initial inhalation occurs through either the nasal cavity or the mouth, past the pharynx and larynx, into the trachea. These structures are known as the upper airways. The trachea is lined with horse shoe-shaped cartilage rings embedded in dense connective tissue, surrounded by a layer of transverse smooth muscle. This structure allows for air conduction into the lower airways. The trachea splits into two main stem bronchi, one for each lung, which are characterized by the presence of smooth muscle and tubuloalveolar glands, surrounded by a fibrocartilage layer (Barnes, 2009). The bronchi branch off with irregular dichotomy into bronchioles and eventually terminal bronchioles, respiratory bronchioles and alveoli (Bai et al., 1994). The path of air from the trachea through to the alveoli may pass through up to 25 generations of branches. This branching structure allows for proper airflow, provides a physical barrier for particle deposition and allows regulation of the humidity and cleaning of the air.

The airway lumen surface is lined with epithelia. Throughout the airways the epithelium forms the first point of contact for inhaled factors such as particles, microbes and pollutants, and provides a physical barrier between the body and outside world. The variety of cell types present in the epithelium and their characteristics provide a host of innate defence mechanisms to protect the body from insult. In the alveoli, the epithelium is comprised of type I and type II pneumocytes which lay in close proximity to the pulmonary capillaries to allow for gaseous exchange (Whitsett and Alenghat, 2015). In the distal airways, i.e. the terminal and respiratory bronchioles, the cells become more cuboidal and club cells replace the goblet cells (Mercer et al., 1994). In the proximal airway, tall columnar pseudostratified mucocilliary epithelia consisting primarily of intermediate, basal, mucus secretory (goblet) and ciliated cells line the trachea to the 6^{th}-10^{th} generation bronchi (Barnes, 2009). The predominant cell type in the proximal airway is the ciliated epithelial cell. Each ciliated cell lining the trachea and bronchi has approximately 300 cilia (Erle and Sheppard, 2014). Cilia are membrane bound structures formed around a microtubule cytoskeleton known as the anexome

(Popatia et al., 2014). The importance of mechanical clearance by the cilia is apparent in patients with primary ciliary dyskinesia (PCD), an inherited disorder of cilia. The clinical phenotype of PCD can be severe and can lead to chronic sinusitis and bronchiectasis as well as infertility and abnormal organ patterning (Whitsett and Alenghat, 2015). The cilia beat in a coordinated, rhythmic fashion which, when combined with ion and water transport across the epithelium, mucus secretion from goblet cells, and coughing, can facilitate the propulsion of mucus and foreign particles towards the mouth. This process is known as mucocilliary clearance, and it is essential for the removal of pathogens and debris from the airways.

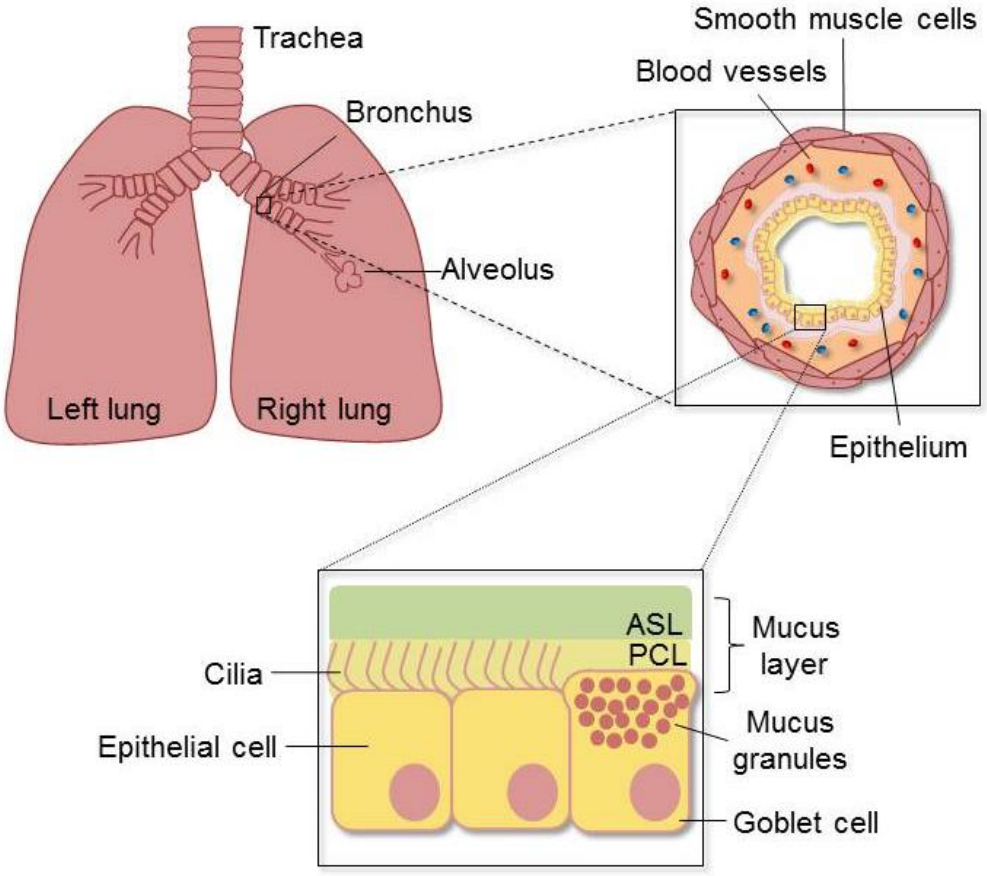

Figure 1-1. The structure of the conducting airways.

Air is breathed in through the mouth or nose, it passes through the trachea, into the bronchi, and down to the small conducting airways. In the alveoli, oxygen exchange occurs. The bronchi allow mucocilliary clearance, they are lined with smooth muscle cells which facilitate coughing and blood vessels which supply the surrounding cells with oxygen. The epithelium lining the bronchi is comprised of goblet cells which secrete mucins and other proteins from granules into the ASL, and ciliated cells, which facilitate mucus clearance by ciliary beat and ion transport.

1.2 Mucociliary clearance

Efficient mucocilliary clearance is maintained by an aqueous environment that bathes the surface epithelium known as the airway surface liquid (ASL). The composition of the ASL is sustained by ion transport at both the basolateral (blood side) and apical (luminal side) membranes of ciliated epithelia, as well as the secretion of mucins and other proteins from goblet cells and submucosal glands. The ASL is comprised of two layers, the periciliary layer (PCL) and the mucus layer. Membrane spanning mucins and tethered mucopolysaccharides protrude from the cilia into the periciliary layer (PCL), providing cell surface lubrication and are critical for propelling the mucus layer through the airway (Erle and Sheppard, 2014). The constituents of the PCL prevent the penetration of the mucus layer into the interciliary space (Button et al., 2012). The mucus layer is considered the 'transport layer'. It is mainly comprised of mucins, MUC5AC and MUC5B, and functions to trap any bacteria and particles that deposit on the surface of the airways, allowing for their clearance from the airways.

Coordinated mucocilliary clearance relies on the mucus layer, the PCL and the cilia, and the properties and mechanisms behind the coordination of these components are complex. The mucus layer must be malleable and able to adapt to a full range of insults within its environment. Furthermore, it must be able to trap pathogens and particles, and maintain its viscoelastic properties which allow the trapped particles and pathogens to be transported towards the mouth (Randell et al., 2006, Cone, 2009). To regulate these diverse properties, the mucus layer acts as a sink for water and can accept or donate liquid in an effort to maintain its hydration status (Tarran et al., 2001a). The hydration status is required for efficient and lubricated ciliary beating, and to maintain the supple properties of mucus which allow it to function as the transport layer. When additional water is added to the airway surface, the rate of mucocilliary clearance increases above that of normal (Tarran et al., 2001b, Tarran et al., 2001a). However, when the mucus layer and PCL lose water and dehydrate, the osmotic pressure of the mucus layer causes the PCL to collapse, and the cilia lose their ability to beat. This dehydration results in an ablation of mucus clearance, and can be seen in diseases such as cystic fibrosis (CF) and chronic obstructive pulmonary disease (COPD).

1.3 Ion transport regulation of the airway surface liquid

Hydration of the ASL is maintained by a balance of transepithelial isotonic electrolyte absorption and secretion, which allows salt and water to flow into and out of the ASL as required. The secretion of Cl^- and the absorption of Na^+ across the epithelia govern the mass of NaCl within the ASL, which in turn regulate the diffusion of water by osmosis into the ASL. The airway epithelium provides a barrier for water transport, between the ASL and the pulmonary vasculature. However, the presence of aquaporins in the basolateral (AQP3) and apical membranes (AQP5) of epithelial cells (Kreda et al., 2001), as well as water transport across the tight and adherent junctions, results in the so called 'leaky epithelium', which enables the epithelium to be highly permeable. Maintaining the hydration status of the ASL is of particular importance in lung health, and dysregulation of the ion channels involved in hydration can lead to mucus dehydration, mucus stasis, and chronic bacterial infections which are common phenotypes of chronic bronchitis (CB) and cystic fibrosis (CF) lung disease.

The osmotic gradients required for water transport across the epithelium are primarily set up by apical and basolateral membrane ion channels in epithelial cells (Boucher, 1994). On the apical surface, the epithelial sodium channel (ENaC) is the rate limiting step in sodium absorption, and the cystic fibrosis transmembrane conductance regulator (CFTR) and calcium-activated chloride channels (CaCCs) are the apical conduits for chloride secretion (Figure 1-2). These channels directly regulate the ion content, and therefore the hydration levels of the ASL.

ENaC is expressed in the epithelia of several organs including the kidney, colon, sweat ducts and lungs and is the primary channel responsible for sodium absorption in airway epithelia (Donaldson and Boucher, 2007). ENaC was originally believed to consist of three different subunits, α β γ, but more recently an additional subunit, δ, has been identified with known isoforms δ_1 and δ_2 (Giraldez et al., 2007, Waldmann et al., 1995). Differential expression of these subunits may provide an alternative method of regulation for ENaC channel function (Haerteis et al., 2009). ENaC is regulated by intracellular second messengers such as cAMP, PIP_2, and PIP_3 (Gaillard et al., 2010). In addition to this, CFTR is thought to inhibit ENaC through both direct and indirect mechanisms. Examples include indirect regulation of ENaC through NHERF1 binding to yes-associated-protein-65 and the c-Src kinase cYes, which inhibits ENaC (Peters et al., 2001), or elevations in intracellular cAMP and PKA (Boucher et al., 1986), or direct regulation of ENaC through

interaction with the intracellular domains of CFTR (Schreiber et al., 1999, Gentzsch et al., 2010). In normal lungs, the ASL is maintained at a relatively consistent depth and level of hydration, and ENaC and CFTR are reciprocally regulated in order to coordinate this volume control. Unregulated ENaC activity is known to deplete ASL volume (Mall et al., 2004). However, CFTR acts as a negative regulator of ENaC, and is able to limit ENaC activity and secrete Cl^- ions leading to hydration of the ASL.

The driving force for sodium absorption is established primarily by the removal of sodium from the cell at the basolateral membrane by the $Na^{+/}K^+$ ATPase exchanger (Crump et al., 1995). Na^+/K^+ ATPase exchanges intracellular Na^+ for extracellular K^+. Potassium is then recycled by potassium channels expressed on the basolateral membrane. The basolateral membrane possesses three types of calcium-activated potassium channel, the large conductance (BK_{Ca}), intermediate conductance ($IK/K_{Ca}3.1$) and small conductance (SK) channels. Sodium/potassium exchange at the basolateral membrane by the Na^+/K^+ ATPase and potassium channels determines the basolateral membrane potential and plays a role in the setup of an electrochemical gradient for the secretion of chloride through CFTR.

The secretion of Cl^- through CFTR at the apical membrane is passive, and is driven by an electrochemical gradient set up primarily by the electroneutral $Na^+/K^+/2Cl^-$ cotransporter (NKCC1). Sodium is taken up by NKCC1 and recycled out of the cell by Na^+/K^+ ATPase, due to its electrochemical gradient. This allows potassium entry into the cell through NKCC1, which facilitates the entry of $2Cl^-$ ions, and allows for the secretion of Cl^- at the apical plasma membrane through CFTR. The coordination of CFTR with ENaC at the apical membrane allows for a balance of absorption and secretion which regulates ASL height and hydration. A study to show that both ENaC and CFTR were involved in ASL volume regulation was carried out by depositing a known amount of liquid onto the epithelial surface-liquid interface and measuring both ASL height and the transepithelial potential difference. After liquid deposition, Na^+ absorption predominantly allowed for the absorption of excess liquid. Once a height of ~7µm was reached, Cl^- secretion increased as Na^+ absorption decreased, which lead to a steady state ASL height of ~7µm (Tarran et al., 2005).

CaCCs are also responsible for a portion of Cl^- secretion into the ASL, and are located in the apical membrane of the airway epithelium (Tarran, 2004). Until recently the molecular identity of CaCCs had not been established. However, in

2008, Anoctamin 1 (Ano1) was found to be located in the airways and was identified independently by three different groups as having similar physiological and pharmacological properties to native CaCCs (Caputo et al., 2008, Schroeder et al., 2008, Yang et al., 2008). CaCCs are both voltage-gated and activated by increases in intracellular Ca^{2+}. These properties allow for tight regulation such that CaCCs are not thought to be responsible for basal changes in ASL height, but are important in regulating changes in ASL height in response to mucosal nucleotides (Tarran et al., 2006).

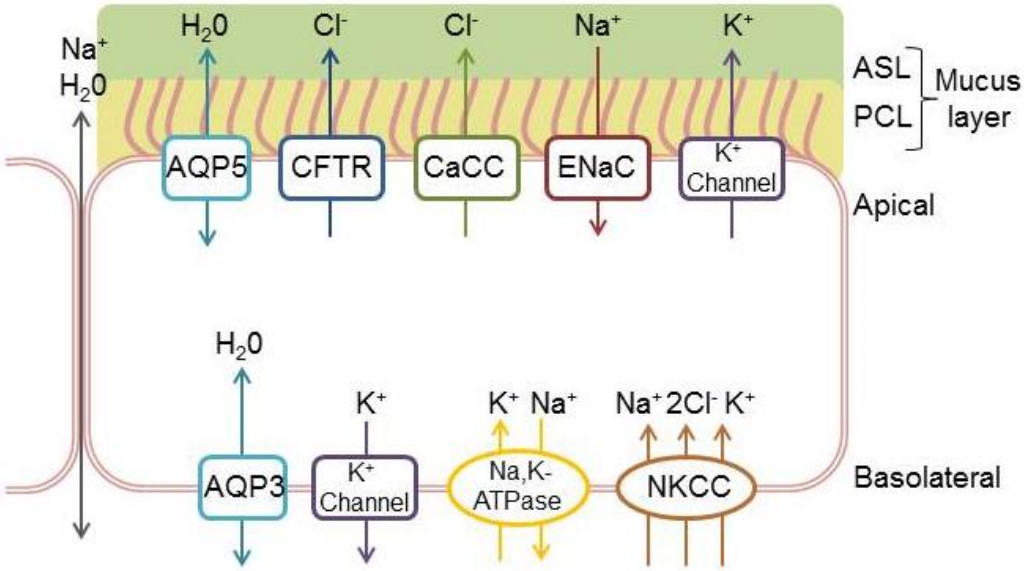

Figure 1-2. A model of ion transport in the airway epithelium.

Mucus clearance requires efficient hydration of the ASL. The ASL is composed of a mucus layer and a pericilliary layer. The volume and composition of the ASL is maintained by epithelial ion transport. Water is taken into the cell down its osmotic gradient at the apical membrane by AQP5, and at the basolateral membrane by AQP3, and across the plasma membrane through epithelial tight junctions. At the apical membrane ENaC regulates sodium absorption and CFTR and CaCC channels facilitate secretion. The net movement of these ions facilitates the movement of water across the cell. Na^+-K^+-ATPase and potassium channels (BK, SK, and IK) at the basolateral membrane maintain an electrochemical gradient and provide a driving force for sodium absorption and chloride secretion at the apical membrane. BK and SK channels at the plasma membrane also have a role in ASL volume regulation.

1.4 The properties of CFTR

CFTR is essential for chloride secretion in the airways. The channel is tightly regulated to allow hydration of the ASL and effective mucocilliary clearance. As such, the structure and regulatory factors of CFTR discussed in this section are incredibly complex and play an important role in CFTR function.

1.4.1 CFTR structure and function

CFTR is a member of the ATP-binding cassette (ABC) transporter superfamily, a large group of transmembrane proteins which use ATP hydrolysis to facilitate the translocation of substrates across the plasma membrane (Sheppard and Welsh, 1999). CFTR is unique as it is the only family member that works as an ion channel and not an ATP-dependent pump. However, consistent with typical ABC transporter structure, CFTR has two membrane spanning domains (MSD1 and MSD2) and two nucleotide-binding domains (NBD1 and NBD2; Figure 1-3). CFTR additionally has a regulatory (R) domain, important for channel activation. Furthermore, CFTR has many motifs which have been identified to play important roles in the trafficking and function of the channel. An example of this are the endocytic motifs present on the C-terminus of CFTR; the tyrosine-based motif, the dileucine motif and the PDZ domain (Figure 1-3). The role of these motifs in endocytosis will be further discussed in section 1.4.3.

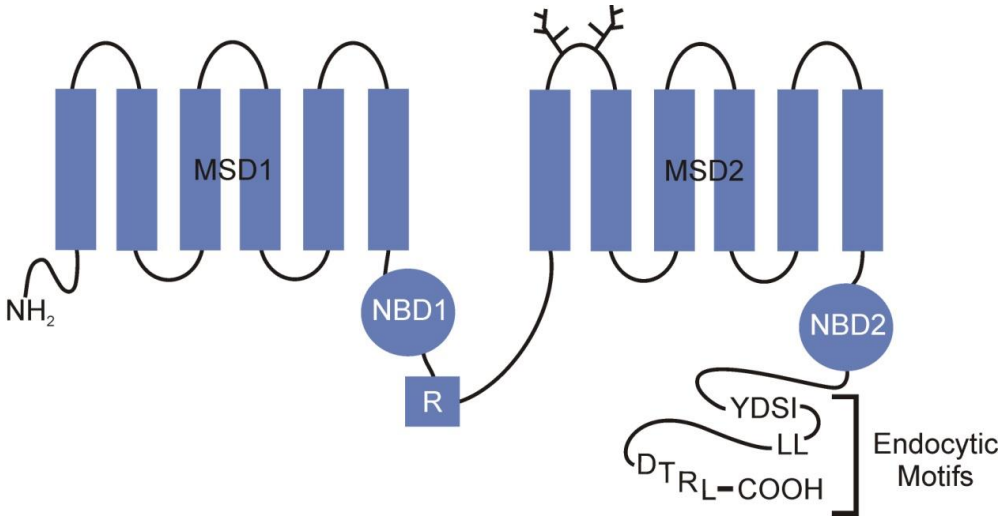

Figure 1-3. The topology of CFTR.

CFTR has two membrane spanning domains and two nucleotide binding domains, as well as a regulatory domain. CFTR has two sites of glycosylation on the extracellular surface as well as three intracellular endocytic motifs; the tyrosine-based motif, the dileucine motif and the PDZ binding motif, represented by their amino acid codes 1424YDSI, 1430LL and 1476DTRL, respectively.

The electrophysiological properties of CFTR channel function are determined by the structure of the channel. The two MSDs assemble to form the pore of the channel for the transport of anions (Hwang and Sheppard, 2009). The pore of the channel is permeable to anions as large as lactobionate, suggesting that the diameter of the channel must be 10 – 13 Å (Linsdell et al., 1998). CFTR has a low single channel conductance of 6-10 pS and a linear current voltage (*I-V*) relationship (Gray et al., 1988). CFTR is preferentially selective for anions over cations, with an anion permeability sequence of $Br^- \geq Cl^- > I^-$ in whole cell patch clamp experiments (Anderson et al., 1991b). The channel is both time- and voltage-dependent, and the activity of CFTR is dependent on cAMP-dependent phosphorylation (Picciotto et al., 1992).

CFTR gating is coupled to ATP binding and hydrolysis at the NBDs, allowing the channel to transition between multiple open and closed states (Vergani et al., 2005, Csanady et al., 2010, Hwang and Sheppard, 2009). In the resting state, one ATP molecule is bound to a NBD. Vergani and colleagues (2005) demonstrated that binding of an additional ATP molecule drives dimerization of the NBDs allowing for a conformational change to be transmitted to the MSDs to open the channel pore for anion transport (Vergani et al., 2005). A second open state occurs after hydrolysis of one of the ATP molecules, leading to dissociation of the NBD dimers and entry into a closed state. Furthermore, Corradi and colleages (2015) recently demonstrated using homology modelling, that the amino acid residue Phe 337 plays a role in gating CFTR in the closed state by blocking the anion pore.

Phosphorylation of the R domain by PKA is a prerequisite for channel gating by ATP and is required for channel activation (Anderson et al., 1991a). The R domain contains many consensus sites for phosphorylation by PKA five of which, plus another in NBD1, are phosphorylated *in vivo* (Cheng et al., 1991, Hegedus et al., 2009). CFTR has extremely low activity when it is not phosphorylated. However, in the presence of PKA the open probability of the channel increases significantly (Mathews et al., 1998, Wang et al., 2000). There are conflicting reports of how phosphorylation by PKA affects channel gating. Mense and colleagues (2006) demonstrated that PKA phosphorylation is necessary for NBD dimerization. Other groups have demonstrated that phosphorylation effects on gating are not only determined by NBD dimerization, but also the interaction of the R domain with the MSDs (Zhang et al., 2011, Hegedus et al., 2008). Thirdly, Kanelis *et al.* (2010) have proposed that phosphorylation of PKA sites in NBD1 may coordinate an interaction between NBD1 and the transmembrane domains. These hypotheses are not

necessarily exclusive, and CFTR gating may be affected by any combination of these events. After gating has occurred, subsequent dephosphorylation of the channel by protein phosphatase (PP) 2C and PP2B controls deactivation and returns the channel to the closed state.

1.4.2 CFTR biosynthesis

Immature CFTR is synthesized in the endoplasmic reticulum (ER). CFTR undergoes complex folding and core glycosylation within the ER. Core glycosylation is the addition of N-linked glycans to the extracellular loop spanning TMD7 and TMD8, resulting in a mannose-enriched protein (Figure 1-3). After processing at the ER, core-glycosylated CFTR is sent to the Golgi apparatus where complex oligosaccharide chains are added to the structure resulting in a mature, fully glycosylated channel (Cheng et al., 1990, Glozman et al., 2009). Maturation of CFTR is somewhat inefficient with only 30% of the wild type CFTR synthesized into a fully mature glycosylated ion channel (Lukacs et al., 1994, Ward and Kopito, 1994). CFTR conformational maturation is mediated by calnexin, calreticulin, and other cytosolic chaperones including Hsc70/Hsp70, Hsp40 and Hsp90. Any protein that is incorrectly folded may be sent for degradation. When the maturation of CFTR is complete, the channel is trafficked to the plasma membrane.

1.4.3 CFTR trafficking

CFTR current (I) is a product of $N \times P_o \times i$ where N is the number of channels at the plasma membrane, P_o is the open probability and i is the single channel conductance. As such, the presence of CFTR at the plasma membrane is tightly regulated. The life cycle of CFTR is considered lengthy, with a total life cycle from synthesis to degradation of more than 24 hours (Lukacs, 1993). Each stage of the life cycle; biosynthesis, exocytosis, function at the plasma membrane, endocytosis, recycling and degradation, is tightly regulated. Following biosynthesis, CFTR is trafficked from the Golgi apparatus to the plasma membrane in coat protein complex (COP) II transport vesicles (Wang et al., 2004). This exocytosis occurs in a syntaxin 3-dependent manner. Syntaxin 3 is a vesicle fusion protein and member of the soluble N-ethylmalemide-sensitive fusion protein attachment protein receptor (SNARE) protein family (Collaco et al., 2010). Stimulation of exocytosis can occur in a number of different manners, for example, in addition to phosphorylating the R domain leading to activation of CFTR, PKA can also stimulate the exocytosis of CFTR to the membrane (Ameen et al., 2003).

At the plasma membrane, active CFTR maintains Cl^- secretion allowing hydration of the ASL. Once CFTR has carried out its function, it is internalized by endocytosis. Despite the lengthy total life cycle of CFTR, chemical labelling demonstrated that CFTR is actually removed from the plasma membrane fairly rapidly, with 25% of CFTR internalized in 2.5 min (Prince et al., 1994, Lukacs et al., 1997). The rate of CFTR internalization is comparable to that of other receptors that undergo clathrin-mediated endocytosis. As discussed in section 1.4.1, CFTR has a number of highly conserved endocytic signals on its C-terminus which assist in allowing CFTR to be endocytosed at such a rapid rate (Hu et al., 2001). Noticeably, two types of endocytic signal have been well characterized, a tyrosine-based motif and a di-leucine-based motif. The tyrosine-based motif has a consensus sequence of YXXϕ, where X is any amino acid and ϕ is a bulky hydrophobic amino acid. In CFTR this sequence is ^{1424}YDSI. Deletion of the tyrosine motif in CFTR resulted in an increase in surface expression of CFTR suggesting that internalization of CFTR was diminished (Weixel and Bradbury, 2000). Di-leucine motifs have consensus sequences D/EXXXLL/I and DXXLL and can be found as ^{1430}LL in CFTR. Mutation of this signal increased the cell surface density of CFTR suggesting that the di-leucine motif facilitates internalization (Hu et al., 2001).

The above signalling motifs mediate the recruitment of CFTR to clathrin-coated vesicles through binding of endocytic adaptors such as adaptor protein (AP) 2 (Hu et al., 2001, Weixel and Bradbury, 2000). Endocytosis is integral to the regulation of cell surface density of many different plasma membrane receptors, transport proteins and ion channels. Of the different types of endocytosis; phagocytosis, micropinocytosis, calveolae-mediated and clathrin-mediated, clathrin-mediated endocytosis is best characterized. Clathrin was first discovered in 1976 (Pearse, 1976), and has since been found to have a triskelion structure comprised of three clathrin-heavy chains which are linked by their C-termini (Brodsky et al., 2001). When the triskelia assemble into a clathrin coated vesicle they form a polygonal lattice which itself cannot bind to the plasma membrane. The clathrin heavy chain within the triskelion formation binds to clathrin light chain, which is oriented into the cytosol and thought to interact with many intracellular adaptor proteins which allow curvature of the plasma membrane and formation of a vesicle (Fotin et al., 2004). Once the vesicle is formed dynamin, a mechanochemical enzyme, oligomerizes in a ring around the plasma membrane stalk that attaches the vesicle to the plasma membrane. It then uses GTP hydrolysis to provide a mechanical force, which

severs the membrane tube allowing entry of the clathrin coated vesicle into the cytoplasm.

Isolation of clathrin coated vesicles from airway epithelial cells revealed a large amount of CFTR present in the vehicles (Dharmsathaphorn et al., 1984). Once CFTR is recruited to clathrin coated vesicles, the vesicle buds off from the plasma membrane. Once the clathrin coated vesicle is taken into the cytosol, the vesicle un-coats. This energy-dependent step is carried out by cofactors including heat shock cognate-70 and auxillin. After un-coating, the vesicles fuse with early endosomes, which are enriched with phosphotidylinositol-3-phosphate and other protein constituents which can play a role in determining the destination of the contents of the endosome (Le Roy and Wrana, 2005). The early endosome is weakly acidic (pH 6.8-5.9) (Maxfield and Yamashiro, 1987) and has low levels of calcium (Gerasimenko et al., 1998). Ras related protein (rab) 5a, a protein that resides primarily in early endosomes, facilitates the trafficking of CFTR to the early endosomes (Roberts et al., 1999, Stenmark et al., 1994, Ameen et al., 2007). The early endosome is known as the main sorting station in the endocytic machinery (Helenius et al., 1983). It primarily functions to sort cargo and target its contents for recycling back to the plasma membrane or for degradation. The different pathways of endocytosis allow the cell to manage the number of CFTR molecules at the cell membrane.

It has been demonstrated in Chinese hamster ovary cells and in polarized T84 epithelial cells that forskolin-stimulated CFTR activity is maintained up to 24 h following stimulation, even in the presence of a protein synthesis inhibitor, cyclohexamide (Lukacs et al., 1993, Ameen et al., 2003). Given that exocytosis of nascent CFTR is slow, and endocytosis of the channel is rapid, these data provide evidence that internalized CFTR must be trafficked back to the plasma membrane. This concept of recycling has been further confirmed using cell surface biotinylation, demonstrating that approximately 50% of internalized CFTR is cycled back to the plasma membrane (Weixel and Bradbury, 2002). Recycling of internalized CFTR allows subapical pools of mature CFTR to form and be rapidly trafficked to the membrane when a dramatic increase in Cl^- secretion is necessary (Thiagarajah and Verkman, 2003). As such, CFTR internalized to the early endosomes can be sent directly back to the plasma membrane through a rab4 dependent mechanism. Alternatively, CFTR is trafficked to recycling endosomes, whereby rab11 functions to traffic CFTR back to the plasma membrane, or to the Golgi apparatus.

Alternatively, CFTR can be targeted for degradation. CFTR can be sorted in the early endosome for degradation. Early endosomes mature into late endosomes, which typically have an oval shape and are approximately 250 – 1000 nm (Poole and Black, 2006). Late endosomes are formed in the periphery of the cell, and move to the perinuclear region for fusion with other endosomes and lysosomes. Early-to-late endosome and late endosome-to-lysosome trafficking is regulated by Rab7. The presence of dominant negative Rab7 caused intracellular CFTR to accumulate since it was unable to traffic to the lysosome (Gentzsch et al., 2004). Upon fusing with lysosomes, the late endosomes provide a unidirectional pathway to degradation (Huotari and Helenius, 2011).

Post synaptic density protein (PSD95), Drosophila disc large tumor suppressor (Dlg1), and zonula occludens-1 protein (zo-1) (PDZ) motifs play a role in polarization localization of membrane proteins, ion channel function and endocytosis by allowing the formation of protein-protein interactions with many PDZ binding proteins (Guggino and Stanton, 2006). Proteins containing PDZ domains often contain other protein interacting modules, and facilitate the interaction of many protein-protein hetero- and homo-typic interactions within macromolecular complexes (Guggino and Stanton, 2006). The C-terminus of CFTR contains a PDZ-interacting motif, ^{1467}DTRL, which binds to proteins containing PDZ domains such as Na^+/H^+ exchanger regulatory factor isoform-1 (NHERF1, otherwise known as the ezrin-binding protein EPB50), NHERF2, and CFTR associated ligand (CAL). NHERF1 and NHERF2 have C-terminal ERM binding domains, which provides a binding site for ezrin, and function to connect CFTR and other membrane proteins to the actin cytoskeleton (Monterisi et al., 2012). In addition to this, NHERF1 has an ezrin-radixin-moesin domain, which allows binding to ezrin, radixin and moesin and subsequently tethers CFTR to the actin cytoskeleton, thus stabilizing CFTR at the apical membrane (Short et al., 1998). Overexpression of CAL decreases the expression of CFTR at the cell membrane, and is thought to play a role in the trafficking of CFTR (Cheng et al., 2002). Furthermore, there is some evidence to suggest that the PDZ binding domain of CFTR is required for recycling of CFTR back to the plasma membrane (Swiatecka-Urban et al., 2002).

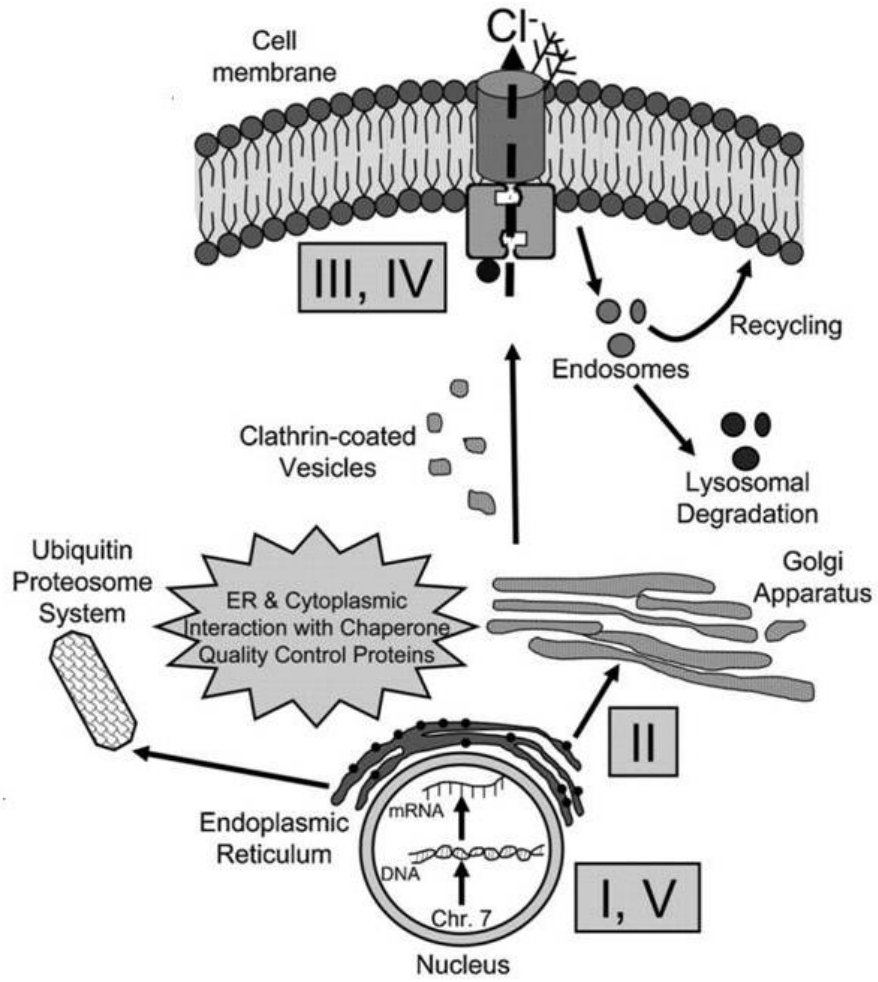

Figure 1-4. CFTR mutations and how they affect biosynthesis, trafficking and endocytosis.

CFTR is synthesized and undergoes quality control in the endoplasmic reticulum. Misfolded proteins are ubiquitinated and trafficked to the proteasome for degradation. Correctly folded CFTR is transported to the Golgi apparatus where N-linked glycosylation occurs. Mature CFTR is trafficked to the membrane to carry out Cl^- secretion. CFTR undergoes endocytosis and can be either recycled or targeted for lysosomal degradation. There are five classes of CFTR mutation which can affect different aspects of these processes. Class I mutations involve premature termination of the production of CFTR, leading to little or no functioning CFTR protein in the membrane. Class II mutations have incorrect folding and affect the trafficking of CFTR to the apical membrane of the cell. Class III mutations include the defective regulation of CFTR at the cell surface, the gating mechanism of CFTR is defective (Walsh, 1993). Class IV mutations reach the cell surface, but Cl^- transport through the cell is impaired due to narrowing of the pore. In class V mutations, mRNA processing is impaired due to defects in splicing. (Image taken and adapted from Rogan *et al.* (2011).

1.5 When CFTR processing goes awry: Airway diseases

As discussed above, the role of CFTR structure, trafficking, and regulation by different factors is crucial for effective mucocilliary clearance. Dysfunction of these components can lead to a variety of disease phenotypes as discussed below.

1.5.1 Cystic fibrosis

Cystic fibrosis (CF) is an autosomal recessive disease caused by mutations in the CFTR gene, which cause a loss of function of the CFTR protein (Donaldson, 2007). There are approximately 2000 identified mutations of CFTR, 242 of which are disease causing (US CF Foundation, 2015). There are five classes of CFTR mutation which lead to changes in CFTR function resulting in a disease phenotype, see Figure 1-4 (Rogan et al., 2011). The most common mutation of CFTR associated with CF is delF508, a class II inframe deletion of the phenylalanine at position 508 (Riordan, 1989). The deletion of phenylalanine 508 results in abnormal folding of CFTR during translation. The misfolded protein is recognized by molecular chaperones which facilitate targeting of the abnormally folded CFTR to proteasomes for degradation (Cheng et al., 1990). Additionally, delF508 has reduced open probability (Denning et al., 1992, Dalemans et al., 1991) and residency time in the plasma membrane upon temperature correction (Lukacs et al., 1993).

Since delF508 CFTR is unable to reach the plasma membrane, secretion of Cl^- into the ASL by CFTR is absent compared to non-CF airways. Though the loss of Cl^- secretion contributes to CF ASL dehydration, the lack of normal CFTR leads to ENaC hyperactivity, which also contributes to dehydration of the airways and ultimately mucus stasis. The combination of both of these factors results in excessive absorption of Na^+, Cl^- and water across the epithelium, leading to depletion of the ASL depth. This depletion directly affects the properties of the ASL, resulting in increased viscosity and decreased elasticity. Mucus transport is impeded and mucus can begin to accumulate. This accumulation in the airways is further exacerbated by the hypersecretion of mucins by goblet cells and submucosal cells. Patients with CF experience chronic inflammation and colonization by microbes, which eventually lead to lung damage and mortality.

Although del508 is the most common mutation, other mutations in CFTR can also cause serious disease phenotypes. Class I mutations are typically nonsense mutations which result in the introduction of premature stop codons into the protein.

This results in unstable truncated proteins, which are non-functional, and are unable to reach the plasma membrane. Class II mutations, like that of delF508 CFTR, also cause CFTR dysregulation by misfolding, leading to premature degradation. Class III mutations are typically caused by missense mutations, leading to the production of CFTR proteins that are able to traffic to the plasma membrane, but have defects in the regulation of CFTR by phosphorylation and ATP. One example of a Class III mutation is G551D-CFTR. This CFTR mutant is folded correctly and trafficked to the plasma membrane, but the gating of the channel, normally regulated by NBD dimerization and ATP binding and hydrolysis, is defective. Class IV mutations are able to traffic to the plasma membrane, but the channels have decreased open probability, and reduced chloride secretion. Class V mutations cause dysregulation of transcription, leading to defects in splicing, and a reduction in the quantity of normally functioning CFTR channels at the plasma membrane (Rogan et al., 2011).

Current therapies for CF patients include anti-inflammatory agents, antibiotics, hypertonic saline and mucolytics (Quon and Rowe, 2016). However, these treatments only address the symptoms rather than treat the underlying cause of the disease. Concerted effort has been undertaken to discover the cellular mechanisms underlying this disease, so that people with CF can have not only medication to treat the symptoms, but to increase the ability of CFTR to reach the membrane in its functional form, and to improve Cl^- secretion across the epithelial surface. To this end, a number of companies within the last five years have produced compounds to directly treat defects of mutant CFTR. Although folding of delF508 is impaired, several studies have demonstrated that when delF508 is able to arrive at the plasma membrane it retains function, although its function is reduced compared to that of wild-type CFTR (Brown et al., 2014, Pedemonte et al., 2005, Denning et al., 1992).

Thus, two types of drugs have been the focus in this effort thus far; potentiators and correctors. Potentiators are intended to improve the ability of mutant CFTR to secrete Cl^- at the plasma membrane. This category of CFTR modulator is primarily targeted at CF patients with class III gating mutations, such as that of G551D. The first compound of this category, Ivacaftor, was approved for patient care in 2012 after results from a randomized controlled trial showed in patients with at least one G551D allele, a 10.6% increase in FEV_1% predicted, and significantly reduced pulmonary exacerbations (Ramsey et al., 2011). However, Ivacaftor alone had no improvements in patients with the delF508 mutation. Correctors function to fix the

cellular misprocessing of CFTR, allowing the protein to fold in its correct form. As such, patients with class II mutations such as delF508 CFTR are primary targets for this therapy. Despite a four-fold increase in delF508 CFTR-mediated chloride secretion in human bronchial epithelial cells (HBECs) (Van Goor et al., 2011), a phase IIa clinical trial demonstrated no improvement in delf508 CFTR homozygous patients (Clancy et al., 2012). A combination co-therapy using both the corrector and the potentiator, to not only improve delF508 CFTR trafficking to the plasma membrane but also to improve channel function, has been shown to have significant effect on CF patients. The combination therapy, Orkambi, was approved for clinical use in 2015, after approximately 3% improvement in FEV_1% predicted in delF508 homozygous patients (Wainwright et al., 2015). Despite the recent success of these drugs in the treatment of CF, many investigations are still being undertaken to discover different and more sophisticated compounds for the correction and potentiation of CFTR, and to address different aspects of CF pathology, with the hope of even more improvements in the lives of patients with CF.

1.5.2 COPD

Chronic obstructive pulmonary disease (COPD) is the third leading cause of death in the world, with a 50% prevalence in heavy smokers (Mannino et al., 2002, Rennard and Vestbo, 2006). COPD is caused by long-term exposure to inhaled pollutants and particles, of which 90% of cases in the developed world are caused by smoke from cigarettes (Barnes, 2000). Two major phenotypes of COPD are emphysema and CB, of which CB is the most prevalent (Hogg et al., 2004). Clinically, CB is known to reflect a chronic productive cough, which lasts for two months over two consecutive years (Boucher, 2004). This productive cough is characterized by sputum production, mucus hypersecretion and the formation of mucus plugs, and can lead to progressive lung function decline and death (Hogg, 2004).

Smoking tobacco stimulates the innate defense system in the lung, which protects against aberrant stimuli. This response involves an acute inflammatory response (Simani, 1974) and mucocilliary clearance (Knowles and Boucher, 2002). Inflammation in CB is located in the central airways and is associated with an increased number of neutrophils, macrophages, and inflammatory mediators such as transforming growth factor (TGF) β (Vignola et al., 1997, Sethi et al., 2006).

Furthermore, the bronchial walls are thickened by the deposition of connective tissue (Thurlbeck and Angus, 1964).

Mucocilliary clearance is deficient in CB and there are many different components that contribute to this. COPD patients undergo delayed mucus clearance demonstrated by reduced mucus velocity in the trachea and a slower removal of radio nuclear particles from the lungs (Morgan et al., 2004, Brown et al., 2002, Moller et al., 2008). This may in part be due to mucus hypersecretion, a common factor of CB. Mucus hypersecretion is multifactorial, and is caused by an increased number of goblet cells (goblet cell hyperplasia) (Saetta et al., 2000), and enlarged mucus glands (glandular hypertrophy) (Reid, 1960). Accordingly, MUC5AC expression in the central airway is increased in patients with COPD (Caramori et al., 2009). Another contributor to deficient mucocilliary clearance is ciliary dysfunction. Patients with COPD exhibit reduced ciliary beat frequency (Yaghi et al., 2012), a phenomenon that is mimicked in smoke exposed subjects (Agius et al., 1998). Also, CS causes shortening of the cilia and impaired ciliogenesis (Tamashiro et al., 2009). The final component of deficient mucocilliary clearance to be addressed here is the hydration status of mucus. Mucus from patients with CB is dehydrated, as determined by increased in percent solids of the mucus of CB patients to ~7% compared to ~2% in normal patients (Clunes et al., 2012, Rubin et al., 1992). When percent mucus solids increases to ~6%, mucus clearance slows down, and the pressure of the mucus layer on the PCL causes the PCL to collapse, leading to the adherence of mucus to the epithelial surface (Button et al., 2012). This phenomenon may be partially responsible for the formation of mucus plugs in the airway.

Current treatments for COPD have centred on inhaled long-acting bronchodilators and corticosteroids. These drugs relax airway smooth muscle, resulting in reduced bronchial obstruction and airflow limitation (Cazzola, 2014). While treatment with inhaled long-acting bronchodilators and corticosteroids reduce exacerbations in CB patients, they do not completely abolish them, and long-term use of long-acting bronchodilators can lead to increased risk of pneumonia (Hurst et al., 2010, Calverley et al., 2011). Ultimately, these treatments are only palliative, and do not address the underlying causes of pathogenesis. Research into new therapeutics for CB has primarily focused on the role of inflammation in the airways in response to CS. Unlike in the treatment of asthma, corticosteroids have no effect on the level of neutrophilic inflammation, and no decrease in inflammatory mediators in COPD (Barnes, 2000). More recently, inhibitors of phosphodiesterase 4 (PDE4) have been

studied in the context of reducing inflammation in patients with COPD and CB, demonstrating improved lung function and reduced exacerbations (Calverley et al., 2009, Fabbri et al., 2009, Rennard et al., 2011, Martinez et al., 2015).

Although some progress is being made by reducing inflammation, new targets for pharmaceuticals are always being investigated. A new focus area for CB therapeutics stems from the concept that CB pathologically resembles CF. Much like CF, the prominent defect in CB is airflow limitation. As discussed in sections 1.5.1 and 1.5.2, patients with CF and CB undergo mucus hypersecretion, mucus accumulation, and goblet cell hyperplasia. These symptoms lead to reduced mucocilliary clearance, chronic neutrophilic inflammation and chronic bacterial colonization (Sethi et al., 2006, Barnes, 2004). As such, some treatments used in CF, i.e. like azithromycin, have also provided marked improvements in symptoms of patients with COPD. On the other hand, the use of mucolytics in CF reduces exacerbations and improves lung function, whereas in CB mucolytics have had few benefits (Decramer et al., 2005, Zheng et al., 2008, Poole and Black, 2006).

More recently, it has become apparent that patients with COPD have dysfunctional CFTR activity. This dysregulation of CFTR activity has been recorded in both nasal potential difference studies and lower airway potential difference studies (Sloane et al., 2012, Cantin et al., 2006b). Interestingly, healthy smokers and COPD smokers exhibit a more severe ablation of CFTR activity compared to COPD former smokers, in which the reduction of CFTR activity is less prominent. These data imply that CFTR deficiency in COPD is a more direct effect of smoke exposure, rather than a downstream effect in COPD pathology. Indeed, healthy ex-smokers that acutely smoke a cigarette also exhibit a rapid decline in nasal potential difference in the presence of low Cl^-/isoprenaline (Clunes et al., 2012). However, the effects of smoke exposure on both healthy smokers and COPD smokers are sustained, even in the absence of acute CS exposure, suggesting there may be long-term effects of CS on CFTR. As such, the expression of CFTR protein was much lower in the bronchial epithelium of COPD GOLD 4 patients ($FEV_1/FVC < 70\%$, $FEV_1 < 30\%$ predicted) when compared to GOLD 0 patients (non-smokers, asymptomatic with normal lung function), indicating that decreases in CFTR function may be attributed to decreases in both mRNA and protein levels.

1.6 Cigarette smoke and CFTR – What do we know so far?

1.6.1 In vitro effects of cigarette smoke on CFTR

The effects of smoke on CFTR can not only be measured in COPD patients and smokers, but have also been recorded *in vivo* across different species. Indeed, the first observation that cigarette smoke (CS) affected chloride secretion was provided by Welsh in 1983, before the identification of the CFTR gene. Welsh demonstrated a decrease in short-circuit current due to an inibition in chloride secretion after acute CS exposure in canine trachea, both *in vivo* and *in vitro* (Welsh, 1983). The ability to measure the effects of CS on CFTR *in vitro* provides a valuable method for investigating the underlying causes of CS-induced CFTR dysfunction. Additionally, *in vitro* studies provide a platform for pharmaceutical manipulation of the smoke response, paving a first step toward the use of CFTR targeted pharmaceuticals in the treatment of CB.

Since the discovery that Cl^- secretion is blunted by smoke exposure in canine trachea (Welsh, 1983), the effects of CS on Cl^- secretion and CFTR *in vitro*, in a variety of different cell types, have been the subject of an increasing number of studies over the last 15 years. In 2005, Kreindler and colleagues presented evidence in HBECs, using measurements of short-circuit current as well as ion flux studies, that net chloride secretion, and specifically cAMP-mediated Cl^- secretion through stimulation by forskolin, was inhibited by CS extract (Kreindler et al., 2005). Sloane and colleagues repeated this work in 2012, again demonstrating a decrease in forskolin-stimulated Cl^- secretion in HBECs by CS extract (Sloane et al., 2012). This data was supplemented by western blots showing that 2% CS extract caused a decrease in CFTR total protein expression, and ASL depth measurements showing that ASL depth is decreased by CS extract. Interestingly, Sloane and colleagues utilized ivacaftor, to potentiate CFTR, and found that both CS extract reduced CFTR- mediated Cl^- secretion and ASL depth recovered in the presence of ivacaftor. However, effects of ivacaftor on CS extract exposed CFTR total protein levels were not determined. In 2006, Cantin and colleagues demonstrated diminished Cl^- secretion in both Calu-3 cells, a human respiratory airway cell line, and T84 cells from the human intestine (Cantin et al., 2006b). Furthermore, Cantin and colleagues also determined that CFTR gene expression in T84 cells and Calu-3 cells was sensitive to oxidative stress (Cantin et al., 2006a). CS itself is a known oxidant and decreased the levels of transcription of CFTR in Calu-3 and T84 cells (Cantin et al., 2006b). Changes in mRNA expression levels do not always directly

result in changes in levels of translated protein. In fact, the majority of studies have shown a weak correlation between mRNA expression data and protein levels (Maier et al., 2009). However, Cantin and colleagues also demonstrated by western blot that CFTR protein levels appear to decrease in Calu-3 cells following exposure to CS. This data has also been reinforced by Cormet-Boyaka's group (Hassan et al., 2014), who have shown that exposure to CS extract results in a time-dependent decrease in both CFTR mRNA expression and protein expression levels in 16HBE14o- cells. In 2009, Cohen and colleagues presented data in murine and human sinonasal epithelial cultures that forskolin-mediated Cl^- secretion was reduced in response to CS extract (Cohen et al., 2009). This was accompanied by a study demonstrating that ciliary beat frequency was also diminished by CS extract. Finally in *Xenopus* Oocytes, Moran and colleagues demonstrated by whole cell patch clamp that CS extract induced reductions in Cl^- are voltage-dependent (Moran et al., 2014).

Thus, CS-induced reduction Cl^- secretion has been confirmed across a number of different cell types, by different methods of smoke exposure. A large number of studies have investigated the changes in chloride secretion by CS, and subsequent effects on mucociliary clearance. However, the underlying cause of reduced Cl^- secretion by CS has not been addressed. Our lab have shown using western blot that CFTR protein levels are reduced following smoke exposure in preparations with a low concentration detergent such as NP40. However, when a detergent with a higher concentration is utilized (1% and 10% SDS) the CFTR the reduction of CFTR protein levels was ablated, suggesting that rather than a decrease in CFTR protein expression, CFTR becomes insoluble after CS smoke exposure. Supplementary to this, Clunes et al. (2012) demonstrated using surface labeling and confocal imaging that CS causes the specific removal of CFTR from the plasma membrane of airway cells leading to intracellular accumulation of CFTR, suggesting that CFTR is internalized following CS exposure. CFTR accumulated in the perinuclear region of the cell, and colocalized with vimentin, an intermediary filament used to identify the location of aggresomes in the microtubule organizing center. Later work from our lab have determined that this internalization of CFTR is dependent on an increase in intracellular Ca^{2+} caused by CS (Rasmussen et al., 2014). Inhibition of the sarcoplasmic/endoplasmic reticulum Ca^{2+} ATPase inhibitor had no effect on CS-induced Ca^{2+} release, the endoplasmic reticulum was ruled out as a source for the rapid release of intracellular Ca^{2+} caused by smoke exposure. However, transfected with LAMP1 tagged with a Ca^{2+}-sensitive FRET pair

demonstrated increased Ca^{2+} concentrations in the vicinity of the lysosomes upon CS exposure.

The *in vitro* studies presented in this section confirm that CS can directly affect the function of CFTR, and studies on ASL height and mucociliary transport (Rasmussen et al., 2014, Sloane et al., 2012) provide further evidence that CS-diminished Cl^- secretion may be associated with the mucociliary transport defects observed in COPD pathology (Hogg, 2004). Thus, investigation into the the cellular mechanisms of CS-induced CFTR internalization will provide valuable insight into the

1.6.2 Components of cigarette smoke

In the original studies of smoke effects on Cl^- secretion, Welsh employed two different smoke exposure protocols for *in vivo* versus *in vitro* work. To smoke the mongrel dogs *in vivo*, puffs of whole cigarette smoke were delivered through an endotracheal tube. In contrast for *in vitro* experiments, whole cigarette smoke was bubbled through mucosal or submucosal bathing solution. This discrepency in smoke exposure methods has been addressed somewhat over the last 25 years although inconsistencies still remain today. This is, in part, due to the complexity of the composition of CS, with over 7000 different compounds identified. At least 69 of these components are known carcinogens, and many others have been identified as toxicants (USDHHS, 2010). CS has two phases; a gaseous phase which accounts for 95% of whole cigarette smoke by weight, and a particulate phase which comprises the remaining 5% of whole cigarette smoke (Keith, 1965). The two phases of CS have different properties. For example, the gaseous phase is strongly oxidizing, whereas in the particulate phase the reducing properties dominate (Church and Pryor, 1985).

The most common *in vitro* methods for smoke exposure, CS extract and CS condensate, isolate the gaseous phase and the particulate phase respectively. CS extract is produced by bubbling smoke through bathing solution or growth medium, whereas CS condensate is produced by smoking the cigarette through a Cambridge filter pad to collect particles larger than 0.1 µm. The collected particulates are then dissolved in a DMSO vehicle. Even within these methods, there are no standards in place to define how many cigarettes or how long the cigarettes should be smoked to produce a response. For example, in their studies of the effects of CS extract on Cl^- secretion in HBECs, Sloane and colleagues

(2012) bubbled the smoke from one reference cigarette (please see section 2.6 for more information on reference cigarettes) through DMSO to make 100% extract, which was then diluted in cell media. Kreindler and colleagues (2005) bubbled 8 reference cigarettes through warmed bath solution to produce 100% CS extract for their studies on CS extract reduced Cl^- secretion in HBECs. For their studies on voltage-dependent reduction in Cl^- secretion using *Xenopus* oocytes, Moran and colleagues (2014) prepared their extract by bubbling the smoke from 50 cigarettes through 50 mL of Frog Ringer solution. Although drastically different methods to produce CS extract were used, both groups observed a reduction in CFTR-mediated Cl^- secretion. Although CS extract is the most commonly used method of CS exposure, St-Laurent and colleagues (2009) demonstrated that the process of bathing HBECs in CSE produced a different inflammatory response to that of whole CS. Thus, in order to use a method of smoking that closely mimics that of the typical smoker, in this thesis, the gaseous phase of cigarette smoke was used to treat the cultures, without the use of a diluent. Although this method closely mimics that of smokers, the removal of the particulate phase by collection on a Cambridge filter pad prevents the cultures from exposure to chemicals only present in the particulate phase. According to data from our lab, the level of nicotine deposition in the lung is reduced following exposure to the gaseous phase of smoke compared to whole CS (Clunes et al., 2008). However, the removal of the particulate phase is necessary to allow fluorescent imaging of the cultures, since the particulate phase of CS contains autofluorescent particles which interfere with the signal.

1.7 Aims

Over the last ten years, increasing evidence suggests that CS can have a direct effect on ion transport across airway epithelium. Specifically, CS causes calcium sensitive internalization of CFTR, resulting in a decrease in CFTR-mediated Cl^- secretion (Clunes et al., 2012, Rasmussen et al., 2014). Given that ASL dehydration and inefficient mucus clearance can lead to symptoms of CB in smokers, elucidating the cellular mechanisms behind diminished Cl^- secretion, as well as the effects on other plasma membrane proteins, in response to CS is an important step towards the discovery of potential new therapies for patients with COPD. To this end, the overall aims of this thesis were to:

1) Investigate the temporal profile of CS-induced CFTR internalization.

2) Elucidate the effects of CS on other plasma membrane proteins.

3) Understand the cell signalling components required for CS-induced internalization.

4) Determine the endocytic route and the terminal destination of CS-internalized CFTR.

2.0 Methods and Materials

2.1 Materials

All cell culture flasks and plates were purchased from Corning Costar. All cell culture medium and supplements were purchased from Life Technologies unless otherwise specified. GFP-CFTR and RFP-CFTR were acquired from Bruce Stanton at Dartmouth College. Anoctamin 1 (Ano1)-mCherry was acquired from C. Hartzell at Emory University. STIM1 labelled on the c-terminus with YFP was acquired from T. Meyer at Stanford University. STIM1-mCherry was created by replacing the YFP tag with mCherry (Park et al., 2009). The following plasmids were acquired as bacteria in agar stabs: mRFP-clathrin light chain was a gift from Ari Helenius (Addgene plasmid # 14435). wt-rab5-DsRed; wt-rab11-DsRed and wt-rab7-DsRed were a gift from Richard Pagano (Addgene plasmid # 13050, # 12679 and # 12661, respectively); wt HA-dynamin 1 pcDNA3.1 and K44A HA-dynamin 1 pcDNA3.1 was a gift from Sandra Schmid (Addgene plasmid # 34682 and # 34683, respectively); Orai1 YFP was a gift from Anjana Rao (Addgene plasmid # 19756). BHK cells stably expressing $CFTR^{15SA}$ were kindly provided by Dr Jack Riordan (UNC). BHK cells stably expressing wtCFTR were kindly provided by Dr Martina Gentzsch.

2.2 Solutions

Pyruvate Ringer's solution: 120 mM NaCl, 12 mM $NaHCO_3$, 24 mM HEPES, 1.2 mM $MgCl_2$, 5.2 mM KCl, 1 mM NaPyruvate, 10 mM Glucose, 1.2 mM $CaCl_2$, 0.25 mM EGTA, 0.1% Albumin (w/v), pH 7.4

Phosphate-buffered saline (PBS): 2.7 mM KCl, 1.8 mM KH_2PO_4, 137 mM NaCl, 9.9 mM Na_2HPO_4, pH 7.4

PBS supplemented with $MgCl_2$ and $CaCl_2$ (PBS++): 2.7 mM KCl, 1.8 mM KH_2PO_4, 137 mM NaCl, 9.9 mM Na_2HPO_4, 1 mM $MgCl_2$, 1 mM $CaCl_2$, pH 7.4

Pierce's lysis buffer: 25 mM Tris-HCl pH 7.4, 150 mM NaCl, 1 mM EDTA, 1% NP-40 (v/v) and 5% glycerol (v/v)

Biotinylation lysis buffer: 0.4% sodium deoxychlorate (w/v), 50 mM EGTA, 10 mM Tris HCl, 1% NP40 (v/v) and 1X protease inhibitor

Borate buffer: 85 mM NaCl, 4 mM KCl, 15 mM NaB_4O_2

Tris-buffered saline with Tween 20 (TBST): 137 mM NaCl, 20 mM Tris, 0.1% Tween-20, pH 7.4

2.3 Routine cell culture

All cell culture work was performed in a sterile laminar flow hood. Cells were cultured in 75 cm^2 culture flasks at 37°C, 5% CO_2 in a sterile humidified incubator. Human embryonic kidney (HEK)293T cells were cultured in Dulbecco's modified Eagle's medium (DMEM) with 4.5 g/L glucose, supplemented with 100 Units/mL penicillin, 100 µg/mL streptomycin, and 10% foetal bovine serum (FBS, Sigma Aldrich, v/v). Baby Hamster Kidney (BHK) cells stably expressing wild type CFTR or mutated CFTR lacking all 15 PKA phosphorylation sites ($CFTR^{15SA}$) were cultured in DMEM:F12 medium supplemented by 100 Units/mL penicillin and 100 µg/mL streptomycin, 10 % FBS (v/v) and 50 mg/mL methotrexate (Teva Pharmaceuticals). All cells were passaged every 2-4 days upon reaching confluency. Once confluent, the growth medium was removed and the cells were washed once with phosphate-buffered saline (Corning) to remove excess FBS. The cells were then incubated for 2-5 min at 37°C in 5% CO_2 with 2 mL trypsin-ethylenediaminetetraacetic acid (EDTA) until cells began to detach from the base of the cell culture flask. At this point, fresh growth medium was added to neutralize trypsin-EDTA. The cells were then mechanically rinsed with growth medium to form a cell suspension. The cell suspension was transferred to a 50 mL conical and centrifuged at 800 rpm for 5 min to remove any remaining trypsin-EDTA. The supernatant was removed and the cells were resuspended in fresh growth medium. From here, continuation flasks were prepared with a subcultivation ratio of 1:10. Cells were counted and seeded directly on 6 well plates for western blots or on 22 mm number 1 glass coverslips (Fisherbrand) in 6 well plates for imaging as appropriate. HBECs were obtained from main stem and lumbar bronchi from human excess donor lungs under protocol previously approved by the University of North Carolina Medical School Institutional Review Board (Fulcher et al., 2005). Primary HBECs were seeded on collagen coated 0.4 µm polyester membrane semi-permeable 12 mm culture inserts (Corning, transwell-clears) and maintained at air liquid interface in 37°C and 5% CO_2. The cultures were 3 weeks post-seeding after becoming fully differentiated.

2.4 Transfections

Approximately 24 h after seeding, at 70-80% confluency HEK293T cells were transiently transfected with appropriate plasmids using Lipofectamine 2000 (Invitrogen). The transfection mix was prepared according to manufacturer's instructions in Opti-MEM (Life Technologies) using a ratio of 3 µL Lipofectamine 2000 to every 1 µg DNA. The growth medium of the cells was switched to antibiotic free medium (DMEM + 4.5 g/L glucose and 10 % FBS (v/v). The transfection mix was added dropwise to the cultures which were then incubated at 37°C and 5% CO_2 for 4 h prior to the replacement of antibiotic free medium with normal growth medium (DMEM + 4.5 g/L glucose, 10 % FBS, 1 x penicillin/streptomycin solution). The cultures were then returned to the incubator at 37°C and 5% CO_2 for 48 h before experiments were performed.

2.5 Construction of CFTR mutants

C-terminal truncation mutants of CFTR were constructed to investigate the role of the C-terminal interactions in CS-induced internalization of CFTR. Human wt-CFTR was previously tagged N-terminally with green fluorescent protein (GFP) and a 23 amine acid linker sequence. This construct was subcloned into vector pcDNA3.1 (Moyer et al., 1998). Truncation mutations of CFTR (K1174X and L1254X) were created using polymerase chain reaction (PCR)-based site-directed mutagenesis to introduce site specific stop codons at lysine 1174 and leucine 1254. Site-directed mutagenesis was performed using the Quick Change Site Directed Mutagenesis Kit (Agilent Technologies) according to manufacturer's instructions. Primers (Table 2-1) were designed using Quick Change Primer Design program (Agilent Technologies) and purchased from Eurofins/MWGOperon. Site-directed mutagenesis requires a series of thermal cycling which allows denaturing of plasmid DNA, annealing of the primers to introduce the mutation and the elongation of primers using a Pfu-based polymerase, yielding both parental DNA and daughter DNA complete with the mutation. Methylated parental DNA was digested with 10 µL *Dpn* 1 for 10 min at room temperature to increase the yield of mutated DNA. The plasmid was then transformed into XL 10-Gold Ultracompetent cells (Agilent Technologies) according to manufacturer's protocol. The plasmid was then amplified by miniprep (Qiagen) and all mutant plasmids were subsequently verified by sequencing across the open reading frame before use.

Mutation	Direction	Primer	Annealing Temp (°C)
K1174X	Forward	ACATGCCAACAGAAGGTTAACCTACCA AGTCAACC	69.4
K1174X	Reverse	GGTTGACTTGGTAGGTTAACCTTCTGTT GGCATGT	69.4
L1254X	Forward	GATCAGGGAAGAGTACTTTGTAATCAG CTTTTTTGAGACTACT	68.5
L1254X	Reverse	AGTAGTCTCAAAAAAGCTGATTACAAA GTACTCTTCCCTGATC	68.5

Table 2-1. Forward and reverse primers designed for the construction of CFTR point mutations

2.6 Cigarette smoke exposure

Kentucky 3R4F Reference Cigarettes were used in all smoke exposure experiments (University of Kentucky, 2016). Kentucky Reference Cigarettes are produced for research purposes only. The constituents of Kentucky Reference Cigarettes indicated in Table 2-2 undergo tight regulation to allow for reproducibility between experiments. An LM1 smoke machine (Borgwaldt) was used to perform all CS exposure (Figure 2-1). The smoke machine functions by automated syringe action to draw CS from a lit cigarette. The CS is then pumped down tubing, through a Cambridge filter pad, into a chamber containing cell cultures. The Cambridge filter pad is designed to capture the particulate phase of smoke. It captures up to 99% of 0.1 µg diameter particulates to ensure that only the gaseous phase of smoke is exposed to the cells. Automation of the smoke machine allowed for reproducible CS puff volume, puff time, and length of time between puff. All cigarettes were smoked with a puff volume of 35 mL over a duration of 2 s. Approximately 13 puffs of CS were applied at a rate of 1 puff every 30 s until the entire cigarette was smoked. This volume of CS is considered standard by the International Organization for Standardization (ISO, 2000) and closely mimics the volume of CS and length of CS intake taken by the typical smoker.

For smoke exposure experiments, HEK293T, BHK^{CFTR} or $BHK^{15SA\text{-}CFTR}$ cells were cultured in 6 well plates on glass coverslips and transfected as described in section 2.4 as necessary. Transfected HEK293T cells were utilized for smoke exposure 48 h following transfection, and BHK^{CFTR} and $BHK^{15SA\text{-}CFTR}$ were utilized 48 h after seeding. In all CS exposure experiments, normal growth medium appropriate for each cell type (section 2.3) was aspirated from cultures and replaced with 1 mL pyruvate Ringer's solution. All cultures were incubated at 37°C for 5 min to equilibrate to the experimental conditions. After incubation, the plates

were tipped to remove excess Ringer's solution providing a thin film of liquid on the coverslips to mimic thin film conditions present in the airway. The plates were placed in a CS only, or air only chamber and exposed to CS as described above. After CS exposure, the cultures remained in the smoke chamber for a further 5 min before removal of the thin film and replacement of original cell media. Cells were then incubated in a CO_2 incubator at 37°C. For internalization time course assays the cultures were incubated at 37°C for 0, 5, 15, 30, 60, or 120 min prior to fixation. All other smoke exposures were carried out with 60 min incubation at 37°C prior to fixation unless otherwise specified. Air exposed cells underwent the same steps, but were kept in an air only chamber, and no cigarette smoke was exposed. Where indicated, HEK293T cells were pre-treated with pharmacological agents including forskolin (5 µM), dynasore (80 µM), nocodazole (33 µM), U0126 (10 µM), AG1478 (30 µM) or cytochalasin D (2 µM). Treatments were maintained throughout the smoke exposure and incubation periods.

Cigarette Reference	Tobacco Component	Amount of each component (%)
3R4F	Flue Cured	35.41
	Burley	21.62
	Oriental	12.07
	Maryland	1.35
	Reconstituted (Schweitzer Process)	29.55
	Glycerine (dry-weight basis @ 11.6% OV)	2.67
	Isosweet (sugar)	6.41

Table 2-2. Tobacco constituents of Kentucky Reference Cigarettes.

The ingredients present in Kentucky Reference Cigarettes closely resemble that of commercial cigarettes, and are maintained from batch to batch to allow for reproducibility across experiments (University of Kentucky, 2016).

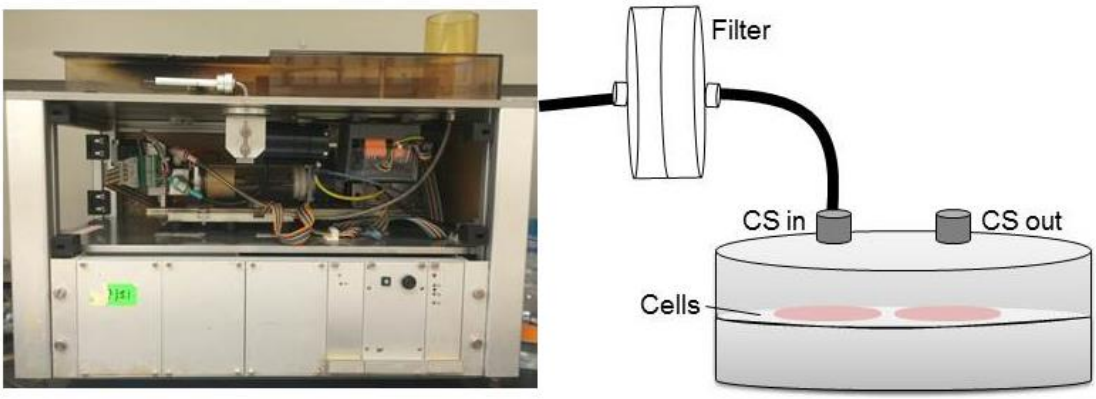

Figure 2-1. Experimental set up for cigarette smoke exposure.

A cigarette is placed in the smoke machine and lit. CS is taken in through an automated syringe and pumped down output tubes, through a Cambridge filter pad and into a chamber containing the cells.

2.7 Immunocytochemistry

Immunocytochemistry was used to detect wt-CFTR and CFTR^{15SA} in BHK cells stably transfected with each construct. Additionally, immunocytochemistry was used to detect natively expressed calreticulin in HEK293T cells. For labelling, cells were treated as appropriate and washed once in ice cold PBS prior to fixation in 4% paraformaldehyde (v/v) for 5 min at room temperature, or 100% methanol for 10 min at -20°C. Following fixation, the cultures were blocked at room temperature with agitation for 1 h in blocking buffer consisting of 10% (v/v) normal goat serum, 5% (v/v) bovine serum albumin and PBS. Wild-type CFTR and CFTR^{15SA} were labelled with monoclonal anti-CFTR 596 IgG2b antibody, obtained via Cystic Fibrosis Foundation Therapeutics and were kindly provided by Dr J. Riordan (UNC). Antibodies were diluted 1:300 in blocking buffer for 3 h at room temperature. Calreticulin was labelled with polyclonal anti-calreticulin antibody (Affinity Bioreagents) at 1:1000 in blocking buffer for 3 h at room temperature. Following incubation with primary antibody, the cultures were washed using PBS for a minimum of 3 x 10 min prior to incubation with secondary antibody goat anti-mouse IgG diluted at 1:300 for 1 h at room temperature. For CFTR labelling, an anti-mouse secondary antibody conjugated to Alexa 488 (Life Technologies) was utilized. For calreticulin labelling, an anti-rabbit secondary antibody conjugated to Alexa 647 (Life Technologies) was utilised. After labelling with secondary antibody, the cultures were washed for a minimum of 3 x 5 min, prior to imaging on the confocal microscope as described in Section 2.8.1.

2.8 Fluorescence microscopy

2.8.1 Confocal microscopy

For all internalization time course assays the cells (HEK293T and BHK^{CFTR}) were seeded at 75,000 cells per well on 25 mm glass coverslips in a 6 well plate. The HEK293T cells were transfected 24 h after seeding with 0.5-1 µg DNA according to manufacturer's instructions. Experiments were performed 48 h after transfection. BHK^{CFTR} cells were used for experiments 48 h post-seeding. All cells were exposed to CS or air as described previously (Section 2.3). After CS or air exposure the cells were incubated for 0, 5, 15, 30, 60 or 120 min in 1 mL normal media before fixing in 4% paraformaldehyde for 5 min at room temperature or 100% methanol for 15 min at -20°C. The cells were then washed three times with PBS and stored at 4°C in PBS until ready for imaging. For imaging, the coverslips were removed from the six well plate and mounted in a metal ring, with 400 µL PBS covering the cells. All cultures were imaged on a Leica SP8 confocal microscope using a 63x 1.40 numerical aperture (NA) plan apochromatic Leica objective. To quantify the internalization of plasma membrane proteins 6 images per coverslip were taken as indicated in Figure 2-2 A. Using Image J (NIH Freeware, http://rsb.info.nih.gov/ij/), 6 regions of interest (ROI) were assigned to measure the fluorescence intensity of the entire plasma membrane, and 6 ROIs to measure the fluorescence intensity of the entire cytosol were taken from all cells present in the image. Examples of the ROIs selected for each cell are presented in Figure 2-2B. The mean fluorescence intensity of the 6 plasma membrane ROIs and 6 intracellular ROIs were calculated to provide an average plasma membrane and an average intracellular fluorescence intensity for each cell. To normalize the data, the mean fluorescence intensity of the plasma membrane and cytosol from all cells on air exposed control coverslips were measured and taken as a value of one, and all other conditions were expressed as a fraction of this value. Data presented as mean ± SEM unless stated otherwise.

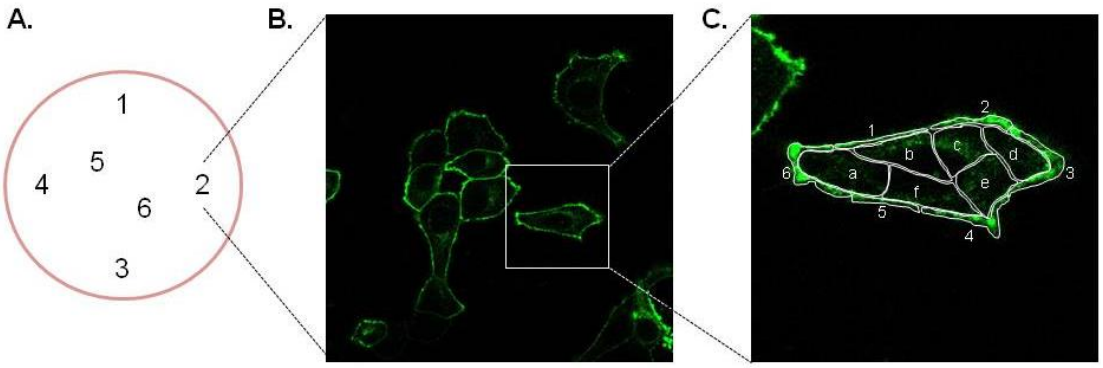

Figure 2-2. Cell and region of interest selection for image analysis.

A diagram outlining the method of data acquisition during confocal imaging. (A) The pink circle indicates a cover slip, and numbers represent the 6 areas of the coverslip in which a confocal image was taken. (B) A representative image taken at ROI 2. All complete cells within the frame are quantified. (C) In each cell, 6 ROIs from the plasma membrane and 6 ROIs from the intracellular region were measured for an average of fluorescence intensity of the entire plasma membrane and the entire intracellular content, respectively.

2.8.2 Acceptor photo bleaching Förster resonance energy transfer

HEK293T cells were seeded in 6 well plates on 25 mm glass coverslips at a density of 75,000 cells per well. The cells were co-transfected with 0.5 µg wt-GFP-CFTR and 0.5 µg wt-RFP-CFTR 24 h after seeding (transfection performed as described above in section 2.4). Cultures were treated with air or CS and fixed 48 h after transfection as described in Section 2.6. Förster resonance energy transfer (FRET) experiments were performed using a Leica SP5 confocal microscope with a 63x 1.30 NA plan apochromatic glycerol immersion objective. The donor, wt-GFP-CFTR or Ano1-GFP, was excited at 488 nm and the emission collected between 495 nm to 549 nm, and the acceptor, wt-RFP-CFTR or Ano1-mCherry, was excited at 561 nm and emission collected between 580 nm to 654 nm. Acceptor photobleaching FRET was measured using ImageJ by measuring a change in donor fluorophore fluorescence intensity after photobleaching of the acceptor fluorophore, using the following calculation:

$$\text{FRET efficiency (\%E)} = ((\text{donor}^{\text{postbleach}} - \text{donor}^{\text{prebleach}}) / \text{donor}^{\text{postbleach}}) \times 100$$

All data presented as mean FRET efficiency (%) ± (standard error of measurement).

2.8.3 Colocalization assay

HEK293T cells were seeded at a density of 75,000 cells per well on a 25 mm glass coverslip. The cells were transiently co-transfected (Section 2.4) with 0.5-1 µg wt-GFP-CFTR and the organelle markers rab5-DsRed, rab7-DsRed, rab11A-DsRed, mRFP-clathrin light chain, and STIM1-mCherry. The cells were exposed to CS 48 h after transfection, as described in section 2.4, and incubated at 37°C and 5% CO_2 for 0, 5, 15, 30, 60 or 120 min before fixing with 4% paraformaldehyde. For colocalization studies of CFTR and calreticulin, a marker of the endoplasmic reticulum, or GM130, a marker of the Golgi apparatus, the cells were fixed in the same manner prior to blocking in 10 % normal goat serum and 1% bovine serum albumin. Calreticulin was detected with anti-calreticulin polyclonal IgG antibody (Affinity BioReagents) and GM130 was detected with anti-GM130 D6B1 rabbit monoclonal IgG antibody (Cell Signalling Technology). Cells were washed a minimum of 3 x 10 min in PBS and incubated with secondary antibody anti-rabbit labelled with Alexa 633. A Leica SP8 confocal microscope was used to take 6 images per coverslip. To measure wt-GFP-CFTR, the cells were excited at 488 nm and the emission collected between 495 to 549 nm. To measure the ds-Red tagged constructs, the cells were excited at 561 nm and the emission was collected between 580 and 654 nm. For mRFP the cells were excited at 555 nm and the emission was collected between 565 nm and 655 nm. For mCherry, the cells were excited at 587 nm and the emission collected between 600 nm and 662 nm. For cultures labelled with Alexa 633, the cells were excited at 633 nm and collected between 640 and 700 nm. The images were overlaid, and the percentage colocalization was quantified using the Leica Application Suite: Advanced Fluorescence (LAS AF) software. Background was set at 20%. A region of interest (ROI) was selected by hand around each cell, and the colocalized pixels (foreground) were presented as white, whilst background pixels were presented as black. The following calculation was automatically used by the LAS AF software to determine the percentage colocalization rate between colocalized areas and background within the ROI.

Percent colocalization = colocalization area / area foreground, where area foreground = image area / area background.

An average of each coverslip was taken and all data are presented as mean colocalization ± SEM.

2.8.4 Intracellular calcium imaging

HEK293T cells were seeded at a density of 100,000 cells per well on 25 mm glass coverslips in 6 well plates. 24 h after seeding, the cells were loaded with 5 µM Fura-2, AM in pyruvate Ringer's (Section 2.3) for 30 min at 37°C in 5% CO_2 before rinsing with pyruvate Ringer's. Briefly, Fura-2, AM is a ratiometric Ca^{2+}-sensitive, membrane permeable dye. Measurements of Ca^{2+}-stimulated fluorescence can be taken at excitation wavelengths of 340 and 380 nm and the emission collected at collected at 510 nm. The ability to excite the dye at two different wavelengths allows for accurate measurement of $[Ca^{2+}]_i$ by minimizing the effects of photobleaching, uneven loading and cell thickness. During the load process 1 µL DMSO or MEK/ERK inhibitor U0126 (10 µM final concentration) was added to the loading solution. To measure changes in intracellular Ca^{2+} after CS exposure, the coverslips were moved to a metal imaging chamber. Pyruvate Ringer's solution (150 µL) was added to mimic thin film conditions as described above, and cultures were exposed to air or CS as described in Section 2.6. Fura-2, AM fluorescence was collected using a Nikon Ti-S microscope with Orca CCD camera (Hamamatsu), Ludl Filter wheels and a 40x 1.3 NA plan fluor oil immersion lens. Fluorescence intensity was measured and presented as mean fluorescence ratio 340/380 ± SEM, mean area under the curve ± SEM and mean maximum change in fluorescence ratio 340/380 ± SEM. Data were collected using HCImageLive software, and GraphPad Prism 4.00 for Windows (GraphPad Software).

2.8.5 Plate reader fluorescence intensity

To estimate the total number of Orai1 transfected cells following CS exposure, HEK293T cells were seeded at a density of 75,000 cells per well on a 6 well plate, and were transfected with Orai1-YFP 24 h after seeding as described in section 2.4. Cells were treated with air or CS 48 h after transfection. Fixation and permeablization with methanol was performed prior to staining with propidium iodide (20 µM) to according to manufacturer's protocol. The fluorescence intensity of propidium iodide, excited at a wavelength of 535 nm and collected at a wavelength of 617 nm, was measured using a Tecan Infinite M1000 plate reader. To normalize the data, the mean fluorescence intensity of the air exposed control cultures were measured and taken as a value of one, and all other conditions were expressed as a fraction of this value. Data presented as mean ± SEM unless stated

otherwise. These cultures were also used for confocal imaging as described in Section 2.8.1.

2.9 Cell surface biotinylation

Biotin can bind primary amines and is not cell soluble; it can therefore be used to bind to cell surface proteins as a technique for the purification of plasma membrane bound proteins. For cell surface biotinylation of primary HBECs, cells were cultured at air liquid interface on semi-permeable culture inserts (Corning, transwell-clears) and exposed to air or CS as noted. Following air/CS exposure, the cultures were cooled to 4°C and washed 3x in ice cold PBS++. The cultures were then agitated at 4°C with 100 µg/µL biotin in borate buffer on the apical surface of the monolayer. FBS (10% v/v) was applied to the basolateral side and was maintained throughout incubation with biotin to ensure biotinylation of only the apical membrane. Excess biotins unable to bind to the cell surface glycoproteins were then quenched with 10% FBS. Cells were washed with ice cold PBS^{++} before lysis with 100 µL biotinylation lysis buffer at room temperature for 10 mins. The lysates were centrifuged for 5 min at 5000xg to remove cell debris. Protein concentrations were calculated using the Bradford assay (Pierce) and samples were diluted in lysis buffer to ensure the same amount of protein was loaded in each tube. The lysates were rotated overnight with NeutrAvidin beads (Thermofisher). The next day, the beads were washed 3 times with ice cold PBS and eluted with 10% 2-mercaptoethanol and 2x lithium dodecyl sulphate (LDS) buffer (Biorad; 40% glycerol (v/v), 4% lithium dodecyl sulfate, 4% Ficoll-400, 0.8 M triethanolamine-Cl pH 7.6, 0.025% phenol red, 0.025% Coomassie G250, 2 mM EDTA disodium). The membrane fractions were loaded on a gel and separated by western blot (for more details on western blot protocol, see Section 2.10). Briefly, the gel was run at 150 mV until the protein ladder reached the bottom of the gel. Gels were transferred wet to (polyvinylidene fluoride) PDVF membranes overnight at 4°C. Membranes were blocked in 5% milk for 1 h at room temperature and probed for total CFTR with primary anti-CFTR 596 IgG2b and for dephosphorylated CFTR with primary anti-CFTR 217 IgG1 acquired from the Cystic Fibrosis Foundation Therapeutics and kindly provided by Dr J. Riordan (UNC). The membranes were washed a minimum of 3 x 10 min in TBST and probed with anti-mouse conjugated to horseradish peroxidase (Jackson ImmunoResearch). The PVDF membrane was visualised using a Chemidoc western blot imager (Biorad).

This work was carried out by Dr Chong Da Tan at the University of North Carolina, at Chapel Hill.

2.10 Western blot

BHK^{CFTR} and $BHK^{15SA\ CFTR}$ cells were seeded on six well plates (Corning) at a density of 75,000 cells per well. The cells were utilized for experiments 48 h after seeding. The cultures were lysed in Peirce's lysis buffer. To quantify protein concentration, bicinchoninic acid (BCA) assay was performed according to manufacturer's protocol. The BCA assay utilizes the biuret reaction (the reduction of Cu^{2+} to Cu^{+}). The combination of two BCA molecules with one Cu^{+} molecule results in the production of a purple coloured reaction product. This product can be detected at an absorption of 562 nm, which is linear with protein concentration within the sample (Thermofisher, 2015). Total protein concentration in the sample was calculated from a standard curve generated from known concentrations of BSA (Figure 2-3).

Lysates, or samples from biotinylation elution (Section 2.9) or were loaded on 4-15% Mini-PROTEAN tris-glycine gel (Biorad) as well as 2 µL dual colour protein standard (Biorad). Gel electrophoresis was performed at 150 mV for 1 h. The gels were then transferred wet, overnight at 4°C, to nitrocellulose or PDVF membranes. Membranes were blocked in blocking buffer consisting of PBS + 0.01% Tween (v/v) and 3% (v/v) dried skimmed milk for 1 h at room temperature prior to incubation overnight at 4°C with primary anti-CFTR 596 monoclonal antibody (UNC CFTR Antibodies) in blocking buffer. The membrane was then washed in PBST for 3 x 5 min at room temperature, prior to the addition of horseradish peroxidase tagged anti-mouse secondary antibody (Jackson ImmunoResearch) at a concentration of 1:1000 in blocking buffer for 1 h. The membrane was then washed 3 x 5 min in PBST to remove any unbound secondary antibody. To detect HRP activity, two components of Clarity enhanced chemiluminescence (ECL) western substrate (Biorad), luminol/enhancer solution and peroxide solution, were combined in equal parts, and were added to the blot for 2 min before the blots were developed using the Chemidoc western blot imager (Biorad).

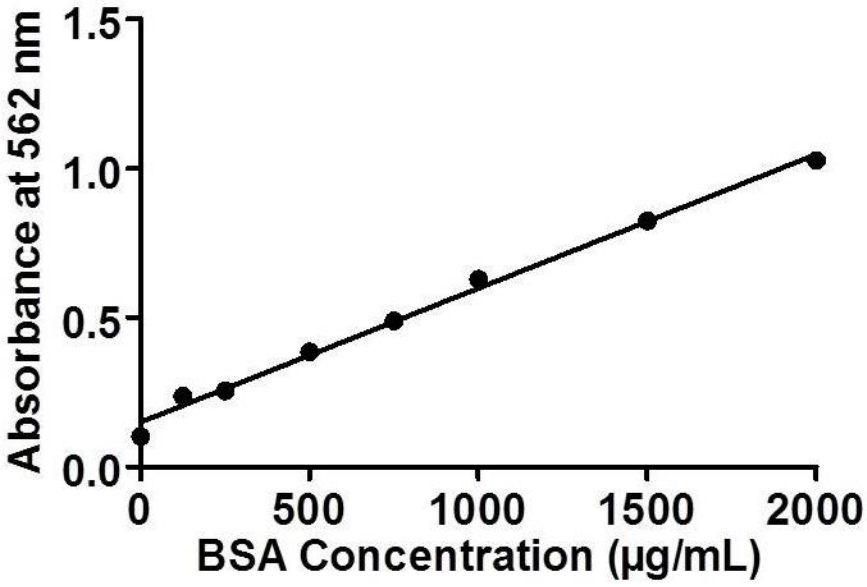

Figure 2-3. Standard curve for BCA assay protein quantification.

BCA protein standard curve was produced using BSA protein standards of known concentration (25, 125, 250, 500, 750, 1000, 1500, 2000 µg/mL). This was utilized for the calculation of the concentration of unknown proteins using regression analysis. Data represents mean of samples ran in duplicate; r^2 = 0.9931.

2.11 Image analysis and statistics

Internalization, FRET assays and densiotometry of western blots were analyzed using ImageJ. All data were collected using Microsoft Excel 2007 (Microsoft Corporation, USA), and graphs were produced using GraphPad Prism 4.00 for Windows (GraphPad Software). All data are given as mean ± SEM unless stated otherwise. Where applicable, statistical significance was calculated using the Kruskal-Wallis test with Dunn's multiple comparison post-test or two-way ANOVA with Dunn's or Sidak's multiple comparison post-test where appropriate. A P value of $p < 0.05$ was considered significant.

3.0 The effect of cigarette smoke on the cellular location of CFTR and other plasma membrane proteins

3.1 Introduction

Airflow limitation and progressive loss of lung function are symptoms which characterize both CF and COPD. CF is an autosomal recessive disease in which mutations of CFTR lead to loss of function, affecting approximately 70,000 people worldwide (CFF., 2015). In contrast, there are more than 1 billion smokers worldwide, and as such, COPD also poses a prominent health risk to society (WHO., 2015). Genetic, epigenetic, and host factors likely contribute to the pathogenesis of COPD. However the primary risk factor is smoking tobacco. Patients with COPD can exhibit both emphysema, characterized by the destruction of the alveolar surface, and CB, characterized by recurrent cough, excessive mucus production and mucus accumulation of the airways (Kim and Criner, 2013). Approximately two-thirds of patients with COPD exhibit CB, which typically has a higher prevelence than that of emphysema (Rab et al., 2013). CB characteristically displays a similar phenotype to CF, with increased mucus accumulation, inflammation and chronic bacterial infection, indicating that there may be a commonality in the pathogenesis of both CF and CB.

Our lab and others have shown blunted chloride secretion following acute CS exposure. This is associated with a rapid internalization of CFTR, leading to decreased ASL depth. Indications that internalization of CFTR and diminished Cl^- secretion may be linked to mucus dehydration and accumulation in patients with COPD present an important challenge. Thus, better understanding of the cellular mechanisms required for this smoke response may reveal potential therapeutic targets to address the underlying causes of smoking related lung disease. To this end, the specific aims of this chapter are to:

1) To develop a protocol to measure the kinetics of CS-induced internalization
2) To determine the importance of the interaction of CFTR-CFTR interactions in CS-induced internalization
3) To better understand the breadth of the effects CS has on plasma membrane proteins

3.2 Results

3.2.1 Cigarette smoke causes time-dependent internalization of CFTR

HEK cells are well suited for biochemical, pharmacological and genetic manipulation (Domingue et al., 2014), and have been shown to exhibit CS-induced calcium release and CFTR internalization much like that of airway epithelia (Rasmussen et al., 2014). This cell line has therefore been selected to carry out the majority of investigations in this thesis.

To investigate the effects of CS on the cellular localization of CFTR, it was first necessary to establish a protocol for visualizing the internalization of CFTR after CS exposure. The N-terminally tagged GFP-CFTR used in this thesis exhibited typical plasma membrane expression and comparable activity in functional experiments to non-tagged CFTR (Moyer et al., 1998). To investigate the cellular location of CFTR following CS exposure, GFP-CFTR was transiently expressed in HEK293T cells. Cells were then exposed to a standard smoking protocol (see methods section 2.6) prior to incubation at 37°C for a series of time points, i.e. 0, 5, 15, 30, and 60 min after CS exposure to better understand CFTR trafficking post-CS exposure. Cells were fixed and visualized using confocal microscopy (Figure 3-1 A), and images were quantified as described in methods section 2.8.1 In Figure 3-1 B, quantification of each time point demonstrated no change in fluorescence intensity at the plasma membrane (PM; red, dashed line) or intracellularly (red, solid line) over 60 min following air exposure. However, following CS exposure CFTR PM fluorescence intensity (blue) decreased with a half-life of 10.5 min and a τ of 15.2 when fit with a single exponential with R^2 value of 0.094 (n = 45 - 125 cells). Intracellular fluorescence intensity increased with a half-life of 27.7 min, τ of 39.9 and R^2 value of 0.085 (n = 45 – 125 cells), consistent with data from Rasmussen *et. al*. which demonstrated that CFTR internalized following CS exposure. To confirm that the change in CFTR distribution within the cell was due to changes induced by CS rather than a result of expression, the transfection efficiency of GFP-CFTR was measured in HEK293T cells (Figure 3-1 C). The number of transfected cells was taken as a percentage of total cells in the frame after 15 min of air or CS exposure. No significant difference was observed in transfection efficiency between air and smoke exposed samples indicating that internalization measured is due to specific effects of CS rather than differences in expression.

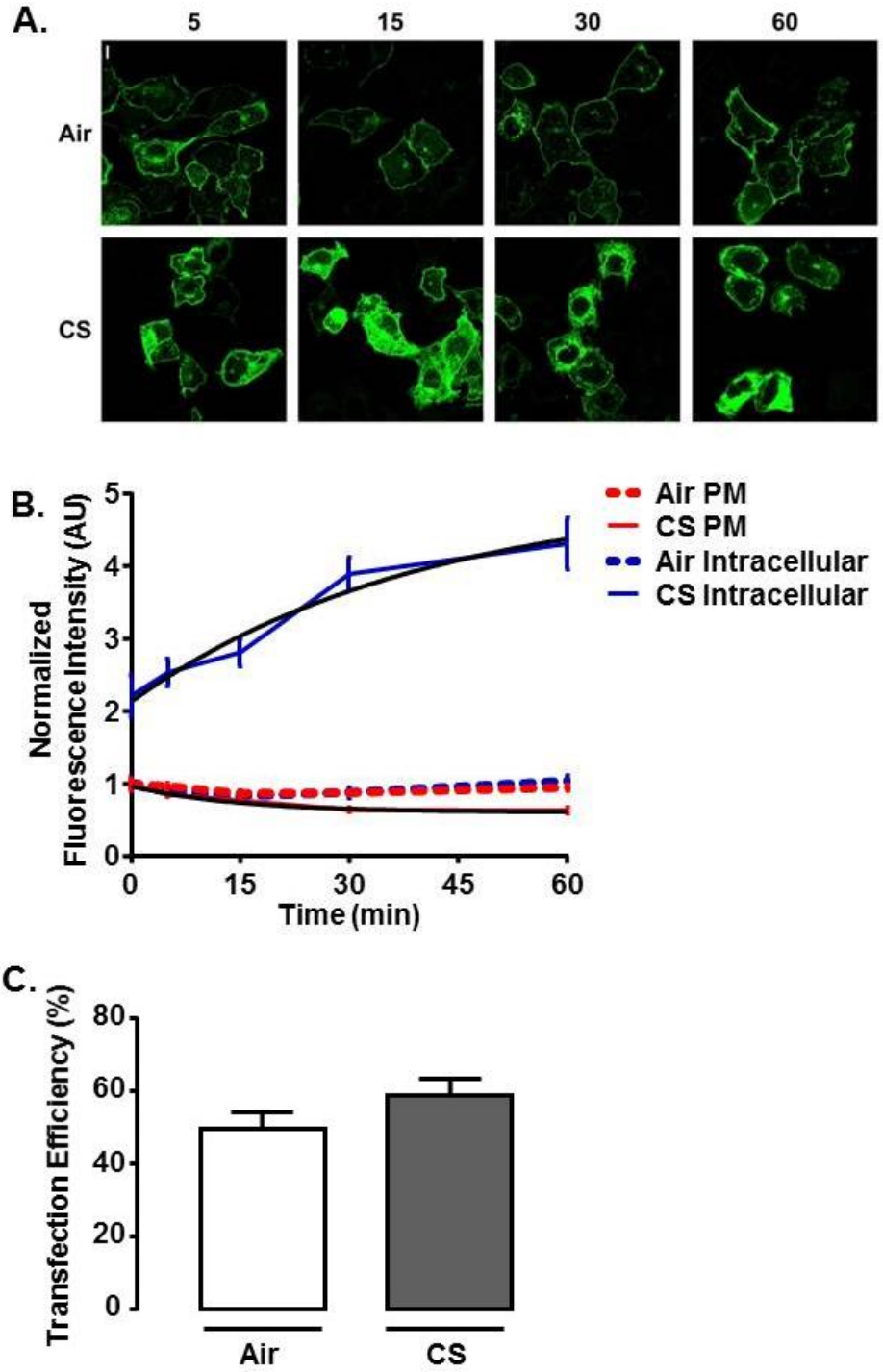

Figure 3-1. Cigarette smoke-internalized CFTR accumulates intracellularly with a half-life of ~27 min.

HEK293T cells transfected with GFP-CFTR were exposed to CS and incubated at 37°C for specified time durations prior to fixation using 4% paraformaldehyde. A) Representative confocal images of GFP-CFTR (green) following air or CS exposure at incubation times 5, 15, 30, and 60 min. B) Plasma membrane (PM; red) and intracellular (blue) fluorescence intensity over time of air (dashed lines) and CS (solid lines) exposed GFP-CFTR. Smoke exposed time points at the PM (r^2 = 0.094) and intracellularly (r^2 = 0.085) were fit with a single exponential (black line). n = 45 - 149 cells from four independent experiments. C) Percentage of cells in frame transfected with GFP-CFTR in air and CS exposed conditions. n = 26 – 30 images per condition. Scale bar = 10 µm.

3.2.2 CFTR dissociates upon internalization by cigarette smoke

CFTR can cluster into distinct microdomains with its interacting partners in the plasma membrane (Li and Naren, 2005). The formation of these microdomains allows CFTR molecules to accumulate in close proximity to one another, ensuring the tight regulation of CFTR and its binding partners. One technique to investigate the interaction of molecules within binding domains is Förster resonance energy transfer (FRET). FRET microscopy relies on the ability to capture fluorescent signals from the through-space interactions of labelled molecules (Sekar and Periasamy, 2003). This is based on the phenomenon that a donor fluorophore can become quenched by donating photons to an acceptor fluorophore, but only when the proximity between the two fluorophores is closer than 10 nm (100 Å). In acceptor-photobleaching FRET, the quenching of the donor is relieved when the acceptor fluorophore is photobleached, which can be measured as a change in apparent FRET efficiency (%).

To investigate CS-induced changes in CFTR-CFTR interactions, the apparent FRET efficiency of GFP-CFTR (donor fluorophore) and RFP-CFTR (acceptor fluorophore) were measured at the plasma membrane of HEK293T cells after smoke exposure and incubation at 37^{o}C for the previously defined time points (section 3.2.1). GFP- and RFP-CFTR were transiently transfected into HEK293T cells. 48 hours after transfection, both constructs expressed predominantly at the plasma membrane (Figure 3-2 A). Plasma membrane FRET levels 15, 30 and 60 min post-CS exposure (Figure 3-2 B; 15.0 ± 1.2%, 16.2 ± 1.5%, and 10.8 ± 1.4%, respectively; n = 33 - 42 cells) remained unchanged compared to plasma membrane FRET levels of air exposed at the same time points (17.4 ± 1.6%, 12.7 ± 1.1%, 12.3 ± 0.8%, respectively; n = 41 - 60 cells). As in previous experiments (Section 3.2.1), a large amount of CFTR accumulated in the perinuclear region of the cell following CS exposure (data not shown). However, upon measuring the apparent FRET efficiency of internal GFP-CFTR and RFP-CFTR post-CS exposure, the FRET efficiency measured at 15, 30, and 60 min (Figure 3-2 B; 4.8 ± 0.6%, 7.6 ± 1.3%, 5.1 ± 0.5%; $p < 0.001$, n = 31 - 53) was significantly lower than plasma membrane FRET efficiency in air and smoke exposed conditions as reported above. It is possible that the high levels of FRET at the plasma membrane in both air and CS exposed conditions may be due to an overcrowding effect due to the overexpression of both RFP- and GFP-CFTR. To test for this, the donor

fluorescence intensity was plotted against the percentage FRET efficiency for each condition (Figure 3-3). The correlation of donor intensity and FRET efficiency in plasma membrane FRET efficiency after both air and CS exposure is slightly negative with r values of -0.47 and -0.24 respectively. A positive correlative relationship would indicate overcrowding, suggesting that the higher the expression of the proteins, the higher the FRET value observed. However, since the values demonstrated here are not positive, the possibility that FRET is occurring due to overcrowding can be ruled out. Therefore, these data suggest that intracellular FRET efficiency is decreased compared to plasma membrane FRET efficiency, suggesting that CFTR may dissociate from its macromolecular complex following CS exposure.

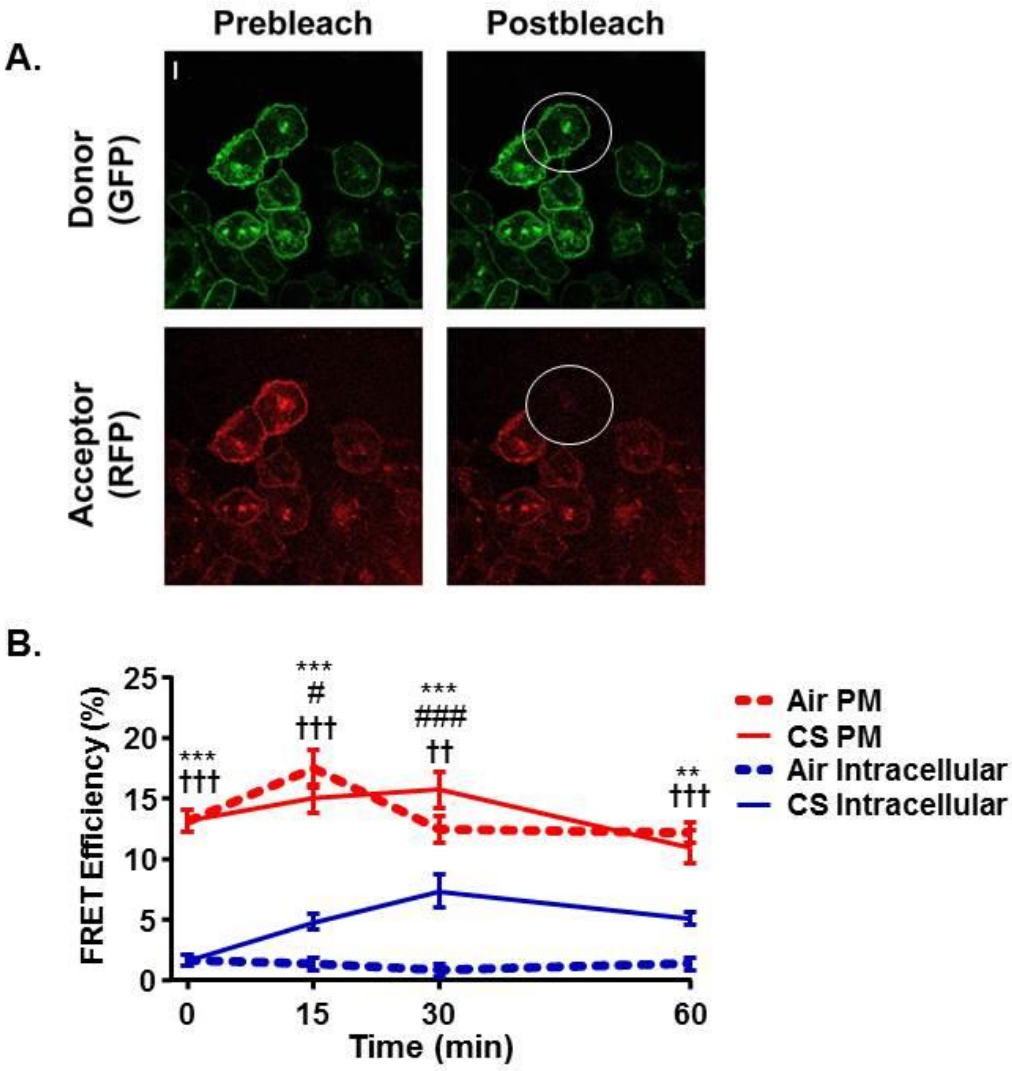

Figure 3-2. Cigarette smoke causes dissociation of CFTR-CFTR interactions.

HEK293T cells co-expressing GFP-CFTR and RFP-CFTR were incubated at 37°C for 0, 15, 30 or 60 min following smoke or air exposure prior to fixing in 4 % PFA. Acceptor photobleaching FRET was performed. (A) Typical confocal micrographs of GFP-CFTR (green) and RFP-CFTR (red) expressing air exposed cells before and after photobleaching of the acceptor fluorophore. (B) FRET efficiency of RFP-CFTR and GFP-CFTR measured at the PM (Red; Air = dashed line, CS = solid line) and intracellularly (Blue; Air = dashed line, CS = solid line) following air and CS exposure. *** = $p < 0.001$ of CS PM compared to CS intracellular, ** = $p < 0.001$ of CS PM compared to CS intracellular, # = $p < 0.05$ of air intracellular to CS intracellular, ### = $p < 0.001$ of air intracellular to CS intracellular, ††† = $p < 0.001$ of air PM to CS intracellular, †† = $p < 0.01$ of air PM to CS intracellular by two-way ANOVA with Sidak's multiple comparison test. All n = 31 - 60 cells from four independent experiments. Scale bar = 10 µm.

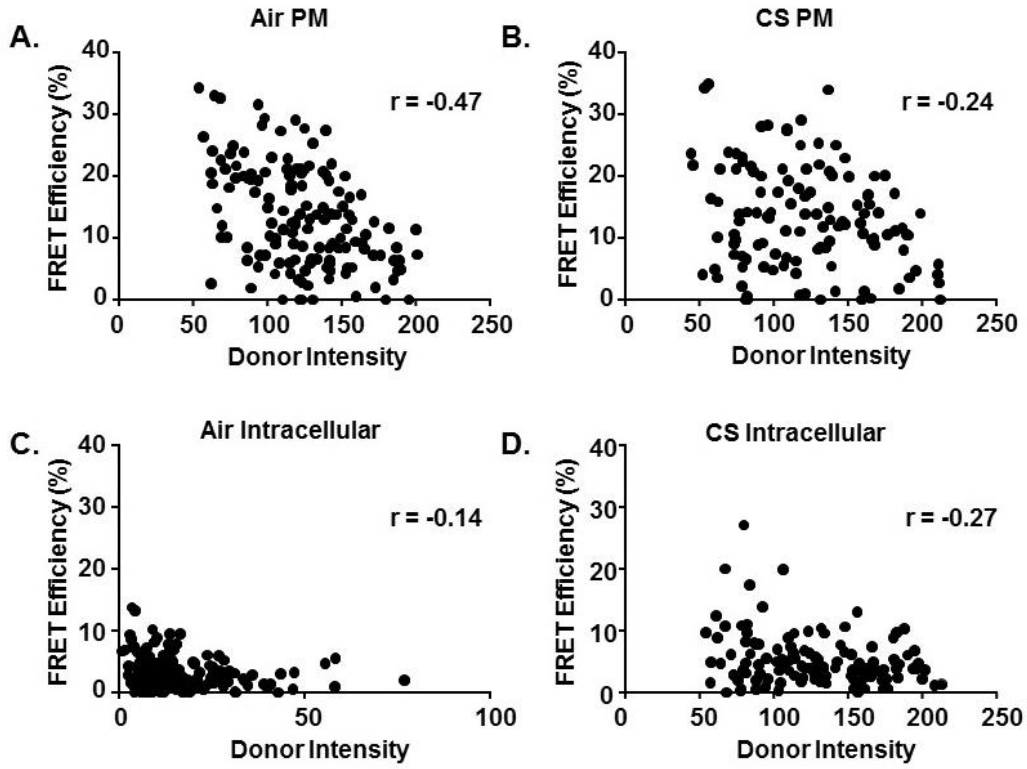

Figure 3-3. The dependence of FRET efficiency on donor intensity.

The FRET efficiency of donor (GFP) and acceptor (RFP) plotted in relation to donor fluorescence intensity after air exposure at the plasma membrane (A) and intracellularly (C) and after CS exposure at the plasma membrane (B) and intracellularly (D). Correlation relationships are indicated by the r value on each graph. Zero or negative correlation indicates that changes in FRET efficiency are not due to increased fluorescence intensity.

3.2.3 CS-induced internalization of CFTR occurs independent of nucleotide-binding domain 2 and the C-terminal endocytic motifs

The C-terminus of CFTR is host to a plethora of motifs important for CFTR regulation, including NBD2, C-terminal endocytic motifs, and the PDZ-binding motif. The PDZ-binding motif permits the interaction of CFTR to the actin cytoskeleton through NHERF1 and ezrin binding. In order to better understand the role of the actin cytoskeleton and CFTR-CFTR interactions, as well as the typical endocytic motifs of CFTR in CS-induced internalization, C-terminal truncation mutants of CFTR were constructed using site-directed mutagenesis. Premature stop codons were introduced to remove the PDZ-binding motif and the endocytic signals including tyrosine- and di-leucine-based motifs (GFP-CFTR-L1254X) and NBD2 (GFP-CFTR-K1174X). After 48 h of expression, both mutants localized to the plasma membrane in HEK293T cells (Figure 3-4 A). After CS exposure, intracellular fluorescence intensity increased in GFP-CFTR-L1254X and GFP-CFTR-K1174X expressing cells from 1.1 ± 0.1 to 2.5 ± 0.2 AU, and 1.2 ± 0.1 AU to 3.4 ± 0.3 AU, respectively ($p < 0.05$, $p < 0.01$, and $p < .001$, $n = 103$ -213). These values were similar to that of wt-GFP-CFTR, which increased from 1.0 ± 0.1 AU to 3.1 ± 0.3 AU following CS exposure, suggesting that removal of the C-terminal endocytic motifs or NBD2 had no effect on CS-induced internalization of CFTR.

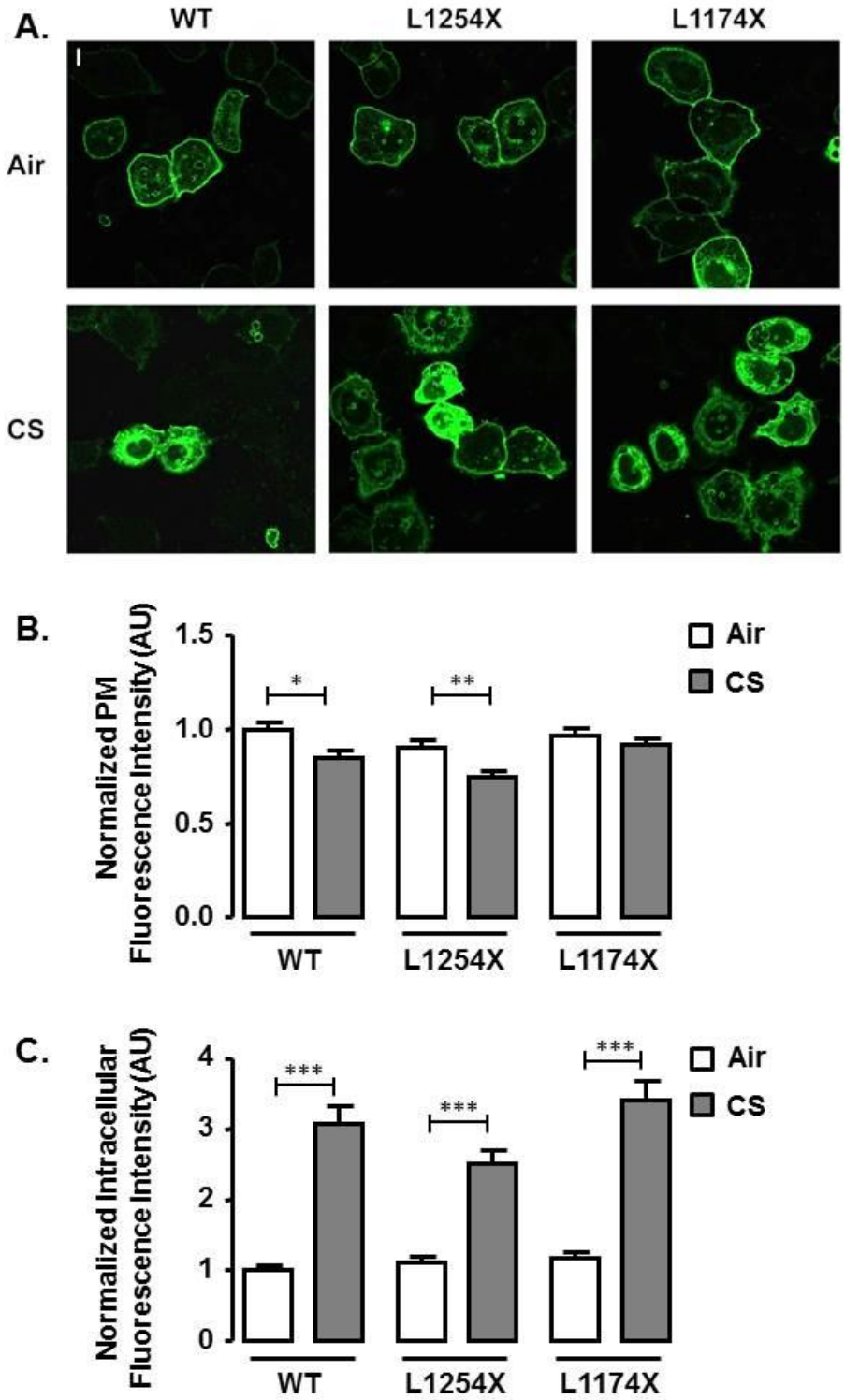

Figure 3-4. The C-terminus and NBD2 of CFTR are not required for CS-induced CFTR internalization.

HEK293T cells on a glass coverslip were transiently transfected with the above constructs and exposed to air or CS, 48 h after transfection. Cells were fixed in 4% PFA at room temperature for 5 min and imaged on a confocal microscope. (A) Representative images of HEK293T cells expressing wt-GFP-CFTR, GFP-CFTR-K1174X or GFP-CFTR-L1254X after air and CS exposure. (B) Mean PM fluorescence intensity in air (open bars) or CS (grey bars) of HEK293T cells transfected with WT-, L1254X-, or K1174X-CFTR. * $p < 0.05$, ** $p < 0.01$, *** $p < 0.001$ by Kruskal-Wallis test with Dunn's multiple comparison post-test, n = 103 – 213 cells from three independent experiments. (C) Mean intracellular fluorescence intensity in air (open bars) or CS (grey bars) of HEK293T cells transfected with WT-, L1254X-, or K1174X-CFTR, * $p < 0.05$, ** $p < 0.01$, *** $p < 0.001$ by Kruskal-Wallis test with Dunn's multiple comparison post-test, n = 103 - 213 cells from three independent experiments. Scale bar = 10 µm.

3.2.4 The effects of cigarette smoke on other membrane proteins

Thus far, we have determined that C-terminal motifs including NBD2, endocytic domains, as well the PDZ domain of CFTR are not required for CS-induced internalization, and that CFTR-CFTR interactions dissociate following internalization by CS. For further investigation into the mechanisms behind CS-induced internalization, it is important to understand whether this phenomenon is specific to CFTR, or whether other ion channels or membrane proteins have an abnormal response to smoke.

Another ion channel responsible for mediating correct hydration of the ASL is Ano1 (Section 1.3). Evidence provided by knockout mice have shown that Ano1 has a distinctive role in the mediation of ASL and further to this, the CaCC has shown to have a minor yet important role in Cl^- transport CF airway epithelia (Knowles et al., 1991, Mason et al., 1991, Stutts et al., 1992, Namkung et al., 2011). Despite the reported role of CaCC in the regulation of Cl^- secretion, observations in HBECs suggest that CS can alter the transepithelial electric potential difference in response to adenosine but not adenosine triphosphate (ATP) (Clunes et al., 2012). These data suggest that CS has a direct effect on the adenosine-mediated Cl^- secretion by CFTR, rather than ATP-mediated Cl^- secretion by CaCC. To investigate the effects of CS on Ano1 more directly, HEK293T cells co-transfected with GFP-CFTR and Ano1-mCherry were exposed to air or CS and incubated at 37^{o}C for 60 min. Consistent with previous data, GFP-CFTR showed significant internal accumulation following CS exposure (4.0 ± 0.3 AU, $p<0.001$, n=174 cells) compared to air control (Figure 3-5 C; 1.0 ± 0.1 AU, n = 194 cells). However, no change in Ano1-mCherry PM fluorescence intensity was seen following air (1.0 ± 0.0 AU) or CS exposure (Figure 3-5 B; 1.1 ± 0.0 AU, n = 212 cells), and no change in Ano1-mCherry intracellular fluorescence intensity was seen in air (1.0 ± 0.1 AU) or CS exposed conditions (1.1 ± 0.1 AU, n = 162 - 212 cells). As no change in the plasma membrane or intracellular fluorescence intensity of Ano1 was observed following smoke exposure, these data suggest that the plasma membrane levels of Ano1 are not affected by smoke.

In addition to internalization studies, acceptor photobleaching FRET efficiency was measured in cells expressing Ano1-GFP and Ano1-mCherry (Figure 3-6). Consistent with previous studies showing that CaCC secretion is not affected by CS, no change in Ano1-GFP - Ano1-mCherry PM FRET levels were measured after

CS exposure at all time points (Figure 3-6; baseline FRET was measured at 17.3 ± 1.2%, n = 32).

Another ion channel present in the airway epithelia is the calcium release-activated calcium channel, Orai1. Store operated calcium entry was unaffected by CS exposure (Rasmussen et al., 2014). However, here, when HEK29T cells expressing Orai1-YFP, were exposed to CS, and incubated for 15 min at 37^{o}C, Orai1-YFP plasma membrane fluorescence intensity decreased from 1.0 ± 0.02 to 0.7 ± 0.02 AU (Figure 3-8 A; $p < 0.001$, n = 125 – 145 cells), and intracellular fluorescence intensity increased from 1.0 ± 0.1 AU to 3.9 ± 0.4 AU ($p < 0.001$, n = 125 - 145). After a longer incubation period of 60 min, Orai1-YFP plasma membrane fluorescence again decreased from 0.9 ± 0.0 to 0.7 ± 0.1 AU and intracellular fluorescence intensity further increased from 1.1 ± 0.1 to 5.6 ± 0.7 AU ($p < 0.001$, n = 54 - 137 cells) indicating that Orai1 internalizes in a similar fashion to CFTR. However, in contrast to data published by Rasmussen *et al*. (2014) demonstrating that cell number did not decrease following CS exposure, here, in Figure 3-8 C, the fluorescence intensity of propidium iodide stained Orai1 transfected cultures decreased from 1.0 ± 0.1 AU (n = 9 wells) to 0.6 ± 0.1 AU ($p < 0.01$, n = 9 wells) following CS exposure. The data suggest that the over-expression of Orai1 may cause different effects to CS compared to cells over-expressed with CFTR.

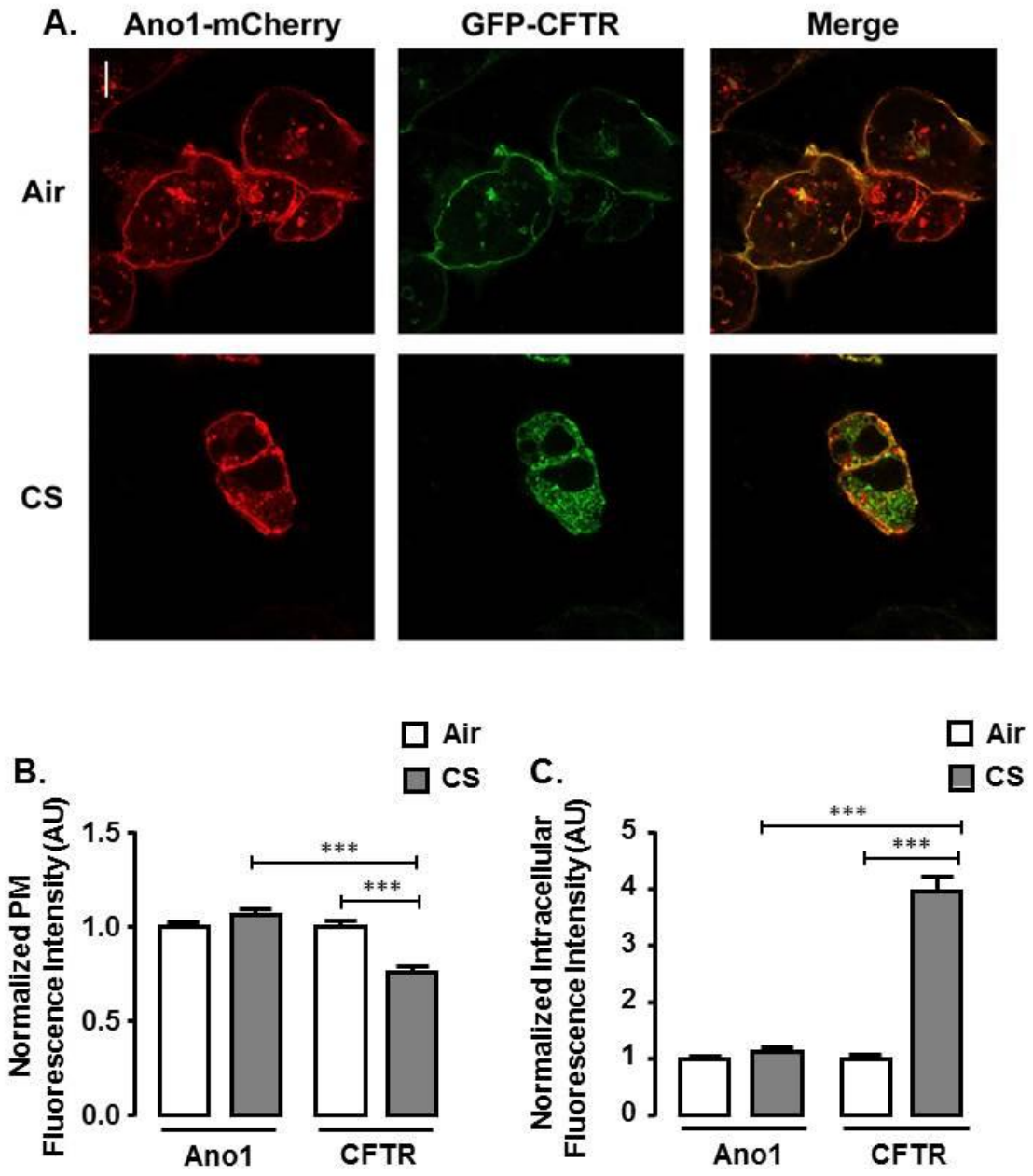

Figure 3-5. Cellular location of Ano1 is not affected by CS.

HEK293T cells co-transfected with Ano1-mCherry and GFP-CFTR were exposed to smoke and incubated at 37°C for 60 min before fixation. (A) Representative confocal micrographs of Ano1-mCherry (red) and GFP-CFTR (green) transfected cells following air and CS exposure. (B) Mean plasma membrane fluorescence intensity of Ano1-mCherry and GFP-CFTR following air (open bars) and CS (grey bars) exposure, normalized to air control for each construct. (C) Mean intracellular fluorescence intensity of GFP-CFTR and Ano1-mCherry after air (open bars) and CS (grey bars) normalized to air control for each construct, *** $p > 0.001$ by Kruskal-Wallis test with Dunn's multiple comparison post-test, n = 162 - 212 cells from four independent experiments. Scale bar = 10 µm.

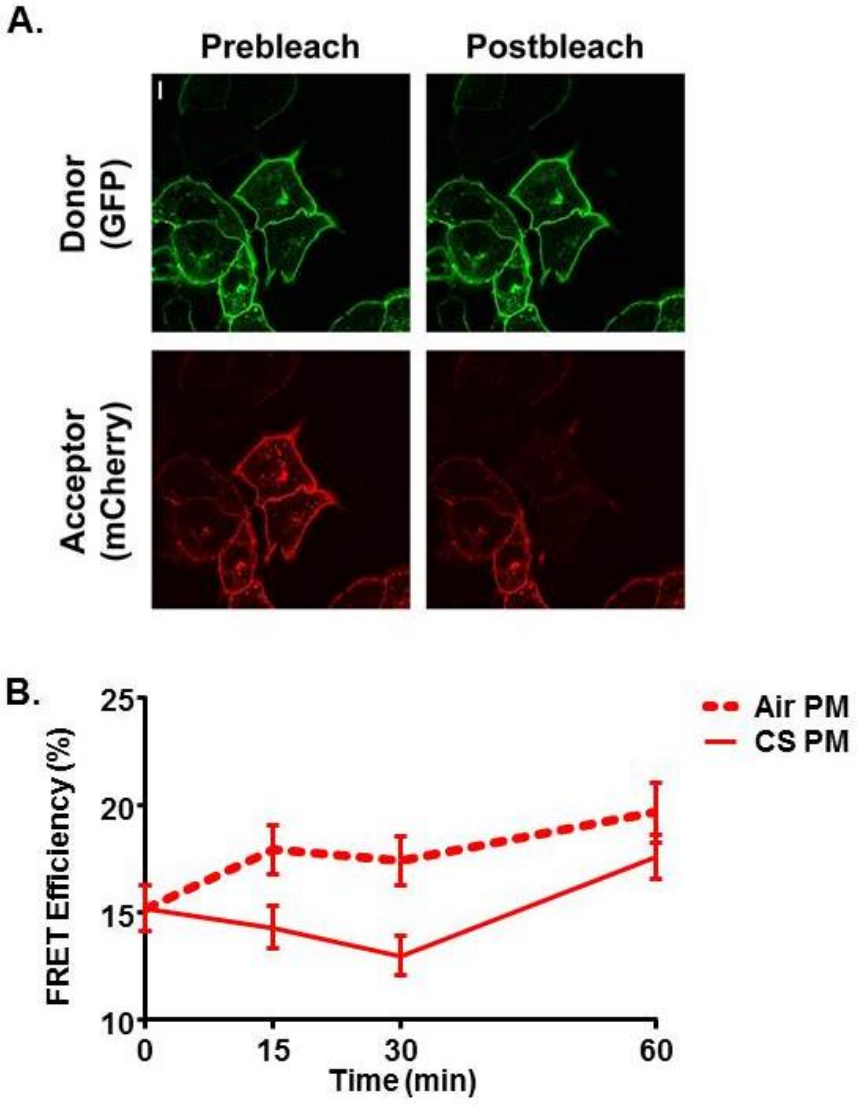

Figure 3-6. Cigarette smoke exposure shows no effect on FRET efficiency of Ano1-GFP and Ano1-mCherry.

HEK293T cells co-expressing Ano1-mCherry and Ano1-GFP were incubated at 37°C for 0, 15, 30 or 60 min following CS or air exposure prior to fixing in 4% PFA. Acceptor photobleaching FRET was performed. (A) Typical confocal micrographs of Ano1-GFP (green) and Ano1-mCherry (red) expressing cells before and after photobleaching of the acceptor fluorophore. (B) Apparent FRET efficiency of Ano1-mCherry and Ano1-GFP measured at the plasma membrane (closed, open and grey bars) following air (open bars) and CS (closed bars). n= 39 - 45 cells from 3 independent experiments. No significant difference of FRET efficiency between air and smoke exposed cultures at all time points. Two-way ANOVA with Tukey's multiple comparison post-test. Scale bar = 10 µm.

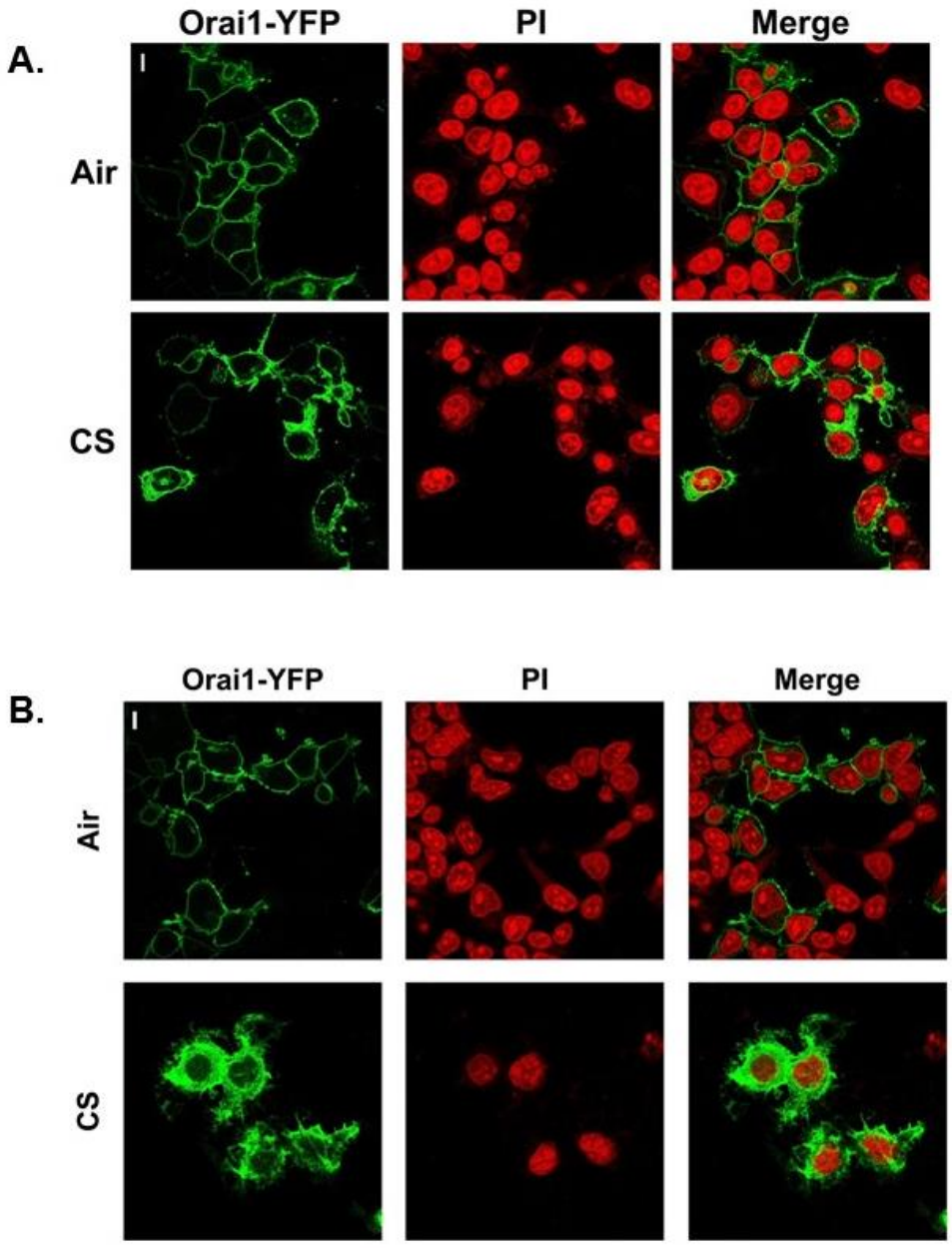

Figure 3-7. Cigarette smoke causes intracellular accumulation of Orai1.

HEK293T cells expressed with Orai1-YFP exposed to air or CS were incubated for 15 or 60 min at 37°C prior to fixation with 4% paraformaldehyde. Cells were stained post-fixation with propidium iodide (red). (A) Representative images of Orai1-YFP (green) and nuclei (red) following air or smoke exposure and 15 min incubation. (B) Representative images of Orai1-YFP and nuclei following air or smoke exposure and 60 min incubation. Scale bar = 10 µm.

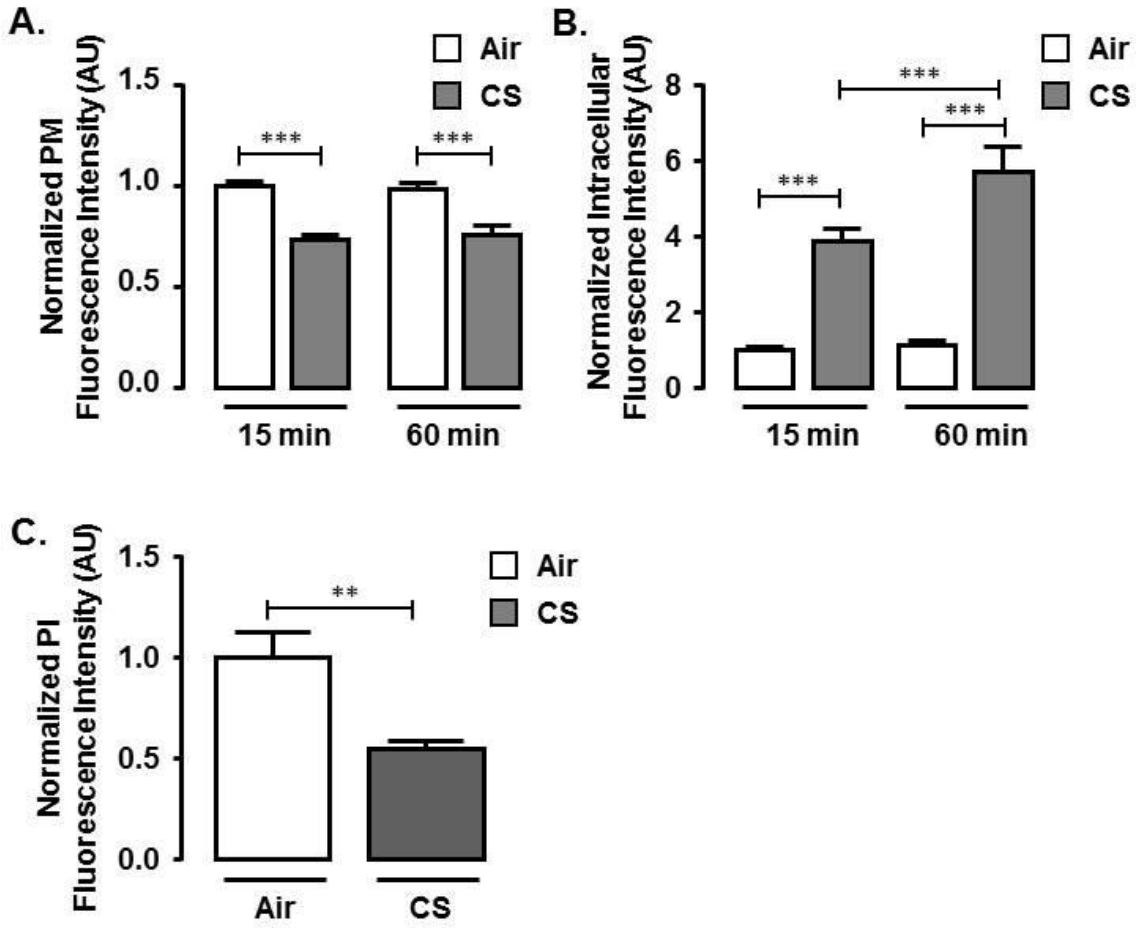

Figure 3-8. Cigarette smoke causes intracellular accumulation of Orai1.

HEK293T cells expressed with Orai1-YFP exposed to air or CS were incubated for 15 or 60 min at 37°C prior to fixation with 4% paraformaldehyde. Cells were stained post-fixation with propidium iodide (red). (A) Mean plasma membrane fluorescence intensity of Orai-1 YFP following 15 min air (open bars) and CS (grey bars) exposure, normalized to air control for each construct. (B) Mean intracellular fluorescence intensity of Orai1 following 60 min air (open bars) or CS exposure (grey bars) normalized to air control for each construct. *** $p > 0.001$ Kruskal-Wallis test with Dunn's multiple comparison test, n =162 - 212 cells from four independent experiments. (C) Propidium iodide fluorescence intensity of cultures incubated with smoke or air was taken using a plate reader (Tecan), as an estimate of total cell number. ** $p < 0.01$ by Student's t test, n = 9 wells per condition from 3 independent experiments.

3.3 Discussion

Diminished CFTR function following CS exposure has now been well documented, and has been attributed to internalization of CFTR as evidenced by surface labelling (Rasmussen et al., 2014). To investigate the dynamics of CS-induced CFTR internalization, in this chapter, we have developed a protocol to assess the temporal profile of CFTR internalization following smoke exposure. Furthermore, this protocol has been adapted to characterize CS-induced CFTR internalization by FRET and the internalization of other plasma membrane proteins. Thus, we have demonstrated that CFTR dissociates from its macromolecular complex following CS exposure, and that CS-induced CFTR internalization is independent of C-terminal endocytic motifs. Moreover, use of the internalization assay to investigate other membrane proteins revealed a similar response of Orai1 to CS exposure.

Rasmussen *et al.* (Rasmussen et al., 2014) used surface labelling of HA-tagged CFTR to assess internalization, however this technique requires a multistep protocol. The use of fluorescently tagged proteins allows the cells to be imaged directly after fixing, and reduces the protocol time by a number of days. Although surface labelling allows the tracking of the movement of CFTR from the plasma membrane into the cell, the technique used in this assay provides a broader analysis of internalization by intracellular accumulation. During the internalization assay, CFTR significantly accumulated intracellularly over time. Although GFP-CFTR plasma membrane fluorescence intensity decreased steadily over time, the amount of GFP-CFTR reduction at the plasma membrane was far lower than the amount of intracellular accumulation, and the half-life for the removal of CFTR from the plasma membrane (10.5) was much faster than that of the half-life for CFTR to accumulate inside the cells (27.7 min). There are two main hypotheses for the reduced removal of CFTR from the plasma membrane following CS exposure. Firstly, the delivery of nascent or recycled CFTR to the plasma membrane may have increased the plasma membrane signal. Secondly, the close proximity of the ER, a potential destination for CS-internalized CFTR (see chapter 5.0), to the plasma membrane may result in plasma membrane fluorescence being intensified by that of ER fluorescence. Despite this limitation, intracellular GFP-CFTR consistently increased following CS exposure much like that seen by Rasmussen *et al.* therefore providing a quantifiable signal for measuring the effects of CS on the cellular localization of CFTR.

CFTR takes part in a variety of physical and functional interactions with different proteins including ion channels, transporters, kinases, phosphatases, cytoskeletal components and signaling factors (Li and Naren, 2005). Evidence suggests that CFTR and its interacting proteins are confined to specific microdomains in the plasma membrane. The compartmentalization of interacting proteins into macromolecular complexes allows for tight regulation of CFTR trafficking and activity, as well as the ability of CFTR to regulate other signaling pathways such as inflammation (Dudez et al., 2008). These macromolecular complexes not only function to bring CFTR in close proximity to a matrix of proteins including actin, NHERF1, and ezrin but also to bring CFTR molecules within close proximity to one another (Li, 2005). FRET, a tool to measure the proximity of proteins, functions as a molecular ruler, allowing the determination of distances between molecules based on the ability of the fluorophore to share photons with one another. Here, FRET efficiency of N-terminally tagged GFP-CFTR and RFP-CFTR was determined in HEK293T cells. Despite the previous report of no appreciable FRET efficiency between N- or C-terminally tagged CFP-CFTR and EYFP-CFTR (Berdiev, 2008), in air conditions membrane GFP-CFTR and RFP-CFTR FRET efficiency was between 12.3 and 17.4%. The presence of different fluorescent tags may be responsible for the discrepancy between the reports of CFTR-CFTR FRET efficiency. Following CS exposure, membrane GFP-CFTR and RFP-CFTR FRET efficiency was unaffected, however, cytosolic CFTR-CFTR FRET efficiency was reduced compared to that of plasma membrane FRET efficiency air and smoke exposed samples. This data suggests that CFTR molecules become further apart upon internalization. In basal conditions, CFTR dissociates from NHERF1 within its microdomain, allowing the AP-2-clathrin complex to interact and leading to endocytosis of CFTR. It is reasonable to assume that the increased distance between the CFTR molecules is due to dissociation from its microdomain to allow the entry of endocytic machinery (Guggino and Stanton, 2006). However, the use of an agonist of endocytosis would give a clearer understanding of whether this phenomenon is specifically due to CS-induced internalization, or whether it is a feature of CFTR endocytosis in general.

The role of actin in CS-induced CFTR internalization was further therefore investigated by the removal of the PDZ-binding motif, a region of CFTR that facilitates the interaction of CFTR with the actin cytoskeleton. The introduction of a stop codon at leucine 1254 produced a mutant of CFTR with the PDZ-binding motif removed. L1254X CFTR maintained normal levels of internalization following CS exposure, suggesting that the interaction of CFTR with the actin cytoskeleton is not

required for CS-induced internalization of CFTR. Furthermore, the C-terminus of CFTR is predominantly involved in the regulation of normal CFTR endocytosis. The L1174X CFTR mutant also had crucial endocytic motifs, including the tyrosine- and di-leucine based motifs, removed. Despite the necessity of the tyrosine and di-leucine based motifs in normal endocytosis, these are not required for CS-induced CFTR endocytosis, suggesting that the mechanism of internalization by CS may be different from that of normal endocytosis. In addition to the C-terminal endocytic motifs of CFTR, NBDs have been implicated in maintaining the stability of CFTR at the plasma membrane (Cheng et al., 1990) Additional removal of NBD2 by the introduction of a stop codon at lysine 1174 had no effect on CS-induced CFTR internalization, suggesting that this domain is not necessary for CS-induced internalization.

Having confirmed that the C-terminus of CFTR is not required for CS-induced internalization, other proteins were investigated to determine their response to CS exposure. CS caused reduction in ASL height, which has been attributed to internalization of CFTR from the plasma membrane. UTP-stimulated nasal PD was not affected by CS (Clunes et al., 2012), further to this CS has no effect on the cellular location of Ano1 at 5, 15, 30 or 60 min. Plasma membrane FRET efficiency of Ano1-mCherry and Ano1-GFP was not affected in air or CS conditions, confirming that CS has no effect on the cellular localization of Ano1. It is possible that much like in CF; CaCC activity provides a compensatory mechanism for chloride secretion in the absence of plasma membrane CFTR (Ousingsawat et al., 2009, Rock et al., 2009)

In native conditions Orai1 is activated by STIM1, an ER localized calcium sensor, following its aggregation induced by calcium store depletion. STIM1 aggregation is unaffected by CS exposure (Rasmussen et al., 2014). In native conditions, Orai1 interacts with CFTR in a macromolecular complex, and the absence of CFTR leads to increased SOCE (Balghi et al., 2011). Despite this, previous research has shown that SOCE mediated by Orai1 is not responsible for increases in intracellular calcium observed during smoke exposure (Rasmussen et al., 2014). Furthermore, we have observed a rapid accumulation of Orai1 in the cytosol following CS exposure. A possible explanation for the CS-induced internalization of Orai1 observed in Section 3.2.4 is that internalization of Orai1 functions to balance changes in SOCE caused by CFTR removal from the membrane by CS. However, since these cells do not endogenously express CFTR, it is more likely that Orai1 internalizes in response to increases in cytosolic calcium.

As such, Orai1 plasma membrane residence and activity is highly sensitive to intracellular Ca^{2+}. For example, as previously mentioned, SOCE by Orai1 is stimulated by the depletion of Ca^{2+} by endoplasmic reticulum stores and interaction with STIM1. Furthermore, increases in intracellular calcium stimulate the recruitment of protein kinase C (PKC) β1 to the plasma membrane. PKCβ1 causes downregulation of SOCE by Orai1 through phosphorylation of the N-terminal sites, S527 and S30, of Orai1 (Hooper et al., 2015, Kawasaki et al., 2010). As CS exposure leads to dephosphorylation of CFTR at a PKA sensitive site (see section 4.2.5), a literature review to reveal putative sites of phosphorylation was performed. Indeed, western blotting and co-immunoprecipitation of Orai1 with antibodies against both Orai1, and the phosphorylated consensus site RRXpS/T confirmed the presence of a putative site of PKA phosphorylation in this channel (Howe, 2011). Thus, investigation of the effects of CS on this site of phosphorylation would be extremely useful in determining whether Orai1 and CFTR are internalized by CS by a similar mechanism. In contrast to Orai1 and CFTR, Ano1 remained at the plasma membrane following smoke exposure. Ano1 is regulated by Ca^{2+}/calmodulin dependent kinase II (Ho et al., 2001, Xie et al., 1996), and although its structure contains putative sites of phosphorylation by PKC, a range of inhibitors against PKC and PKA had no effect on Ano1-mediated chloride section (Tian et al., 2011). Thus, the lack of this site may provide an explanation for the lack of response of the channel to CS.

The major findings of this chapter are summarized below:

- CS causes rapid internalization of CFTR, with intracellular accumulation of CFTR occurring with a half-life of 27.7 min.

- CFTR-CFTR interactions dissociate following internalization by CS exposure.

- C-terminal endocytic motifs of CFTR are not required for CS-induced internalization, suggesting that C-terminal endocytic.

- CS causes internalization of CFTR and Orai1, but not Ano1.

4.0 Cigarette smoke exposure causes dephosphorylation of CFTR leading to its internalization

4.1 Introduction

Despite clear evidence that CS causes rapid internalization of CFTR, little is known about the cell signalling pathways that initiate this phenomenon. Our lab has shown that CS-induced CFTR internalization is dependent on the release of Ca^{2+} from lysosomes following CS exposure (Rasmussen et al., 2014), but whether Ca^{2+} directly stimulates CFTR internalization, or works through downstream signalling pathways remains to be seen.

Historically, CFTR has been considered a cAMP-mediated chloride channel which cannot be activated by calcium (Evans and Marty, 1986). However, more recently it has become known that CFTR may additionally be regulated by Ca^{2+}. For example, cholinergic stimuli which mediate Ca^{2+} release from the endoplasmic reticulum cause activation of CFTR in BHK cells expressing the muscarinic receptor M3R (Billet et al., 2013). This response is partially due to the Ca^{2+}-sensitive activation of adenylyl cyclase, which leads to phosphorylation and activation of CFTR by PKA. Some CFTR activity remained upon inhibition of PKA, indicating that Ca^{2+} stimulation of CFTR must additionally occur by an alternative mechanism. One proposed pathway suggests that Ca^{2+} causes upregulation of Src, a proto-oncogene tyrosine kinase, which prevents dephosphorylation and deactivation of CFTR by inhibiting protein phosphatase (PP) 2A (Billet and Hanrahan, 2013). Furthermore, a more direct effect of Ca^{2+}-loaded calmoduliin on CFTR has been reported in abstract form (Bozoky et al., 2015).

It is therefore important to consider which Ca^{2+}-mediated down stream effectors are responsible for the Ca^{2+}-sensitive internalization of CFTR by CS. Researchers have shown that CS stimulates mitogen-activated protein kinase (MAPK) pathways including the mitogen-activated protein kinase kinase/extracellular signal-regulated kinase (MEK/ERK1/2) pathway (Mercer and D'Armiento, 2006). The MAPK pathway is a potent regulator of cell survival and proliferation (McCubrey et al., 2007). Furthermore, MEK/ERK can regulate the expression of ENaC through the interaction of E3 ubiquitin ligase Nedd4-2, resulting in the degradation of ENaC (Falin and Cotton, 2007, Booth and Stockand, 2003). The MEK/ERK1/2 pathway has been implicated in the upregulation of CFTR through INFɣ (Kulka et al., 2005). More recently, the Cormet-Boyaka group have demonstrated using CS extract that

the inhibition of MEK/ERK reduces CS-induced CFTR internalization, suggesting that CS-induced internalization is MAPK-dependent (Xu et al., 2015).

The hypothesis that cytosolic kinases may regulate CFTR is not a new one. Hormonal stimulation of the airway epithelium activates CFTR through an increase in cytosolic cAMP. This increase in cAMP levels causes activation of the serine threonine kinase, protein kinase A (PKA) (Taylor et al., 1990). The coding sequence of CFTR contains many consensus sequences for PKA phosphorylation, many of which are located in the R domain (Figure 4-5). The phosphorylation of CFTR by PKA increases the affinity of CFTR to bind ATP, increases the channel bursting rate and increases the open probability of CFTR (Cheng et al., 1991). As well as PKA, a number of different kinases activate, inhibit or have a dual effect on CFTR including PKC (Li et al., 2007), casein kinase 2 (CK2) (Treharne et al., 2009), and Src (Billet et al., 2013). PKC, another serine threonine kinase, increases the magnitude of the PKA response (Jia et al., 1997, Liedtke and Cole, 1998, Middleton and Harvey, 1998, Tabcharani et al., 1991). CK2 regulates CFTR processing and membrane trafficking (Luz et al., 2011). Src kinase, a tyrosine kinase, activates CFTR by direct phosphorylation and indirectly by inhibiting PP2A (Billet et al., 2013). Many of the kinases that regulate CFTR have been shown to be located in macromolecular complexes with CFTR (Luo et al., 1998).

Several phosphatases regulate CFTR; serine and threonine phosphatases have two distinct functional classes, protein phosphatase (PP) 1 and PP2, and the latter class itself is categorised into three groups PP2A, PP2B and PP2C. All three classes of PP2 phosphatases interact with CFTR. PP2A can physically associate with CFTR via its C-terminus (1451-1476), leading to rundown of CFTR channel activity (Thelin et al., 2005). Not only does PP2A directly regulate CFTR, it may also lead to important signalling events by other proteins that regulate CFTR. For example, AMP-activated protein kinase (AMPK) directly interacts with both PP2A and CFTR and down regulates CFTR activity via residues 1420-1457 (Hallows et al., 2000). PP2B (otherwise known as calcineurin) is Ca^{2+}-dependent., and inhibition of PP2B with cyclosporin A and deltamethrin activates CFTR in cell-attached patch clamp studies (Fischer et al., 1998). CFTR and PP2C co-immunoprecipitate, and PP2C can co-purify with his-tagged CFTR using nickel affinity chromatography (Zhu et al., 1999), suggesting that CFTR and PP2C form a stable regulatory complex.

Investigation into the relationship of CS-induced calcium signalling and the role of the MAPK pathway will provide useful insights into the effects of CS on CFTR. Thus, the aims of this chapter were to:

1) Determine the relationship between calcium signalling and MAPK regulation of CS-induced CFTR internalization.
2) Understand the effects of CS on the phosphorylation state of CFTR.
3) Determine which consensus sites of phosphorylation are important for CS-induced CFTR internalization.

4.2 Results

4.2.1 CS-induced internalization of CFTR is dependent on MEK signalling

Activation of the MEK/ERK pathway is required for CS extract to internalize CFTR. (Xu et al., 2015). However, bathing cultures in CS extract has been shown to stimulate a number of abnormal responses compared to cells exposed to fresh CS. The method for fresh CS exposure developed by Phillips *et al.* (2005) and used in this thesis is an established technique for the delivery of CS *in vitro*, which provides a similar volume and rate of smoke intake to that of human smokers. Therefore, to confirm the effects of MAPK inhibitors on the response of CFTR to gaseous CS U0126, an inhibitor of MEK, was used. HEK293T cells transiently transfected with GFP-CFTR were exposed to either air or CS (see methods section 2.6) in the presence of vehicle (0.001 % DMSO) or 10 µM U0126 (Figure 4-1 A). In the presence of vehicle (Figure 4-1 B), plasma membrane fluorescence intensity significantly decreased from 1.0 ± 0.0 AU after air/vehicle exposure to 0.7 ± 0.04 AU following CS/vehicle exposure (Figure 4-1 B; $p < 0.001$, n = 100 - 129 cells). Intracellular GFP-CFTR fluorescence intensity significantly increased from 1.0 ± 0.1 AU after air/vehicle exposure to 4.9 ± 0.3 AU following CS/vehicle exposure (Figure 4-1 C, n = 100 – 129 cells). However, in Figure 4-1 C, in the presence of U0126, the intracellular accumulation of CFTR by CS was significantly reduced by U0126 from 4.9 ± 0.3 AU in CS/vehicle treated cells, to 1.3 ± 0.2 AU in CS/U0126 treated cells, consistent with data using CS extract from the Cormet-Boyaka group (Xu et al., 2015). However, a small but significant increase was measured in intracellular fluorescence intensity in CS/U0126 treated cells (1.3 ± 0.2 AU, n = 106 cells) compared to air/U0126 treated cells ($p < 0.001$, 0.8 ± 0.1 AU, n = 106 cells). However, the intracellular fluorescence intensity of CS/U0126 exposed cells was not significantly different from that of air/vehicle treated cells (1.0 ± 0.1 AU, n = 129 cells). These data indicate that treatment with U0126 prevented CS-induced GFP-CFTR internalization, confirming that MEK is an important regulator of CS-induced CFTR internalization.

Since the CS-induced internalization of CFTR is dependent on both MEK activation and the release of lysosomal calcium, it was important to determine whether the two signalling pathways interact. To this end, we investigated the effect of MEK inhibitor U0126 on CS-induced calcium release in fura-2 loaded HEK293T cells (Figure 4-2). Following CS smoke exposure in vehicle treated cells, the mean

change in intracellular $[Ca^{2+}]_i$ trended towards an increase in $[Ca^{2+}]_i$ which was sustained over time, but was not significantly different from that of air/vehicle treated cultures (n = 3 coverslip). CS exposed cells treated with U0126 exhibited a similar profile to that of vehicle/CS treated cells, suggesting that inhibition of U0126 may not affect CS-induced Ca^{2+} release, but again the trend in increase of U0126/CS treated cells was not significantly different from U0126/air treated cells. Thus, increasing the number of cultures measured may reduce variability, and further clarify the effect of U0126 on CS-induced Ca^{2+} release.

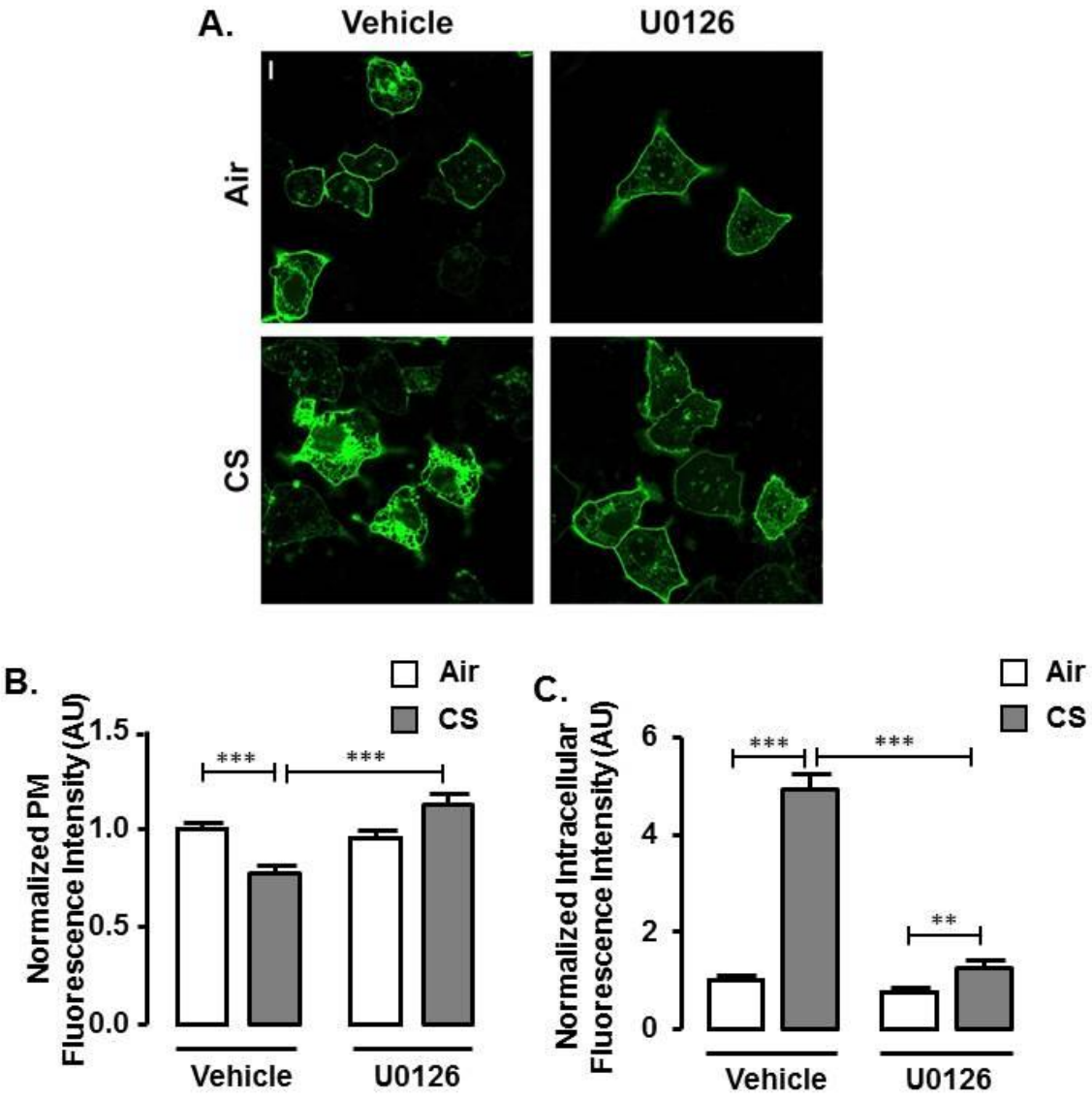

Figure 4-1. Exposure to the MEK inhibitor, U0126, inhibits CS-induced CFTR internalization.

HEK293T cells transiently transfected with GFP-CFTR were pre-treated for 30 min with vehicle (0.01% DMSO) or 10 µM U0126 prior to exposure to air or CS exposure. Following exposure, cells were incubated at 37°C for 60 min before fixation with 4% PFA. (A) Representative confocal images of GFP-CFTR in all conditions. (B) Mean plasma membrane fluorescence intensity in air (open bars) or CS (grey bars) of cells treated with vehicle or 10 µM U0126. (C) Mean intracellular fluorescence intensity in air (open bars) or CS (grey bars) of cells treated with vehicle or 10 µM U0126, *** $p < 0.001$ by Kruskal-Wallis test with Dunn's multiple comparison post-test. n = 106 - 120 cells from 3 independent experiments. Scale bar = 10 µm.

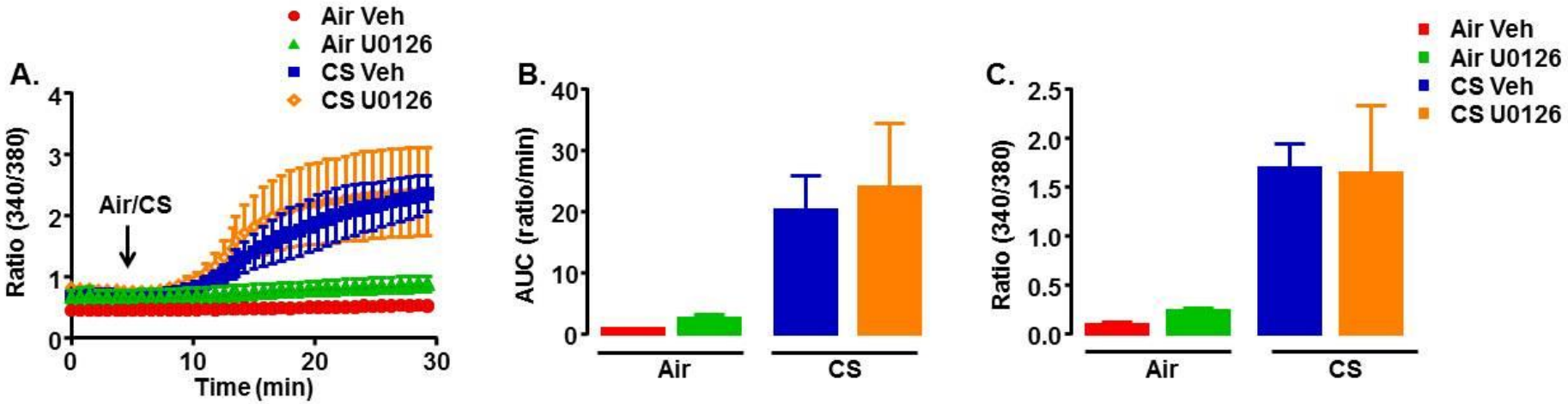

Figure 4-2. U0126 does not affect CS-induced Ca^{2+} release.

HEK293T cells were loaded with 5 µM Fura-2, AM and exposed to air or CS. (A) Mean change in intracellular [Ca^{2+}], in response to air or CS, in cultures treated with vehicle (0.01% DMSO) or 10 µM U0126. Mean change in area under the curve (B; AUC). And (C) maximum change in fluorescence ratio in air and CS exposed conditions following treatment of vehicle or U0126. n = 3 coverslips from 2 independent experiments.

4.2.2 The epidermal growth factor receptor regulates plasma membrane expression of CFTR

The epidermal growth factor receptor (EGFR), an upstream regulator of the MAPK pathway, is endogenously expressed in low levels in HEK293T cells (Maegawa et al., 2009). Activation of EGFR by the binding of EGF leads to autophosphorylation of the receptors C-terminus. Phosphorylation at this site allows the downstream binding of docking proteins such as growth factor receptor bound protein 2 (GRB2) and son of sevenless (SOS). SOS promotes the binding of Ras to GTP, allowing its interaction with RAF, and subsequent activation of MEK (Ullrich and Schlessinger, 1990). Unlike MEK/ERK, EGFR has no reported effects on the activity or trafficking of CFTR. Therefore, the effects of AG1478 an EGFR antagonist on the cellular location of CFTR in both control and CS conditions were investigated. Inhibition of EGFR with AG1478 significantly increased the amount of GFP-CFTR at the plasma membrane in air control conditions (Figure 4-3 A and B; 1.1 ± 0.1 AU, n = 117 cells) compared to vehicle ($p < 0.01$, 1.0 ± 0.0 AU, n = 101 cells). These data suggest that EGFR may play a role in CFTR plasma membrane trafficking and surface density. Consistent with data demonstrating that CS can cause resistance of EGFR to AG1478 (Filosto et al., 2012), following CS exposure (Figure 4-3 B), AG1478 treatment no longer increased GFP-CFTR plasma membrane fluorescence intensity. Furthermore, plasma membrane fluorescence intensity was reduced to levels consistent with that of cells undergoing CS-induced CFTR internalization (Figure 4-3 B). Despite this, inhibition of EGFR with AG1478 partially reduced intracellular accumulation of CFTR. The fluorescence intensity of intracellular GFP-CFTR following smoke exposure with was reduced from 5.7 ± 0.4 AU (n = 82 cells) in CS/vehicle treated cells to 4.3 ± 0.3 AU ($p < 0.001$, n = 113 cells). Thus, despite the resistance of EGFR to AG1478 in the presence of CS, some inhibition of internalization was recorded.

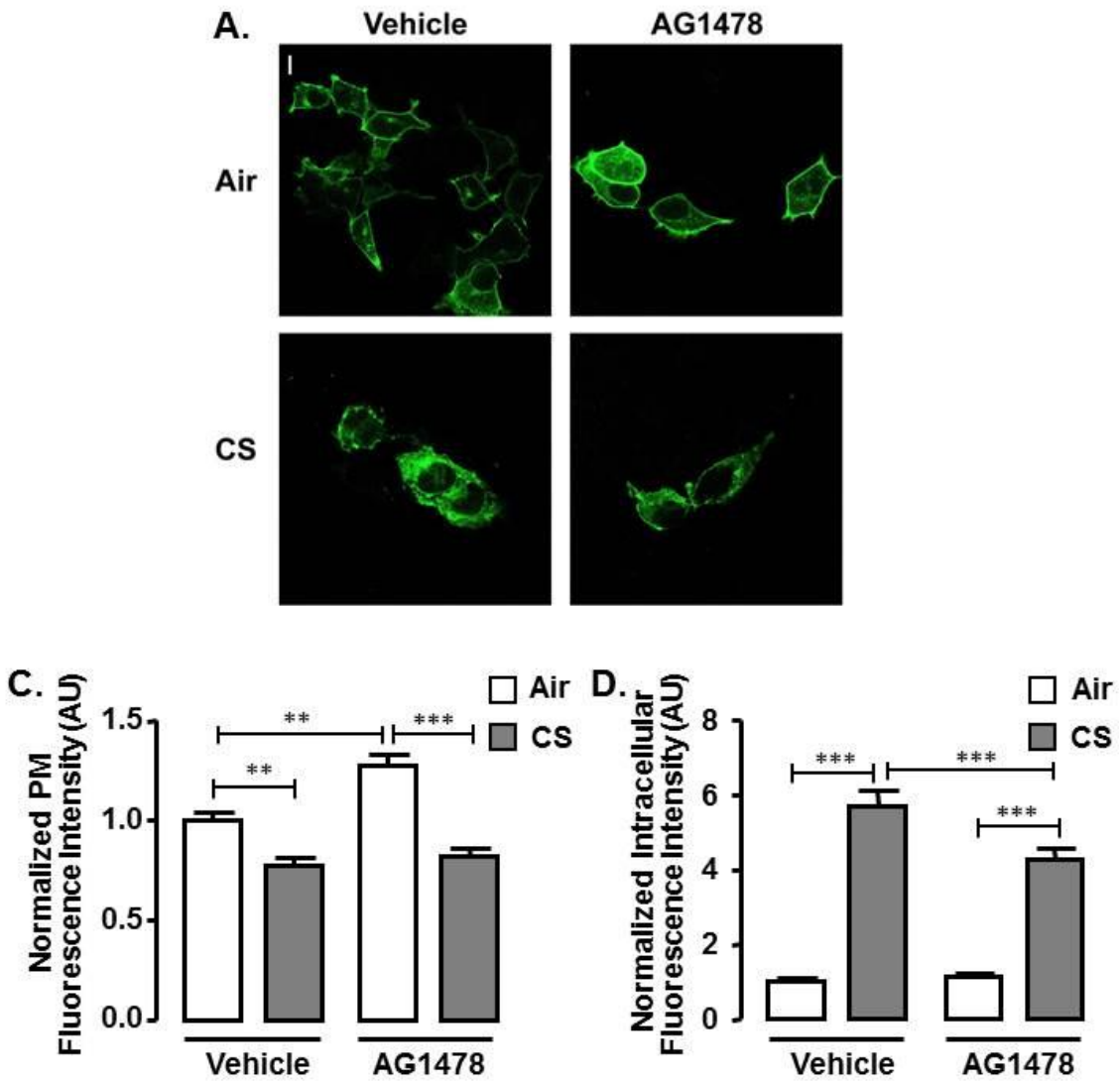

Figure 4-3. The EGFR regulates levels of CFTR in the plasma membrane and may influence CS-induced CFTR internalization.

HEK293T cells transiently transfected with GFP-CFTR were pre-treated for 30 min with vehicle (0.1 % DMSO) or 30 µM AG1478 prior to exposure to air or CS. Cells were subsequently incubated at 37°C for 60 min before fixation with 4% PFA. (A) Representative confocal images of GFP-CFTR in all conditions. (B) Mean plasma membrane fluorescence intensity in air (open bars) or CS (grey bars) of cells treated with vehicle or 30 µM AG1478. (C) Mean intracellular fluorescence intensity in air (open bars) or CS (grey bars) of cells treated with vehicle or 30 µM AG1478. ** $p < 0.01$, *** $p < 0.001$ by Kruskal-Wallis test with Dunn's multiple comparison post-test. n = 82 - 117 cells from 3 independent experiments. Scale bar = 10 µm.

4.2.3 Forskolin inhibits CS-induced CFTR internalization

Given that kinases play an important role in CFTR internalization by CS, we next investigated the role of phosphorylation in CS-induced CFTR internalization. PKA phosphorylation activates CFTR (Anderson et al., 1991a), and has been identified as an agonist of endocytosis in T84 cells expressing CFTR (Bradbury et al., 1992). Forskolin, an adenylyl cyclase agonist, stimulates the phosphorylation of CFTR through the production of cAMP, leading to maximal phosphorylation of the channel by PKA (Anderson et al., 1991a). GFP-CFTR was predominantly located at the plasma membrane in HEK293T cells in the presence of both vehicle (0.05 % DMSO) and 5 µM forskolin (Figure 4-4 A). Following air exposure, no significant difference in plasma membrane expression levels were observed in the presence of forskolin (Figure 4-4 C, 1.0 ± 0.0 AU, n = 180 cells) compared to vehicle (1.00 ± 0.03 AU, n = 192 cells). As previously reported, GFP-CFTR accumulated internally following CS exposure (Figure 4-3 D, $p < 0.001$, 2.9 ± 0.1 AU, n = 137 cells) compared to air (1.0 ± 0.1 AU, n = 192 cells). However, in the presence of forskolin, there was no significant difference in plasma membrane GFP-CFTR fluorescence intensity in air conditions (1.0 ± 0.0 AU, n = 180 cells) compared to CS exposed cells (1.0 ± 0.0 AU, n = 142 cells). Additionally, in the presence of forskolin, no significant difference in intracellular GFP-CFTR fluorescence intensity was measured following CS exposure (1.4 ± 0.1 AU, n = 143 cells) compared to air (1.1 ± 0.1 AU, n = 180 cells). Therefore, phosphorylation of CFTR prevents CS-induced internalization. These results suggest that CFTR is likely to be in a dephosphorylated state to undergo CS-induced internalization.

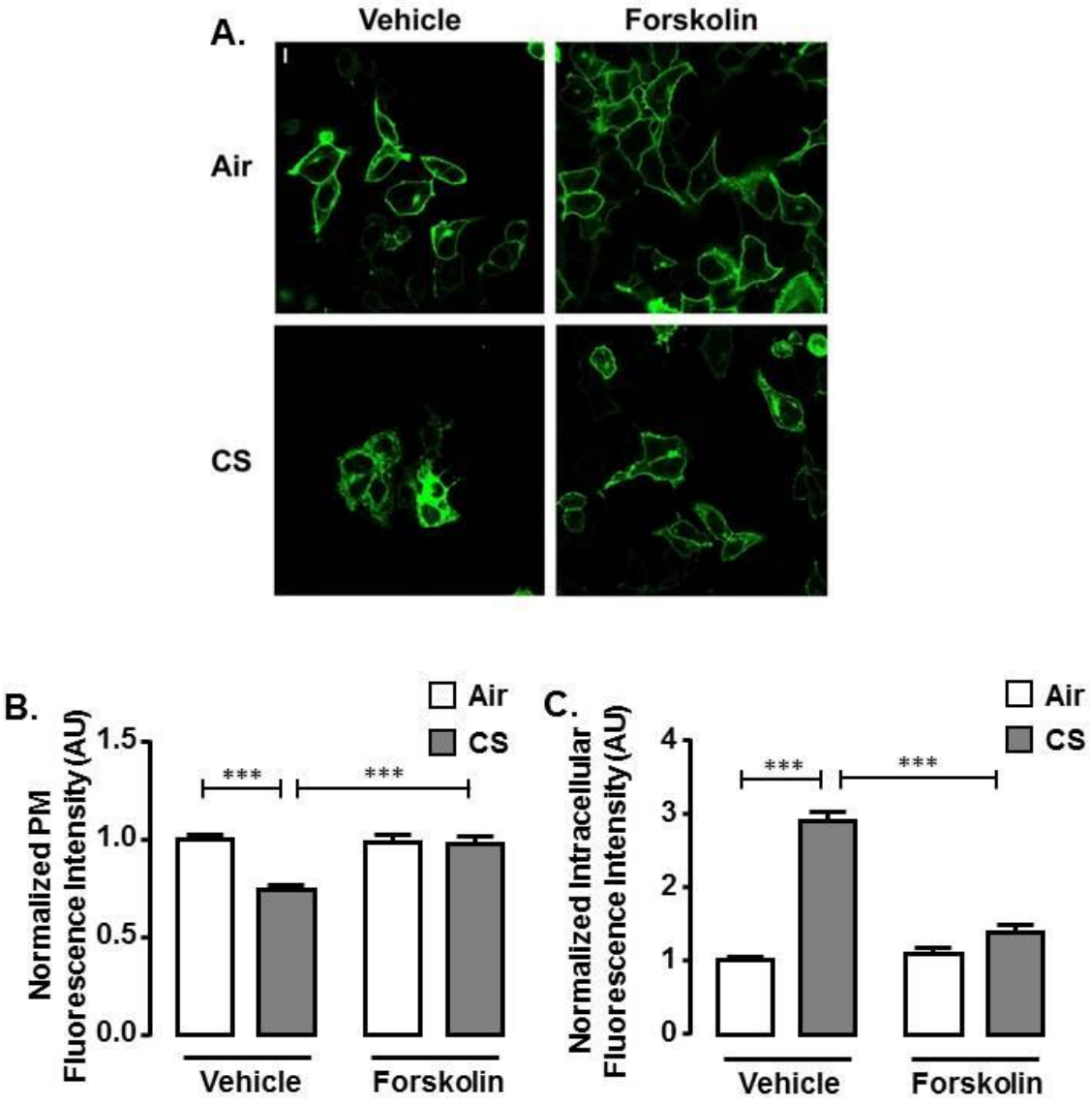

Figure 4-4. Forskolin-dependent phosphorylation of CFTR prevents CS-induced internalization.

HEK293T cells transiently transfected with GFP-CFTR were pre-treated for 30 min with vehicle (0.05 % DMSO) or 5 µM forskolin prior to exposure to air or CS exposure. Next, cells were incubated at 37°C for 60 min before fixation with 4% paraformaldehyde. (A) Representative confocal micrographs of GFP-CFTR in the presence of 5 µM forskolin in air and CS exposed conditions. (B) Mean plasma membrane fluorescence intensity in air (open bars) or CS (grey bars) of cells treated with vehicle or 5 µM forskolin. (C) Mean intracellular fluorescence intensity in air (open bars) or CS (grey bars) of cells treated with vehicle or 5 µM forskolin. *** $p < 0.001$ by Kruskal-Wallis test with Dunn's multiple comparison post-test. n = 137 - 192 cells from 3 independent experiments. Scale bar = 10 µm.

4.2.4 PKA-unresponsive CFTR has an altered pattern of expression

CFTR has a plethora of conserved phosphorylation sites, with a large proportion of sites located in the R domain (Figure 4-5). Many of these sites are specific to PKA phosphorylation (Hegedus et al., 2009). As discussed in section 4.1, phosphorylation of CFTR by PKA plays an important and complex role in the activation of CFTR. The removal of any one of the PKA consensus phosphorylation sites does not abolish PKA-mediated CFTR activity. However, when multiple consensus sites were mutated, PKA-mediated CFTR activity was reduced (Hegedus et al., 2009). Previously, the Riordan group demonstrated that replacement of all nine serine/threonine sites in the R domain with the addition of a tenth site in NBD1 to alanine residues (10SA CFTR) failed to remove all PKA-mediated CFTR activity (Chang et al., 1993). However, further replacement of an additional five sites of serine/threonine PKA phosphorylation ($CFTR^{15SA}$, Figure 4-5 A) resulted in a CFTR channel that is unresponsive to PKA (Hegedus et al., 2009).

Here, BHK cells stably expressing wt-CFTR or CFTR with 15 sites of phosphorylation replaced with alanine residues ($CFTR^{15SA}$, see methods section 2.3) were used to investigate the role of PKA phosphorylation in CS-induced CFTR internalization. Western blot was performed to characterize expression of WT- and $CFTR^{15SA}$. The same amount of protein was loaded for each sample (15 µg), and total expression of $CFTR^{15SA}$ was significantly higher (43 %) than wt-CFTR (Figure 4-5 B, $p < 0.05$ by student's t-test, $n = 3$). The expression of band C (mature, fully glycosylated CFTR) and band B (immature, core glycosylated CFTR) was measured as a percentage of total CFTR expression (Figure 4-5 C). Both WT and $CFTR^{15SA}$ demonstrated significantly more band C expression than band B ($p < 0.001$, $n = 3$). However, no change was observed in the proportion of band C to band B in either wt-CFTR (73.9 ± 1.1 % and 26.5 ± 1.1 %, respectively) and or $CFTR^{15SA}$ (80.2 ± 3.4 % and 19.8 ± 3.4 %, respectively), suggesting that the maturation of $CFTR^{15SA}$ is not different from that of wt-CFTR.

To investigate the effects of CS on the cellular localization of 15SA-CFTR, BHK cells expressing wt-CFTR or $CFTR^{15SA}$ were exposed to CS, incubated for 60 min, and fixed in 100% MeOH (methods section 2.6). The cells were blocked in bovine serum albumin and normal goat serum, prior to probing with anti-CFTR (596) and anti-mouse Dylight 488. In Figure 4-6 A, wt-CFTR expressed primarily at the plasma membrane after air exposure, and was internalized following CS exposure.

The expression pattern of $CFTR^{15SA}$ was similar to that of wt-CFTR following CS exposure (Figure 4-6A), suggesting that phosphorylation may have important role in maintaining CFTR at the plasma membrane. The intracellular fluorescence intensity of $CFTR^{15SA}$ did not increase following CS exposure, rather the fluorescence intensity significantly decreased from 1.4 ± 0.04 AU in air conditions to 1.1 ± 0.1 AU ($p < 0.01$, $n = 80 - 236$ cells) following CS exposure, implying an important role of the 15 sites of PKA phosphorylation in the CS-induced internalization of CFTR.

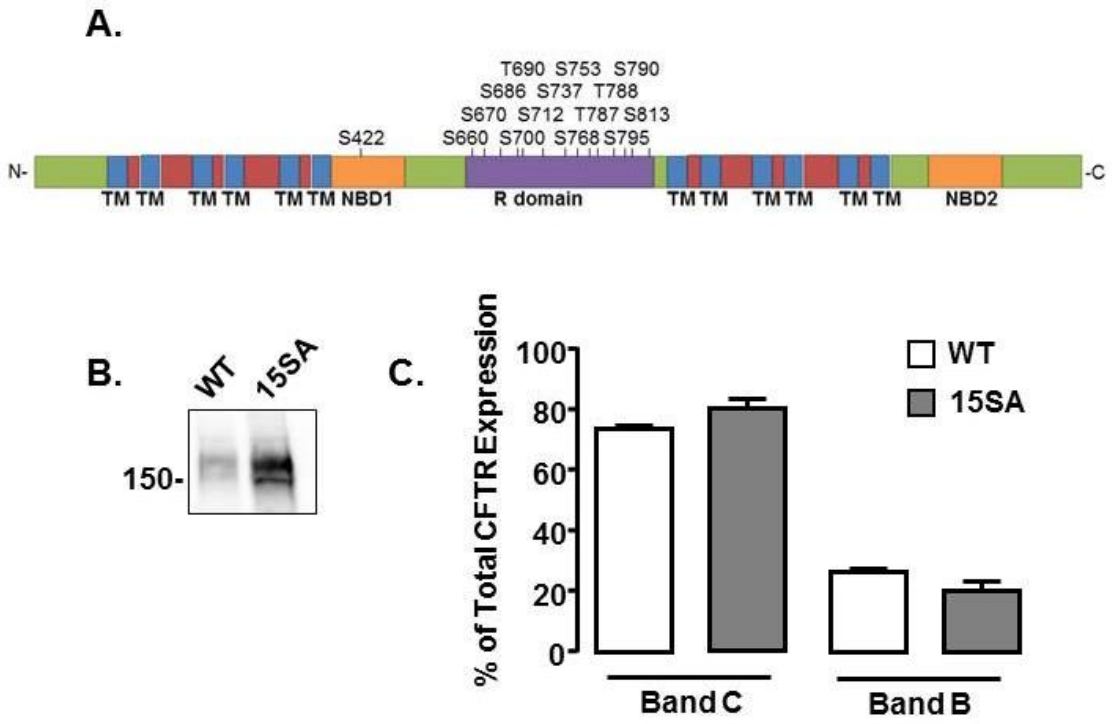

Figure 4-5. PKA-unresponsive CFTR has a different expression pattern and response to CS exposure compared to wt-CFTR.

(A) A schematic showing fifteen consensus sites of serine/threonine phosphorylation in CFTR which are mutated to alanine residues to produce CFTR^{15SA}. (Adapted from Billet *et. al.* (2015)). (B) BHK cells stably expressing wt-CFTR (WT) or CFTR^{15SA} (15SA) were seeded at a density of 100,000 cells per 35 mm dish. The cells from three 35 mm dished were lysed in Pierce lysis buffer and combined. Protein concentration was measured using BCA assay and 15 µg per sample was loaded on a 7-15 % gel (Biorad, USA). The gel was transferred to PDVF by wet transfer and the blots were blocked for 1 hr in 3% milk and TBST, and probed with anti-CFTR (596) (1:1000). Blots were washed 3 x 5 min in TBST and probed with HRP conjugated anti-mouse secondary antibody and developed using the Chemidoc (Biorad, USA). Bands shown are representative of three individual experiments. (C) Densiotometry of WT and CFTR^{15SA} band C (mature) and band B (un-glycosylated). Combined Band C and Band B expression was measured as total CFTR expression. Expression of Band C and Band B were calculated as a percentage of total CFTR expression. n = 3. Statistics were calculated using Kruskal-Wallis test with Dunn's multiple comparison post-test. n = 137 - 192 cells from 3 independent experiments

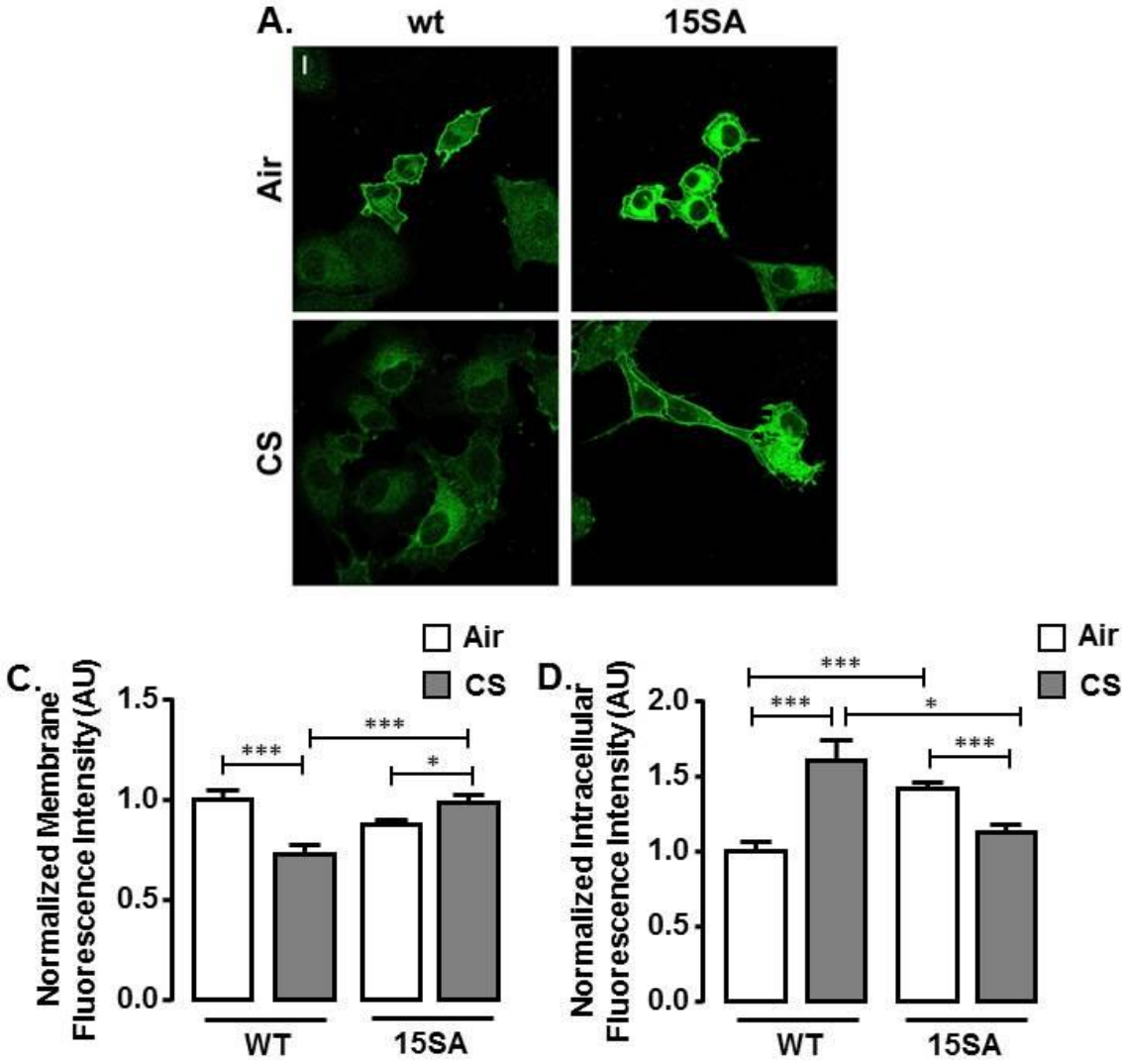

Figure 4-6. PKA-unresponsive CFTR has a different expression pattern and response to CS exposure compared to wt-CFTR.

BHK cells stably expressing either wt-CFTR or CFTR^{15SA} were exposed to air or CS prior to 60 min incubation at 37°C and 5% CO_2. The cells were fixed and permeablized in methanol. Cells were blocked for 1 h in 5 % normal goat serum and 1 % bovine serum albumin in PBS. The cells were incubated with primary antibody (anti-CFTR 596) for 3 h at room temperature, followed by three washes with PBS, and labelling with anti-mouse secondary antibody conjugated to Dylight 488. (A) Representative confocal micrographs of wt- and CFTR^{15SA} in air and CS exposed conditions. (B) Ratios of CS/air at the plasma membrane and intracellularly were calculated for each condition. (C) Mean plasma membrane fluorescence intensity in air (open bars) or CS (grey bars) of cells transfected with WT- or CFTR^{15SA}. (D) Mean intracellular fluorescence intensity in air (open bars) or CS (grey bars) of cells transfected with WT- or CFTR^{15SA}. * $p < 0.05$, *** $p < 0.001$ by Kruskal-Wallis test with Dunn's multiple comparison post-test., n = 80 - 236 cells from three independent experiments. Scale bar = 10 µm.

4.2.5 Cigarette smoke exposure causes dephosphorylation of CFTR

Having established the importance of kinases and phosphorylation by PKA in CS-induced internalization of CFTR, we employed primary human bronchial epithelial cells (HBECs) and an R domain specific antibody whose epitope binding is sensitive to phosphorylation by PKA to investigate the phosphorylation state of CFTR. HBECs were exposed to whole CS generated from 0-3 cigarettes, and plasma membrane CFTR was recovered by surface biotinylation. Consistent with previous findings (Rasmussen et al., 2014), total surface membrane CFTR (measured by anti-CFTR 596) decreased after CS exposure. However, the amount of inactive, dephosphorylated CFTR measured by probing with phosphorylation sensitive anti-CFTR 217 antibody increased following CS exposure, suggesting that CS causes CFTR dephosphorylation which is potentially linked to internalization.

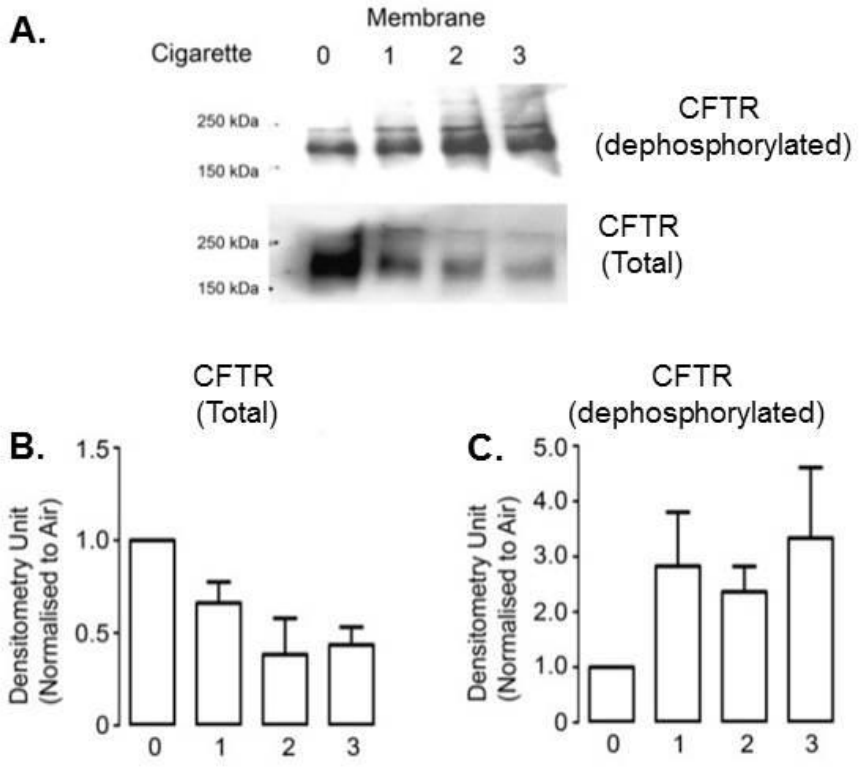

Figure 4-7. Cigarette smoke causes dephosphorylation of CFTR.

HBECs cultured at the air liquid interface on semi-permeable culture inserts (Corning, transwell-clears) were biotinylated, with FBS on the basolateral side. The cells were then lysed in Pierce's lysis buffer and were then spun down to remove cell debris. The remaining lysates were rotated overnight with neutravidin beads. Protein concentrations were calculated using Bradford assay and samples were diluted to ensure the same amount of protein was loaded in each tube. Beads were centrifuged at 14,000xg and pellet was collected. The beads were denatured with sample buffer and 2-mercaptoethanol at 37°C for 1 h. Membrane fractions were loaded on a biorad gel and ran at 150 mV until the protein ladder reached the bottom of the gel. Gels were transferred wet to PDVF membrane overnight at 4°C. Membranes were blocked in 5 % milk and probed for dephosphorylated CFTR with primary anti-CFTR 217 antibody. The membranes were washed a minimum of 3 x 10 min and probed with anti-ms conjugated to horseradish peroxidase. The PVDF membrane was visualised using a Biorad Chemidoc (USA). This work was carried out by Dr Chong Da Tan at the University of North Carolina, at Chapel Hill.

4.3 Discussion

Recently, studies into the effects of cigarette smoke on airway epithelia have lead to the discovery that CS causes the release of lysosomal calcium, leading to internalization of CFTR (Rasmussen et al., 2014). This internalization causes dehydration of the airway surface liquid, which is hypothesized to be an important risk factor for mucus accumulation in smokers and patients with COPD (Clunes et al., 2012). In the previous chapter, it was determined that the normal motifs which signal CFTR for endocytosis are not necessary for its internalization by smoke. Thus understanding the cell signaling pathway(s) that do lead to CS-induced calcium release and CFTR internalization are important steps towards the development of new therapeutics for COPD. The aims of this chapter were to better understand the relationship between the CS response and the MAPK pathway, and to determine how CS-induced calcium release and CFTR internalization is affected by phosphorylation of CFTR.

The Cormet-Boyaka group have provided evidence that CS extract, produced by bubbling whole CS through growth medium, can directly activate the MAPK pathway. CS-induced internalization of CFTR is dependent on the activation of this pathway (Xu et al., 2015). Our lab has previously demonstrated using nicotine as a marker of CS, that the effects of smoke on the airway epithelium differ depending on the preparation technique of the smoke (Clunes et al., 2008). Furthemore, whole CS exposure using the exposure chambers as developed by Phillips *et al*. (2005), exposes the epithelia to concentrations of nicotine comparable to nicotine levels *in vivo* (Clunes et al., 2008). To this end, we assessed the effects of the MAPK pathway on CS-induced CFTR internalization using whole CS. Consistent with results from Estelle Cormet-Boyaka's group (Xu et al., 2015), U0126, an antagonist of MEK, diminished the internalization of CFTR by CS thus confirming that CS-induced CFTR internalization is reliant on the activation of MEK. Furthermore, although the CS-induced change in $[Ca^{2+}]$ trended towards an increase in $[Ca^{2+}]_i$, these results were not significantly different from air exposed cells. Despite this, CS exposure cultures treated with U0126 displayed a remarkably similar $[Ca^{2+}]_i$ profile to that of CS/vehicle treated cells. These data lead to the speculation that MEK/ERK may evoke its effects on CFTR downstream of CS-induced Ca^{2+} release. However, further investigation into this matter must be performed. Furthermore, in collaboration with the Cormet-Boyaka group, it was observed that the CS-induced phosphorylation and activation of ERK (Xu et al., 2015) is calcium-dependent

(personal communication with Estelle Cormet-Boyaka, data not shown), further confirming that the MAPK pathway is downstream of calcium signaling, and upstream of CFTR internalization.

The MAPK pathway is upregulated by EGFR, a tyrosine kinase receptor. To investigate the possibility that the tyrosine kinase receptor may be an important factor in the MAPK regulation of CS-induced CFTR internalization, AG1478, an inhibitor of tyrosine kinase receptors was used to investigate CS-induced CFTR internalization. Although the EGFR has been shown to regulate trafficking of the Na^+/K^+-ATPase (Lee et al., 2015), extensive search of the literature revealed that EGFR has no known effects on CFTR trafficking. In the present study, AG1478 treatment alone increased plasma membrane expression of CFTR compared to vehicle control. This effect could be due to a number of different aspects of CFTR trafficking including reduced CFTR trafficking to the plasma membrane, a decrease in native endocytosis, or reduced recycling. Since CS can cause EGFR to exhibit resistence to some tyrosine kinase inhibitors such as AG1478 (Filosto et al., 2012), in the presence of CS, AG1478 no longer increased the plasma membrane abundance of CFTR, rather the levels of plasma membrane CFTR resembled that of smoke exposed CFTR in vehicle conditions. In the presence of AG1478, CS caused significant internalization of CFTR. However, the level of this internalization was slightly reduced compared to vehicle control, suggesting that EGFR may have a role in CS-induced CFTR internalization. One explanation for the slight inhibition of CS-induced internalization by AG1478 despite the CS-induced resistance of EGFR to this drug may be provided by the high concentration of AG1478 (30 μ) utilized in this experiment. Thus, it is apparent that EGFR plays a significant role in CFTR trafficking in both control and CS exposed conditions. However, future experiments will need to determine the true extent of the role of EGFR in CS-induced CFTR internalization. Since the resistance of EGFR to AG1478 can be prevented by PP1 and PP2 (Filosto et al., 2013), inhibitors of Src. These inhibitors could therefore be used to further investigate the role of EGFR in CFTR trafficking. However, since Src itself has been demonstrated to directly effect CFTR (Lepple-Wienhues et al., 2001, Davenport et al., 1996), it is possible that the inhibition of Src may itself play a role in CS-induced internalization of CFTR. Therefore, a more reliable way to investigate the role of EGFR would be to use different antagonists of EGFR, express a dominant negative EGFR, or knockdown EGFR using siRNA. Additionally, stimulation of the cells with exogenous EGF would provide further

insight into the role of the EGFR in CFTR trafficking in both native, and CS exposed conditions.

Given that kinases play an established role in CS-induced CFTR internalization, and that PKA is critically involved in the activation of CFTR, the role of phosphorylation by PKA in the CS response was investigated. Forskolin has previously been identified as an antagonist of endocytosis, and that endocytosis can be regulated in a cAMP-dependent fashion (Bradbury et al., 1992). Bradbury and colleagues (1992) performed this investigation using T84 cells in which CFTR is natively expressed. However, their studies addressed the effects of global endocytosis by measuring fluid-phase uptake, and the direct effects of forskolin on the specific internalization of CFTR were not identified. Our data suggest that the phosphorylation of CFTR by PKA had inhibitory effects on CS-induced internalization of CFTR, and that phosphorylation of CFTR by PKA reduces the ability of CS to cause internalization of CFTR.

To further investigate the effects of PKA phosphorylation on CFTR trafficking and CS-induced internalization, a PKA-unresponsive $CFTR^{15SA}$ with 15 sites of PKA phosphorylation mutated to alanine residues was used. The expression of wt-CFTR and PKA-unresponsive $CFTR^{15SA}$ in BHK cells was investigated using western blotting and confocal microscopy. The relative expression of both band C and band B CFTR were not signifcantly different in 15SA-CFTR compared to wt-CFTR, suggesting that the maturation of $CFTR^{15SA}$ is similar to that of wt-CFTR. Billet *et. al.* (2013) demonstrated that plasma membrane levels of surface biotinylated $CFTR^{15SA}$ were similar to wt-CFTR. However, here the level of immunolabelled plasma membrane $CFTR^{15SA}$ was slightly reduced compared to that of wt-CFTR following air exposure, and intracellular $CFTR^{15SA}$ was significantly increased compared to that of wt-CFTR. The expression pattern of $CFTR^{15SA}$ exposed to air was therefore remarkably similar to that of CS exposed wt-CFTR, suggesting that PKA phosphorylation may play an important role in maintaining CFTR at the plasma membrane, and that dephosphorylation of the PKA consensus sites may drive internalization of CFTR. Furthermore, the effects of CS on the cellular location of CFTR were investigated using confocal imaging. Compared to wt-CFTR, the CS-induced internalization of $CFTR^{15SA}$ was reduced. Together, these data suggest that the lack of PKA phosphorylation on the R domain of CFTR causes internalization, and prevents further internalization of $CFTR^{15SA}$ by CS.

Since CS-induced CFTR internalization was inhibited by forskolin, and the removal of PKA phosphorylation sites causes a shift in the equilibrium to favor internalization of CFTR, the phosphorylation state of CFTR following CS exposure was investigated using a CFTR antibody specific to the R domain that conveys sensitivity to phosphorylation at the epitope. Total CFTR decreased with an increasing number of cigarettes. However, using cell surface biotinylation the amount of dephosphorylated plasma membrane CFTR increased following CS exposure, suggesting that CS causes dephosphorylation of CFTR. Since the phosphorylation-sensitive antibody used to detect dephosphorylated CFTR (anti-CFTR 217) specifically recognizes amino acids 807-819, and the removal of 15 sites of PKA phosphorylation caused CFTR endocytosis, it is possible to pinpoint CS-induced dephosphorylation to phosphorylation concensus sites present within the 807-819 region. There are three highly conserved phosphorylation sites in the 807-819 region of the R domain; serine 809, serine 813 and serine 816. Further investigation of these sites by mutation to alanine, or mutation to a negatively charger amino acid such as glutamate would provide further information on the specific role of dephosphorylation at these sites. Since maximal phosphorylation of CFTR by forskolin prevented internalization, and the removal of 15 sites of CFTR phosphorylation caused the accumulation of intracellular CFTR, suggesting that the phosphorylation state of CFTR, and specifically dephosphorylation, may be a novel physiological regulator of CFTR residence time in the plasma membrane. This data will be of general interest for both CS-mediated CFTR dysfunction, as well as other CFTR diseases such as CF.

To better understand CS-induced dephosphorylation of CFTR, it is important to consider the mechanics of this dephosphorylation event. Dephosphorylation could be caused by activation of a phosphatase, inactivation of a kinase or the relative change in the activation levels of both. There are many kinases and phosphatases known to affect CFTR. PP2A is an important regulator of CFTR, causing its dephosphorylation at the apical surface or airway epithelia (Thelin et al., 2005). PP2A does not require the binding of any cofactors for its activation. However, CS increases the activity of PP2A *in vivo* and in patients with emphysema (Wallace et al., 2012). PP2A interacts with CFTR through its C terminus (1451-1476) (Thelin et al., 2005). However, in the previous chapter (Section 3.2.3) the removal of the C-terminus of CFTR had no effect on CS-induced CFTR internalization, suggesting that dephosphorylation by PP2A does not underly the CS-mediated CFTR response. Assuming that dephosphorylation of CFTR leads to its internalization, we

can eliminate PP2A as a phosphatase of interest based on this information. PP2B is a Ca^{2+} dependent phosphatase whose inhibition in Calu-3 and 3T3 cells leads to the activation of CFTR (Fischer et al., 1998). The activation of PP2B by Ca^{2+} makes this phosphatase an interesting candidate for the dephosphorylation of CFTR by CS, and further investigation into the role of PP2B, and other kinases and phosphatases, in CS-induced CFTR internalization should be performed

The major findings of this chapter are summarized below and in Figure 2-2.

- CS-induced CFTR internalization is inhibited by MEK/ERK inhibitors but not through inhibition of CS-induced Ca^{2+}-release.
- CS causes dephosphorylation of CFTR leading to its internalization.
- CS-induced CFTR internalization is inhibited by maximal phoshorylation of CFTR by forskolin.
- The removal of 15 consensus sites for phosphorylation resulted in intracellular accumulation of CFTR, suggesting that dephosphorylation of CFTR may be a stimulus for internalization. Furthermore, the removal of these sites reduced the amount of CS-induced internalization compared to wt-CFTR.

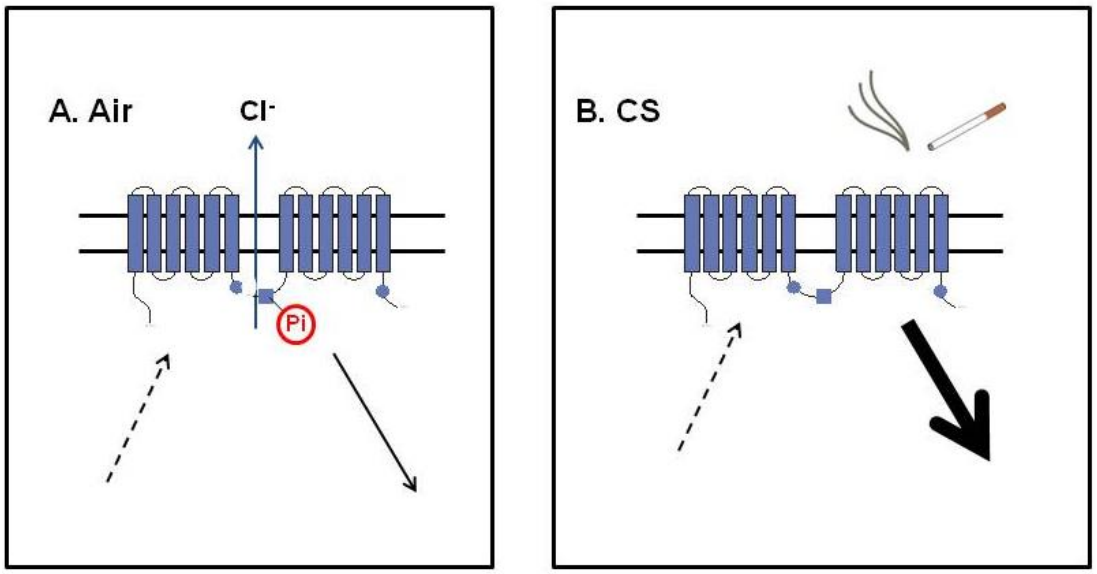

Figure 4-8. A proposed model for the effects of CS on the phosphorylation status of CFTR.

(A) In air conditions, endogenous agonists stimulate the phosphorylation and activation of CFTR to maintain normal Cl^- secretion. (B) In the presence of CS, CFTR is dephosphorylated resulting in augmented CFTR endocytosis, and decreased Cl^- secretion.

5.0 Cigarette smoke-internalized CFTR takes an abnormal endocytic path

5.1 Introduction

The work presented in the previous chapter (4) of this thesis focused primarily on determining the cell signalling pathways leading to cigarette smoke induced CFTR internalization. Thus, CS caused dephosphorylation of CFTR, and maximal phosphorylation of CFTR by forskolin prevented its internalization by CS. The focus of this chapter is to examine CFTR post-internalization, and to determine the destination of CS-internalized CFTR. Thus far, data published by our lab demonstrates that CFTR total protein levels decrease in western blot studies following CS exposure. However, when high concentrations of detergent were utilized, CFTR total protein levels did not decrease in the presence of CS. Furthermore, colocalization studies of CFTR and LAMP1, a lysosomal marker, demonstrated that CFTR does not localize to the lysosomes following CS exposure (Rasmussen et al., 2014). These data suggest that CFTR is not degraded upon rapid internalization by smoke, and that CFTR remains in the cytosolic fraction in an insoluble form upon CS exposure. Studies by the Cormet-Boyaka group have determined that CS-internalized CFTR colocalizes with lysosomes upon inhibition of lysosomal activity with chloroquin (Xu et al., 2015). However, these experiments were performed with by bathing cultures in 100% CS extract, produced using cigarettes with no filter, which may explain the discrepancy between the two publications. CS-internalized CFTR internalizes to the perinuclear region of the cell (Clunes et al., 2012). Immunolabeling of vimentin, an intermediary filament which is known to play a role in aggresome formation, demonstrated a similar expression pattern to that of CS exposed CFTR (Clunes et al., 2012). However, no present data investigates the pathway of CFTR trafficking from the plasma membrane to the perinuclear region of the cell.

Thus, it remains unclear whether CS-induced CFTR internalization occurs through the constitutive clathrin-mediated pathway, or whether it is endocytosed through an alternative mechanism. As such, the aims of this chapter were to:

1) Determine the pathway of endocytosis of CS-induced CFTR internalization
2) Determine the terminal location of the perinuclear accumulations of CFTR

5.2 Results

5.2.1 CS-induced internalization of CFTR is reduced by inhibitors of endocytosis

Hypertonic sucrose has been shown to inhibit endocytosis by causing reduction in the size and number of clathrin-coated pits and is associated with the formation of microcages of clathrin, which deplete the levels cytoplasmic clathrin necessary for endocytosis (Heuser and Anderson, 1989). To investigate the role of the endocytic machinery in the CS-induced internalization of CFTR, HEK293T cells were pre-treated with hypertonic sucrose (0.45M sucrose) for 15 min before exposure to air or CS. Hypertonic sucrose significantly reduced both the increase in intracellular fluorescence intensity and decrease in plasma membrane fluorescence intensity associated with CS-induced CFTR internalization (Figure 5-1). The post-CS intracellular fluorescence intensity was significantly reduced from 1.5 ± 0.2 AU (n = 172 - 182) in CS/vehicle conditions to 0.7 ± 0.1 AU ($p < 0.001$, n = 91 - 147) in the presence of CS/hypertonic sucrose. Hypertonic sucrose treated levels of plasma membrane fluorescence intensity were not significantly different to that of air/hypertonic sucrose treated cells (n = 172 – 182). However, CS/hypertonic sucrose treated cells exhibited a small but significant increase in intracellular fluorescence intensity (1.5 ± 0.2 AU) compared to air/hypertonic sucrose ($p < 0.01$, 0.7 ± 0.1 AU). These data suggesting that while hypertonic sucrose significantly reduces CS-induced CFTR internalization, it does not fully ablate it.

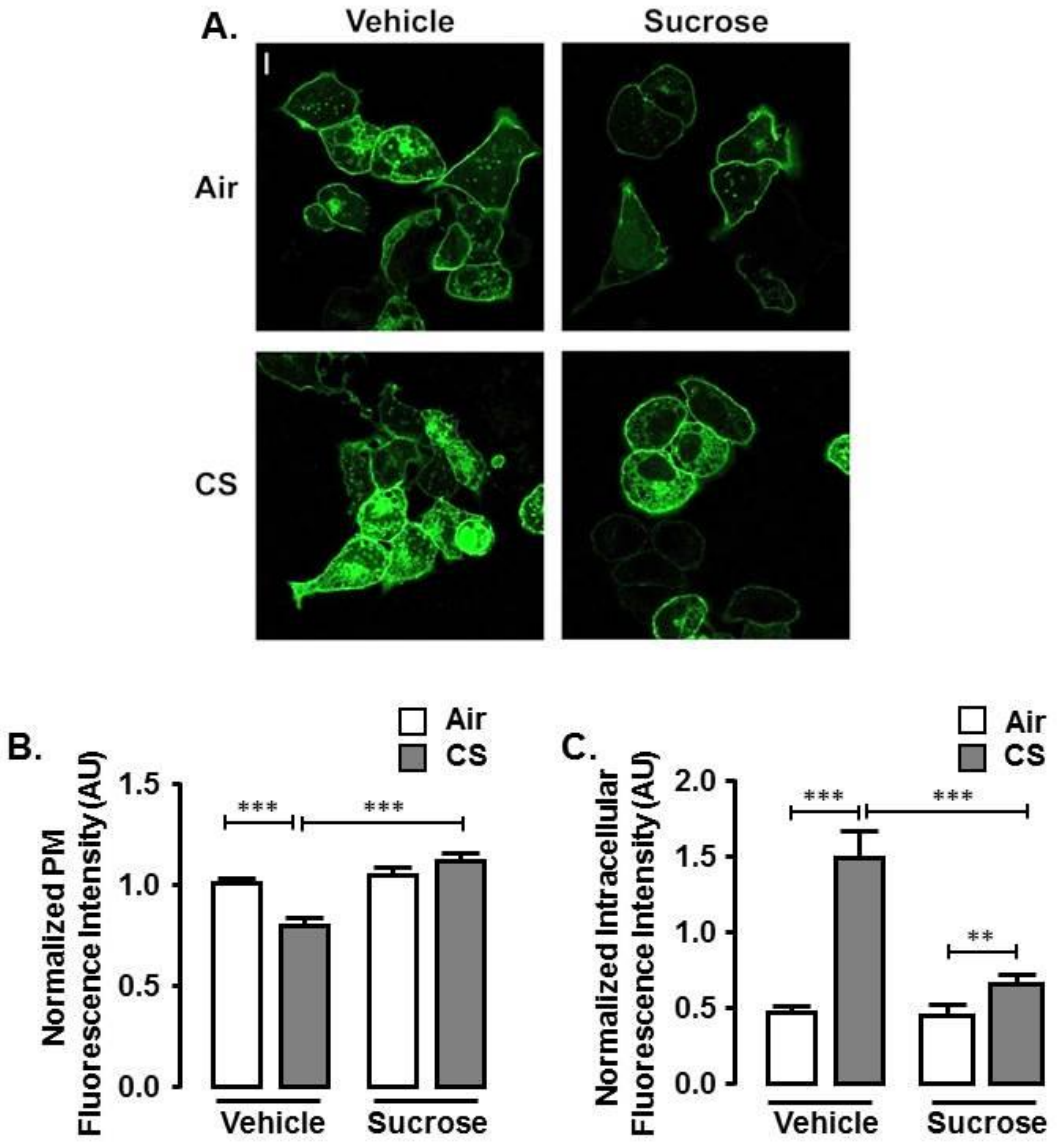

Figure 5-1. Hypertonic sucrose, an inhibitor of endocytosis, reduces CS-induced CFTR internalization.

HEK293T cells were transfected with wt-GFP-CFTR. The cells were pre-treated 48 h after transfection with vehicle (pyruvate Ringer's solution) or 0.45 M sucrose at 37°C for 15 min. The cells were then treated with CS and incubated at 37°C for 60 min before fixing in 4% PFA. A) Representative confocal images of GFP-CFTR in the presence of 0.45 M hypertonic sucrose in air and CS exposed conditions. (B) Mean plasma membrane fluorescence intensity in air (open bars) or CS (grey bars) of cells treated with vehicle or 0.45 M sucrose. (C) Mean intracellular fluorescence intensity in air (open bars) or CS (grey bars) of cells treated with vehicle or 0.45 M sucrose. ** $p < 0.01$, *** $p < 0.001$ by Kruskal-Wallis test with Dunn's multiple comparison post-test. n = 91 - 182 cells from 3 independent experiments. Scale bar = 10 µm.

5.2.2 CS-internalized CFTR is taken in to the cell by clathrin coated vesicles

CS-induced CFTR internalization was reduced by hypertonic sucrose, a chemical inhibitor known to prevent clathrin-dependent endocytosis. Since hypertonic sucrose is known to inhibit other types of endocytosis, including calceolate-mediated endocytosis in addition to clathrin-mediated endocytosis, colocalization studies with clathrin light chain were performed to further determine the internalization pathway of CS-exposed CFTR. As such, HEK293T cells were transiently co-transfected with GFP-CFTR and clathrin light chain tagged with the fluorescent marker mRFP (see methods section 2.8.3). Exposure to air or CS revealed a significant increase in colocalization of GFP-CFTR with clathrin light chain-mRFP after 5 minutes of CS exposure compared to air controls (Figure 5-2 B; $p < 0.01$, $n = 49 - 84$ cells). This increase was sustained across all time points and peaked at 60 min at 55.8 ± 1.9%, but was no longer maintained at 120 min. These data indicate that more CFTR is internalized in a clathrin-dependent manner following CS exposure, and that CS-induced CFTR internalization is therefore clathrin-dependent.

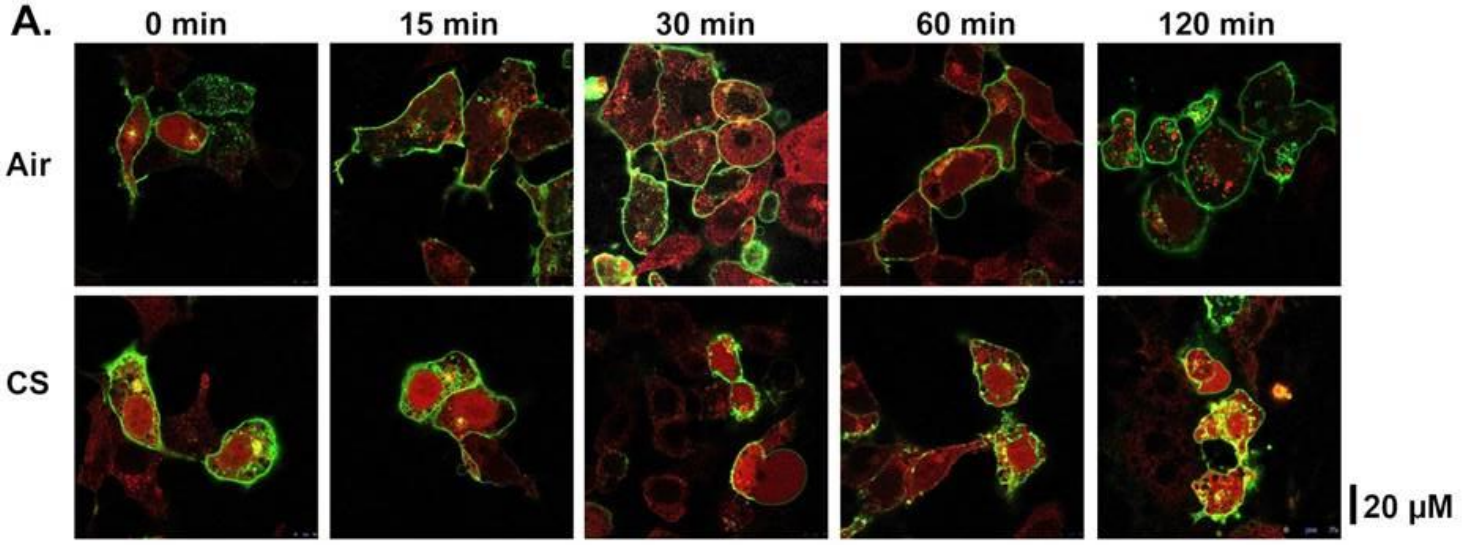

Figure 5-2. Colocalization of CFTR and clathrin light chain increases after cigarette smoke exposure.

HEK293T cells transfected with GFP-CFTR and clathrin light chain-mRFP were exposed to CS and incubated for different time periods fixation. A) Confocal images of air and CS-exposed cells at different times. B) Mean percentage of colocalization were calculated using the LAS AF software (Leica). Percentage colocalization after CS exposure peaked at 60 min (55.8 ± 1.9%; n = 49 - 85 cells, ** $p < 0.01$, *** $P < 0.001$ by two-way ANOVA with Sidak's multiple comparison test.

5.2.3 CS-induced CFTR internalization is dynamin-dependent

Dynamin is required for clathrin-mediated endocytosis, and inhibition of dynamin GTPase activity with dynasore provides a well-studied method for endocytic inhibition. To further investigate the endocytic path of CS-internalized CFTR, HEK293T cells transfected with GFP-CFTR were pre-treated with 80 µM dynasore for 30 min. The post-CS plasma membrane fluorescence intensity was significantly increased from 0.8 ± 0.04 AU in air/vehicle control conditions to 1.13 ± 0.1 AU in CS/dynasore treated cells (Figure 5-3; $p < 0.001$, n = 122 - 172). Additionally, dynasore prevented the increase in intracellular fluorescence intensity typically seen following CS exposure. The post-CS intracellular fluorescence intensity was reduced from 1.5 ± 0.2 AU in CS/vehicle conditions to 0.6 ± 0.1 AU in the presence of CS/dynasore ($p < 0.001$, n = 123 - 172 cells). No changes were observed in air/dynasore or CS/dynasore plasma membrane or intracellular fluorescence intensity.

Although dynasore is widely used across the literature to identify dynamin-mediated endocytosis, it has low specificity due to its ability to inhibit the activity of other GTPases within the cell. To confirm the role of dynamin in CS-induced CFTR internalization a dominant negative dynamin plasmid, dynamin^{K44A}, was transiently co-transfected with GFP-CFTR into HEK293T cells. In the presence of dynamin^{K44A}, CS-induced CFTR internalization was inhibited as demonstrated by a reduction in both CS-stimulated plasma membrane removal and intracellular accumulation of CFTR (Figure 5-3 a). Post-CS exposure plasma membrane fluorescence intensity was increased from 0.70 ± 0.0 AU in GFP-CFTR only control cultures compared to 0.093 ± 0.06 AU in cells co-transfected with dynamin^{K44A}. Intracellular fluorescence intensity post-CS was decreased from 2.52 ± 0.2 AU in GFP-CFTR only control cultures compared to 1.1 ± 0.1 AU in cultures co-transfected with dynamin^{K44A}. Furthermore, similar results were demonstrated in cultures co-transfected with wt-dynamin and GFP-CFTR, in which post-CS exposed plasma membrane fluorescence intensity was increased from 0.8 ± 0.1 AU in wt-dynamin transfected cultures, compared to 0.9 ± 0.1 ($p < 0.01$, n = 63 – 105) in dynamin^{K44A} expressing cultures. Post-CS exposed intracellular fluorescence intensity was decreased from 2.2 ± 0.1 AU in wt-dynamin transfected cells to 1.1 ± 0.1 AU ($p < 0.01$, n = 63 – 105). Together, these data suggest that dynamin GTPase activity is required for CS-induced CFTR internalization.

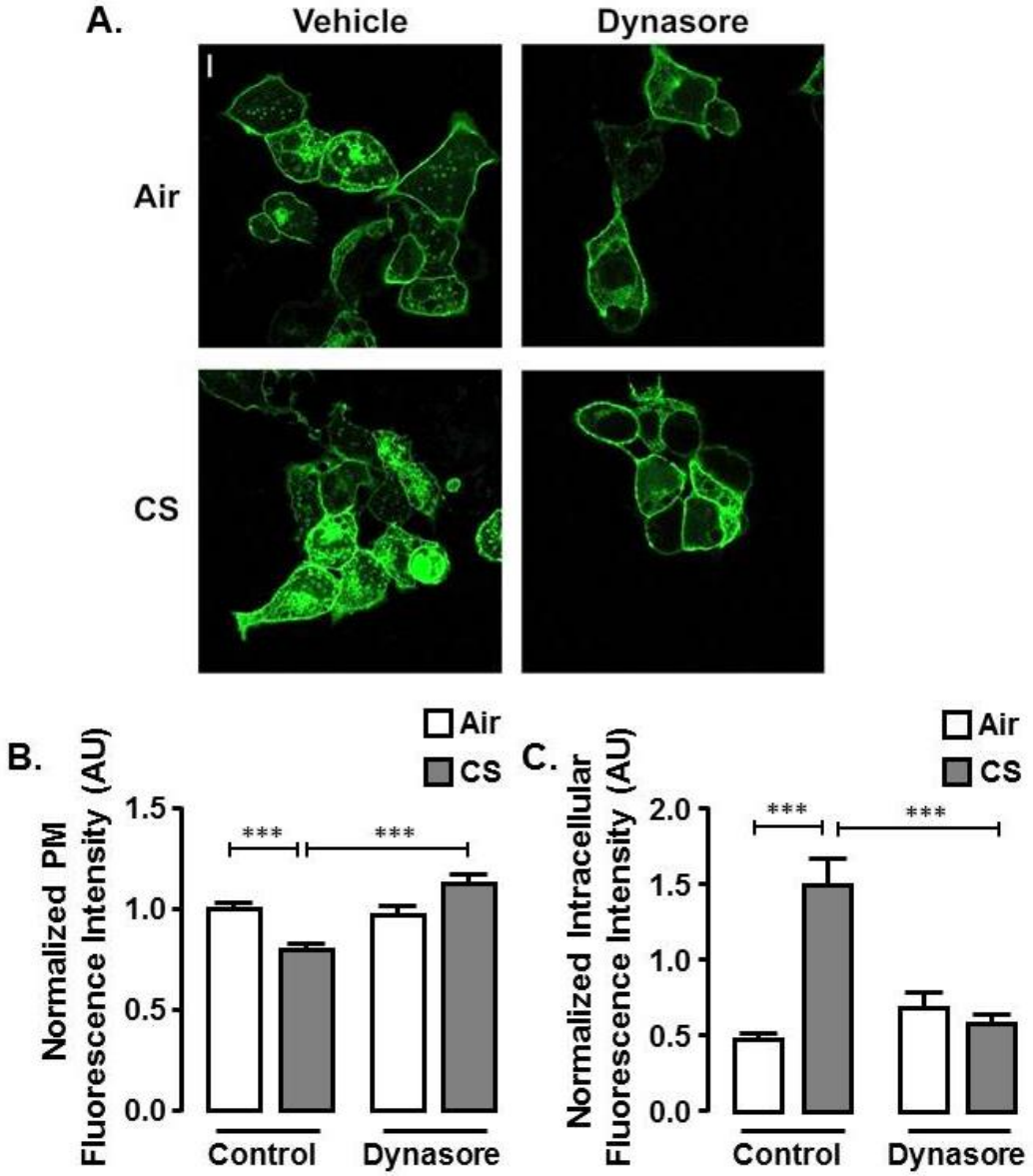

Figure 5-3. Dynasore, an inhibitor of dynamin, prevented the CS-induced internalization of CFTR.

HEK293T cells were transfected with GFP-CFTR. The cells were pre-treated 48 h after transfection with 80 µM Dynasore at 37°C for 30 min. The cells were then exposed to CS or air and incubated at 37°C for 60 min before fixing in 4% PFA. (A) Representative confocal images of GFP-CFTR in the presence of vehicle or 80 µM dynasore in air and CS exposed conditions. (B) Mean plasma membrane fluorescence intensity in air (open bars) or CS (grey bars) of cells treated with 80 µM dynasore. (C) Mean intracellular fluorescence intensity in air (open bars) or CS (grey bars) of cells treated with vehicle or 80 µM dynasore (n = 101 - 182 cells from three independent experiments, *** p > 0.001 by Kruskal-Wallis test with Dunn's multiple comparison post-test). Scale bar = 10 µm.

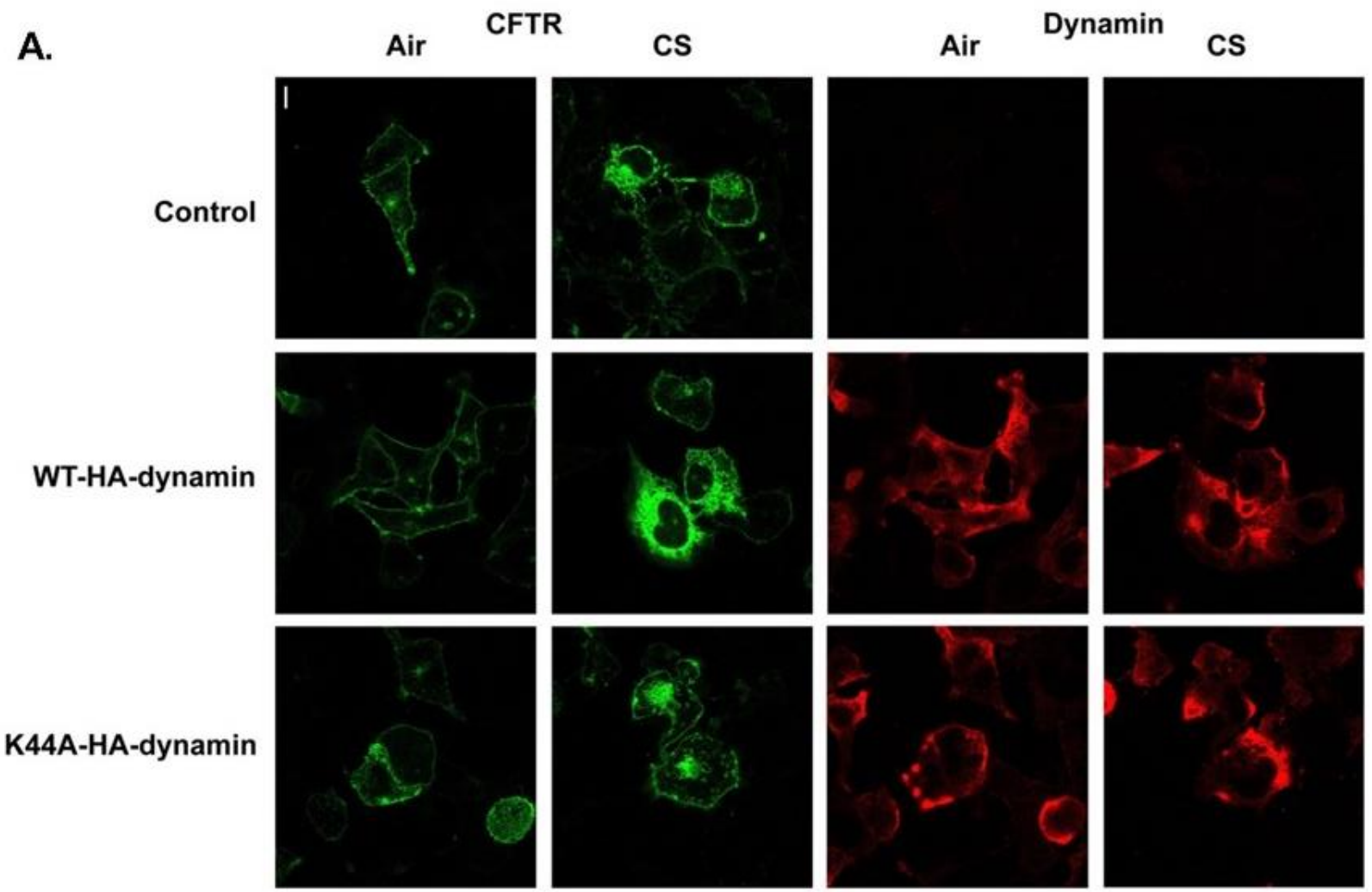
A.
CFTR
Dynamin
Air
CS
Air
CS
Control
WT-HA-dynamin
K44A-HA-dynamin

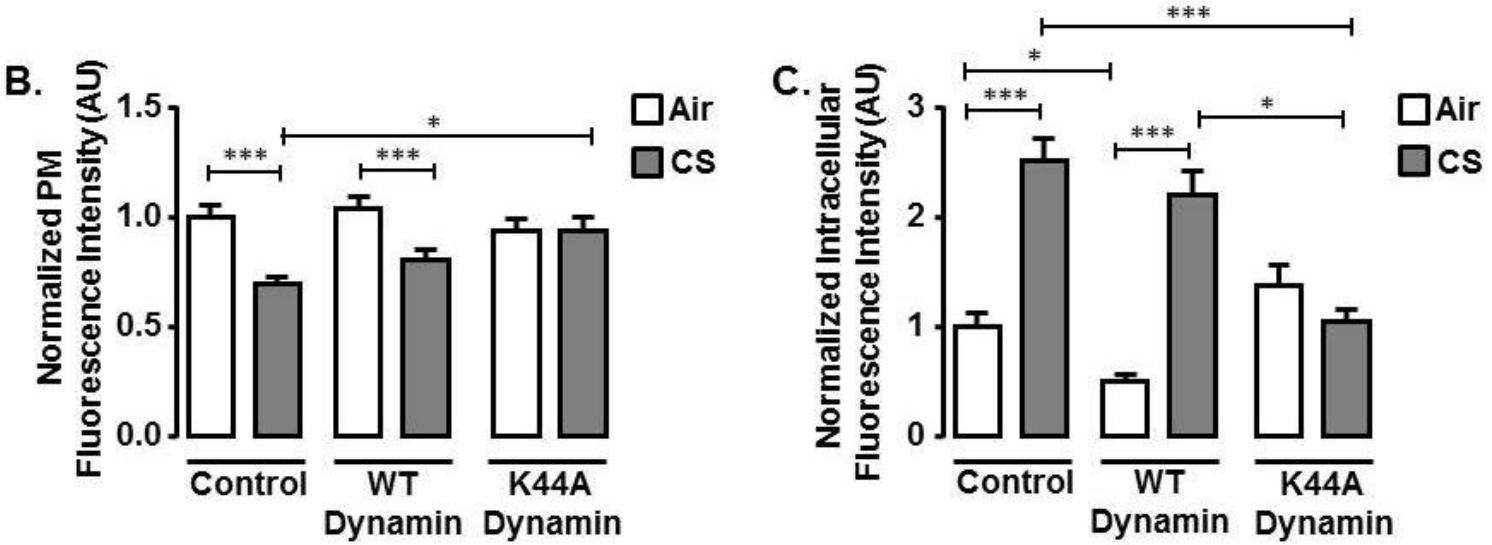

Figure 5-4. Dominant-negative inhibition of endocytosis prevented CS-induced internalization of CFTR.

HEK293T cells transfected with GFP-CFTR ± wt- or K44A-HA-dynamin were exposed to CS and incubated at 37°C for 60 min before fixation. Cells were blocked in 5% NGS and 1% BSA before probing with primary anti-HA antibody and Alexa 647 tagged secondary. (A) Representative confocal images of air and smoke treated cells transfected with GFP-CFTR ± wt- or HA-dynamin^{K44A}. (B) Fluorescence intensity of plasma membrane GFP-CFTR normalized to air control. (C) Fluorescence intensity of intracellular GFP-CFTR. *p<0.05, *** p < 0.001, n = 65 - 105 cells. Scale bar = 10 µm.

5.2.4 Endocytic trafficking of CS-exposed CFTR requires an intact cytoskeleton

Microtubules have been implicated in the bidirectional long-range movement of both clathrin coated vesicles and recycling, early and late endosomes across different cells types (Soldati and Schliwa, 2006). However, in the context of CFTR most research has focused around the role of microtubules in the recycled delivery of CFTR to the plasma membrane. For example, in *Xenopus laevis* oocytes (Weber et al., 2001), colonic T-84 cells (Tousson et al., 1996) and the airway epithelial cell line 9HTEo- (Schwiebert et al., 1994), disruption of microtubule polymerisation by nocodazole reduced cAMP-mediated CFTR current by preventing intracellular pools of CFTR from returning to the plasma membrane. However, contradictory data has been presented in both Calu3 cells (Loffing et al., 1998) and HEK293T cells (Domingue et al., 2014). In these latter cell types, cAMP-stimulated CFTR currents were unaffected by nocodazole, suggesting that microtubules do not play a role in CFTR exocytosis nor endocytosis in these cell types. In agreement with these data, no effect was observed on the cellular location of CFTR in the presence of nocodazole (Figure 5-5). However, when HEK293T cells were pre-treated with 33 µM nocodazole, the accumulation of intracellular GFP-CFTR following CS exposure was reduced from 3.8 ± 0.4 AU (n = 122 cells) in CS/vehicle conditions to 2.5 ± 0.3 AU ($p < 0.001$, n=90 cells) in the presence of nocodazole (Figure 5-5 c). Despite the reduction in post-CS intracellular fluorescence intensity after nocodazole treatment, this value was still significantly higher than the intracellular fluorescence intensity of air exposed vehicle treated cells (1.0 ± 0.2 AU; $p<0.001$, n = 120), suggesting that whilst CS-internalization of GFP-CFTR is reduced by nocodazole, it is not completely abolished in the presence of nocodazole. Furthermore, the reduction in plasma membrane fluorescence intensity in vehicle control cells following smoke exposure (from 1.0 ± 0.0 AU in air exposed conditions to 0.68 ± 0.0 AU in CS exposed conditions; $p < 0.01$, n= 120 - 122 cells) is not affected by nocodazole (Figure 5-5 B; 1.0 ± 0.03 AU air to 0.8 ± 0.03 AU CS; $p < 0.001$, n = 90 - 120 cells). These data suggest that nocodazole does not fully prevent CS-induced removal of CFTR from the plasma membrane. However, given that post-CS internal fluorescence intensity of GFP-CFTR was partially reduced in the presence of nocodazole, and the expression pattern of internal GFP-CFTR (Figure 5-5 A) was different from that of vehicle treated post-CS cells, microtubules may be required for CS-induced CFTR internalization and the disruption of

microtubules with nocodazole may result in CFTR following an alternative internalization pathway to that of vehicle treated post-CS cells.

Actin, through NHERF1 and ezrin, forms interactions with CFTR and plays an important role in regulating the ion channel. The presence of actin within CFTR microdomains and its effects on CFTR are well understood. In 1996, Cantiello's group showed that organization of the actin cytoskeleton is necessary for the cAMP-dependent activation of CFTR (Prat et al., 1995). Furthermore, actin disassembly dramatically decreases the expression of CFTR at the plasma membrane, and upregulates its internalization (Ganeshan et al., 2007, Okiyoneda and Lukacs, 2007). Thus, cytochalasin D a potent inhibitor of actin polymerization was used to investigate the role of actin in CS-induced CFTR internalization. To this end, HEK293T cells transfected with GFP-CFTR were pre-treated with vehicle (0.02 % DMSO) or 2 µM cytochalasin D for 15 min and exposed to CS prior to fixation. As previously reported in control conditions, GFP-CFTR was located predominantly at the plasma membrane and internalized following CS exposure (Figure 5-6 A). However, in the presence of cytochalasin D, GFP-CFTR expressed predominantly in the cytosol in air control conditions (Figure 5-6 A), suggesting that, consistent with previously published data (Ganeshan et al., 2007, Okiyoneda and Lukacs, 2007), actin is important for the normal cellular distribution of CFTR. In the presence of cytochalasin D, no changes were observed in plasma membrane fluorescence intensity following air/cytochalasin D exposure (1.0 ± 0.0 AU) compared to CS/cytochalasin D exposure (0.8 ± 0.1 AU, n = 77 - 104 cells). Additionally, no changes were observed in intracellular fluorescence intensity following air/cytochalasin D exposure (2.9 ± 0.4 AU) compared to CS/cytochalasin D exposure (3.3 ± 0.2 AU, n = 77- 104 cells). These data demonstrate that cytochalasin D has a distinct effect on the distribution of CFTR in control conditions. Furthermore, CS-induced internalization of CFTR was ablated by cytochalasin D.

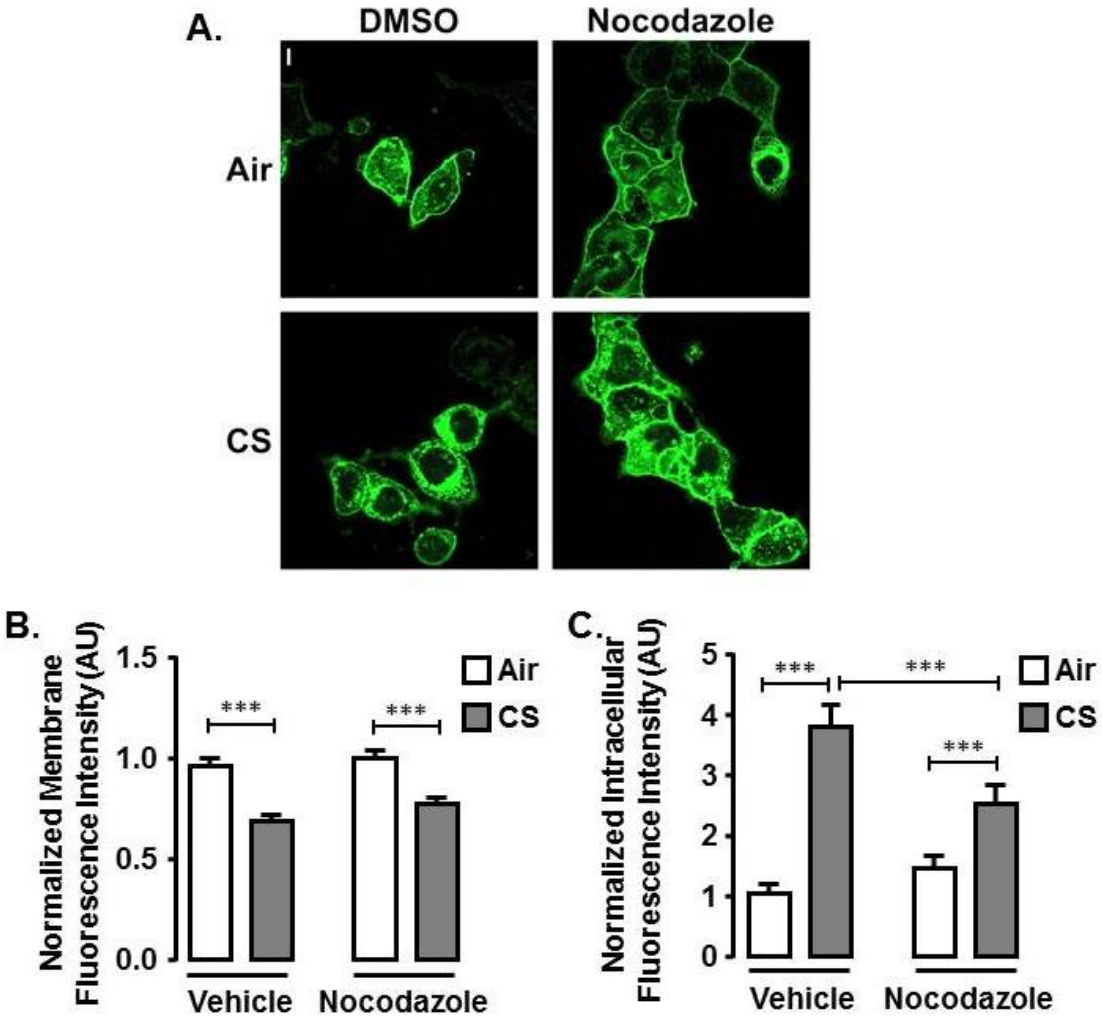

Figure 5-5. Disruption of microtubules alters the course of internalization of CS-exposed CFTR.

HEK293T cells transfected with GFP-CFTR were pretreated with vehicle (0.1% DMSO) or 33 µM nocodazole at 37°C for 30 min. The cells were then exposed to CS or air and incubated at 37°C for 60 min before fixing in 4% PFA. A) Representative confocal images of GFP-CFTR in the presence of vehicle or 33 µM in air and CS exposed conditions. (B) Mean plasma membrane fluorescence intensity in air (open bars) or CS (grey bars) of cells treated with vehicle or 33 µM nocodazole. (C) Mean intracellular fluorescence intensity in air (open bars) or CS (grey bars) of cells treated with vehicle or 33 µM nocodazole (n = 90 - 163 cells from 3 independent experiments). *** $p < 0.001$ by Kruskal-Wallis test with Dunn's multiple comparison post-test. Scale bar = 10 µm.

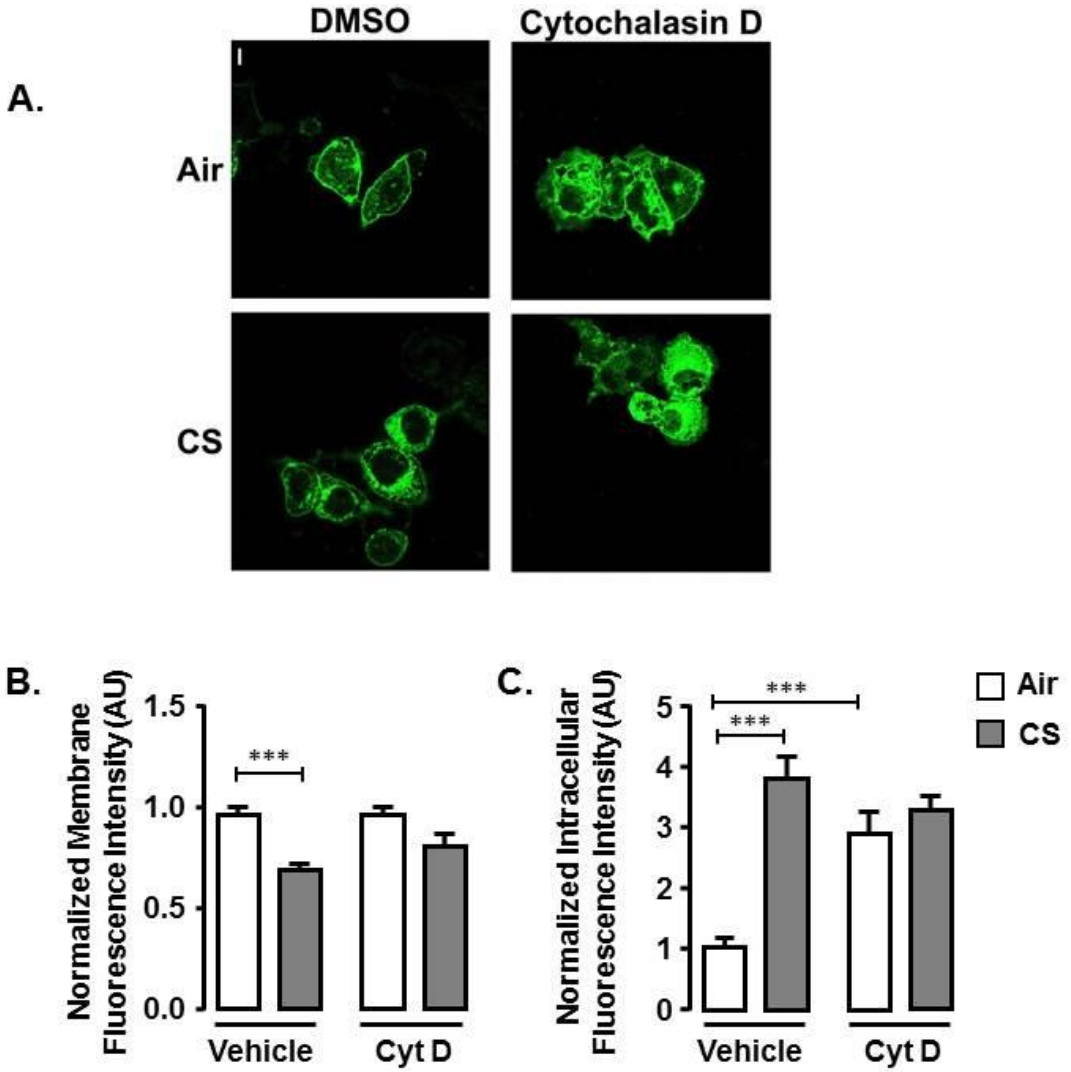

Figure 5-6. Disruption of the cytoskeleton by cytochalasin D prevents CS-induced CFTR internalization.

HEK293T cells were transfected with wt-GFP-CFTR. The cells were pre-treated 48 h after transfection with vehicle (0.02 % DMSO) or 2 µM cytochalasin D at 37°C for 30 and 15 min respectively. The cells were then exposed to air or CS and incubated at 37ºC for 60 min prior to fixing in 4 % PFA. A) Representative confocal images of GFP-CFTR. B) Mean plasma membrane fluorescence intensity in air (open bars) or CS (grey bars) of cells treated with vehicle or 2 µM cytochalasin D. (C) Mean intracellular fluorescence intensity in air (open bars) or CS (grey bars) of cells treated with vehicle or 2 µM cytochalasin D (n = 76 – 163 cells from 3 independent experiments, *** $p > 0.001$ by one-way ANOVA with Tukey's post-test). Scale bar = 10 µm.

5.2.5 More CS-internalized CFTR traffics through the early endosomes than the late or recycling endosomes

In typical CFTR endocytosis following uptake by clathrin coated vesicles, CFTR is trafficked to the early endosomes, and from here is sorted to the late or recycling endosomes (Gentzsch et al., 2004). To the understand effects of CS on this pathway of internalization, colocalization assays utilizing a series of endosomal and organelle markers were performed. Rab5A, a protein primarily expressed in the early endosomes, was transiently co-transfected with GFP-CFTR in HEK293T cells. Following CS exposure, the percentage of GFP-CFTR and rab5A colocalization significantly increased compared to air exposure over time (Figure 5-7). This CS-induced increase was sustained at all time points and peaked at 120 min at 52.3 ± 3.0% (Figure 5-7 B; $p < 0.001$, $n = 71 - 100$ cells). The colocalization rate of air exposed control cells was maintained between 28.6-35.4% across all time points. These data suggest increased uptake of CFTR by early endosomes following smoke exposure. Colocalization of GFP-CFTR with rab7-DsRed, a marker of late endosomes, increased significantly from 23.4 ± 2.6% following air exposure to 32.9 ± 2.1% 30 min following CS exposure and was sustained throughout the 120 min duration (Figure 5-8 B, $p < 0.01$, $n = 73-81$ cells). Furthermore, at all time intervals the percent colocalization of GFP-CFTR with the recycling endosome marker rab11 was not affected by smoke exposure, suggesting that CS-internalized CFTR does not undergo increased recycling, despite increased levels of endocytosis (Figure 5-9). The increase in colocalization of CFTR at the early endosomes post-CS was significantly higher than that of both rab7 and rab11 at all time points (Figure 5-10, $p < 0.001$), indicating that significantly more CFTR traffics through the early endosomes than the late and recycling endosomes.

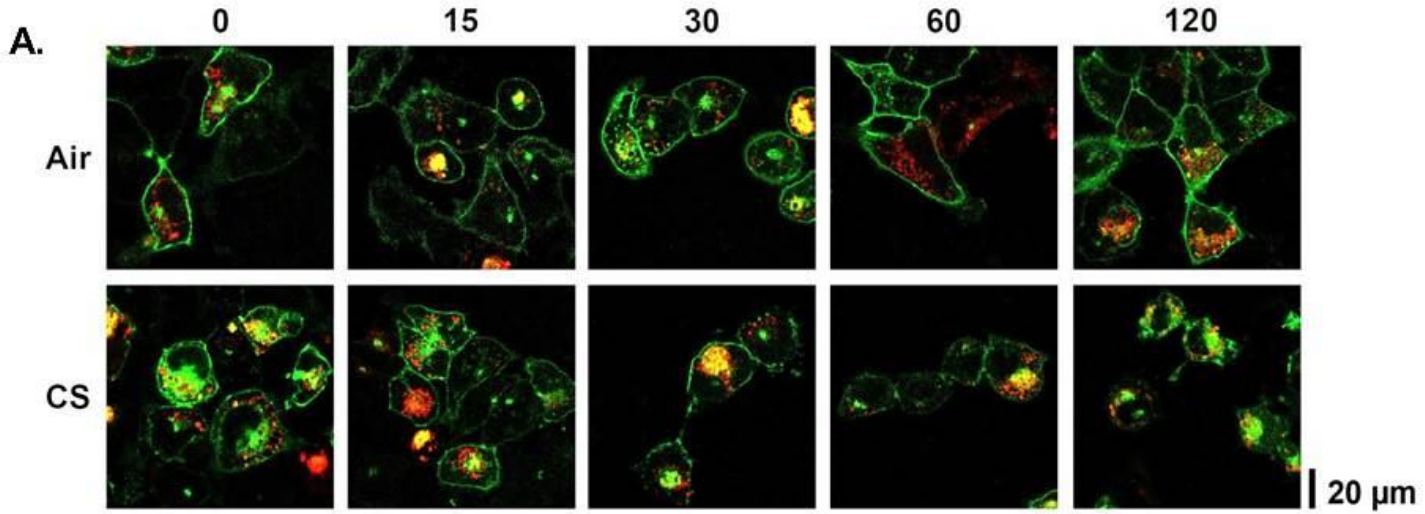

Figure 5-7. Colocalization of CFTR with an early endosomal marker (rab5A) increased after CS exposure.

HEK293T cells transfected with GFP-CFTR and rab5A-dsRed2 were exposed to CS and incubated at different time intervals before fixation. A) Confocal images of air and CS-exposed cells at different time intervals. B) Mean percentages of colocalization were calculated using the LAS AF software (Leica). Percentage colocalization after CS exposure was significantly higher at each time point. *** $p < 0.001$ n = 71 - 108 cells.

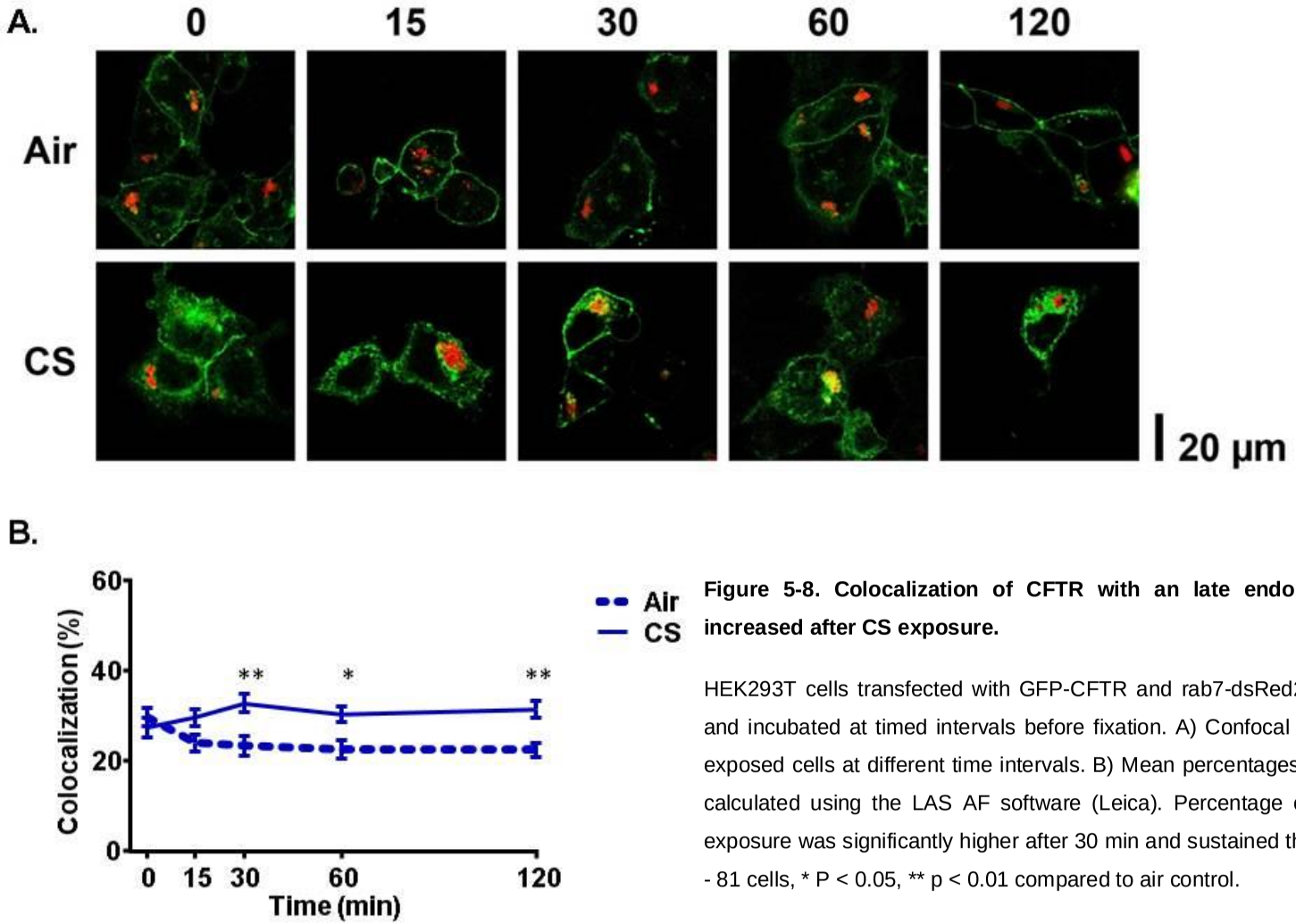

Figure 5-8. Colocalization of CFTR with an late endosomal marker (rab7) increased after CS exposure.

HEK293T cells transfected with GFP-CFTR and rab7-dsRed2 were exposed to CS and incubated at timed intervals before fixation. A) Confocal images of air and CS-exposed cells at different time intervals. B) Mean percentages of colocalization were calculated using the LAS AF software (Leica). Percentage colocalization after CS exposure was significantly higher after 30 min and sustained through 120 min. n = 73 - 81 cells, * $P < 0.05$, ** $p < 0.01$ compared to air control.

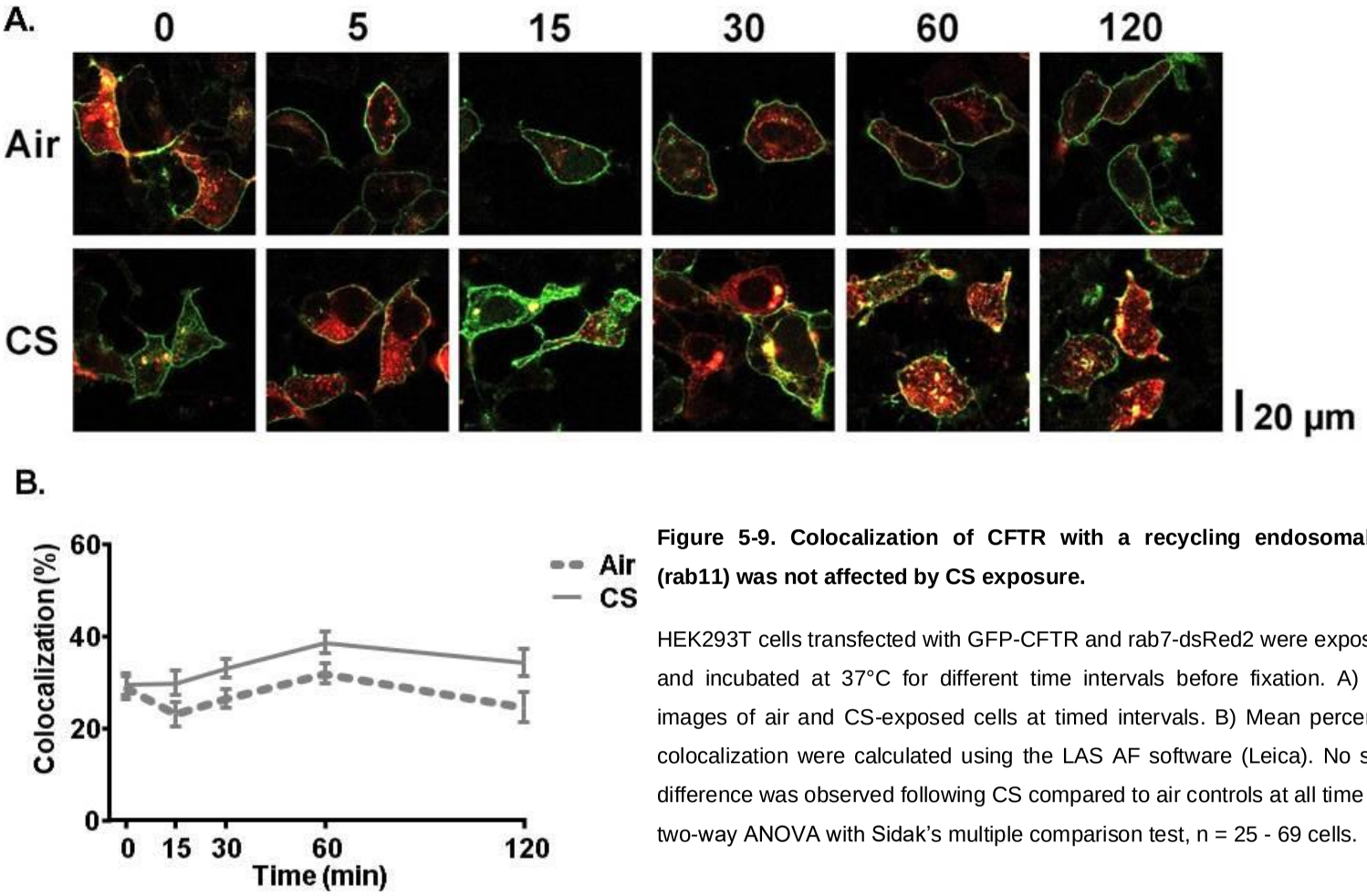

Figure 5-9. Colocalization of CFTR with a recycling endosomal marker (rab11) was not affected by CS exposure.

HEK293T cells transfected with GFP-CFTR and rab7-dsRed2 were exposed to CS and incubated at 37°C for different time intervals before fixation. A) Confocal images of air and CS-exposed cells at timed intervals. B) Mean percentages of colocalization were calculated using the LAS AF software (Leica). No significant difference was observed following CS compared to air controls at all time points by two-way ANOVA with Sidak's multiple comparison test, n = 25 - 69 cells.

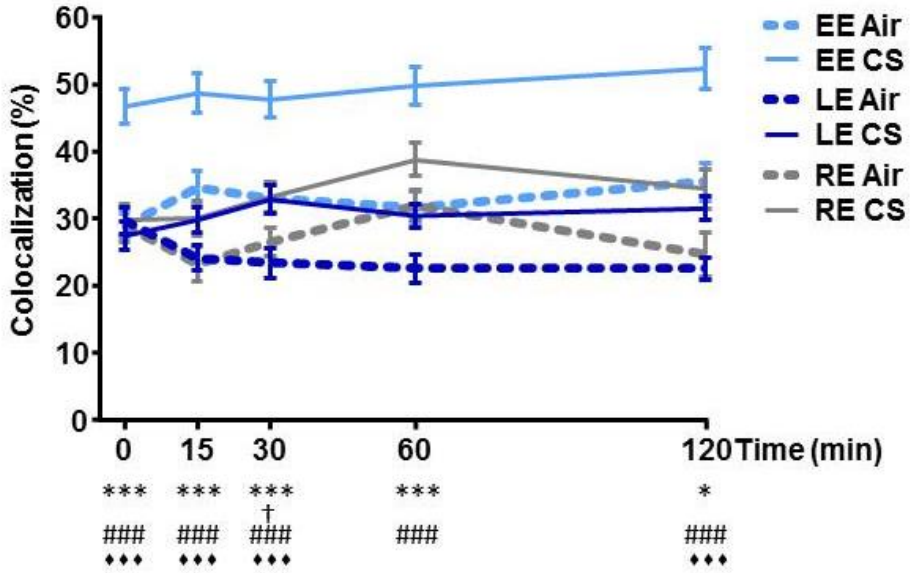

Figure 5-10. More CS-internalized CFTR traffics through the early endosomes than the late or recycling endosomes.

Compiled data from Figure 5-7, Figure 5-8, and Figure 5-9 demonstrates significantly more GFP-CFTR colocalization with rab5A-DsRed than rab7-DsRed or rab11-DsRed. *** = $p < 0.001$ of early endosomes (EE) CS compared to EE air, * = $p < 0.05$ of EE CS compared to EE air, † = $p < 0.05$ of late endosomes (LE) CS compared to air, ### = $p < 0.001$ of EE CS compared to LE CS, ♦♦♦ = $p < 0.001$ EE CS compared to recycling endosome (RE) CS, two-way ANOVA with Sidak's multiple comparison test n = 25 - 108 cells.

5.2.6 CFTR colocalizes with ER and Golgi markers following CS exposure – A hypothesis for retrograde transport

To assess the colocalization of GFP-CFTR in the Golgi apparatus an antibody specific to the *cis*-Golgi protein, GM130, was utilized. Colocalization of GFP-CFTR with the Golgi apparatus significantly increased following CS-exposure compared to air controls from 0-60 min (Figure 5-11; $p < 0.01$, $p < 0.001$, n =43 - 135 cells). To assess the colocalization of CFTR in the ER, HEK293T cells were transiently co-transfected with GFP-CFTR and STIM1-mCherry. Although STIM1 is present primarily in the ER (Smyth et al., 2010), it is not typically used as an ER marker. For this reason, these cultures were immunolabelled with anti-calreticulin, a secondary marker of the ER, to further assess colocalization. Post-CS exposure, both STIM1 (Figure 5-12; $p < 0.01$ at 0 min and $p < 0.001$ through 5-120 min, n = 59 - 143) and calreticulin (Figure 5-13; $p < 0.01$ at 0 min and $p < 0.001$ through 5-120 min, n = 81 - 142) had increased colocalization with GFP-CFTR from 0 – 60 min compared to air controls. Furthermore, the colocalization of both ER markers did not significantly differ from one another (Figure 5-14), suggesting that STIM1 provides a robust marker for the ER. Although CFTR colocalization was significantly increased in both the Golgi and the ER, there was a significantly higher percentage colocalization of CFTR with both ER markers (between 40.0 ± 2.3% and 49.5 ± 2.2%) compared to the Golgi (Figure 5-14; between 17.2 ± 1.3% and 24.6 ± 1.5%).

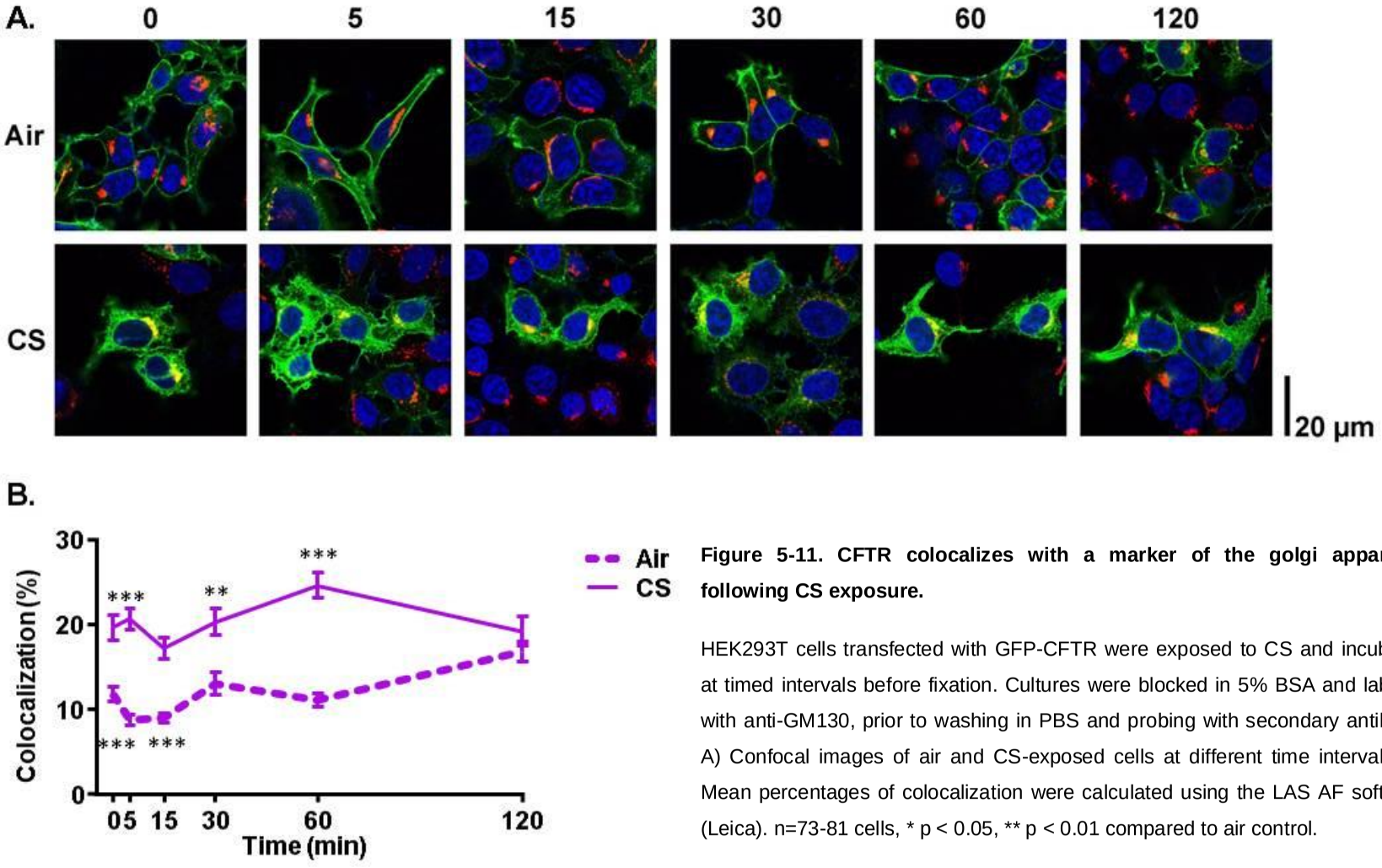

Figure 5-11. CFTR colocalizes with a marker of the golgi apparatus following CS exposure.

HEK293T cells transfected with GFP-CFTR were exposed to CS and incubated at timed intervals before fixation. Cultures were blocked in 5% BSA and labeled with anti-GM130, prior to washing in PBS and probing with secondary antibody. A) Confocal images of air and CS-exposed cells at different time intervals. B) Mean percentages of colocalization were calculated using the LAS AF software (Leica). n=73-81 cells, * $p < 0.05$, ** $p < 0.01$ compared to air control.

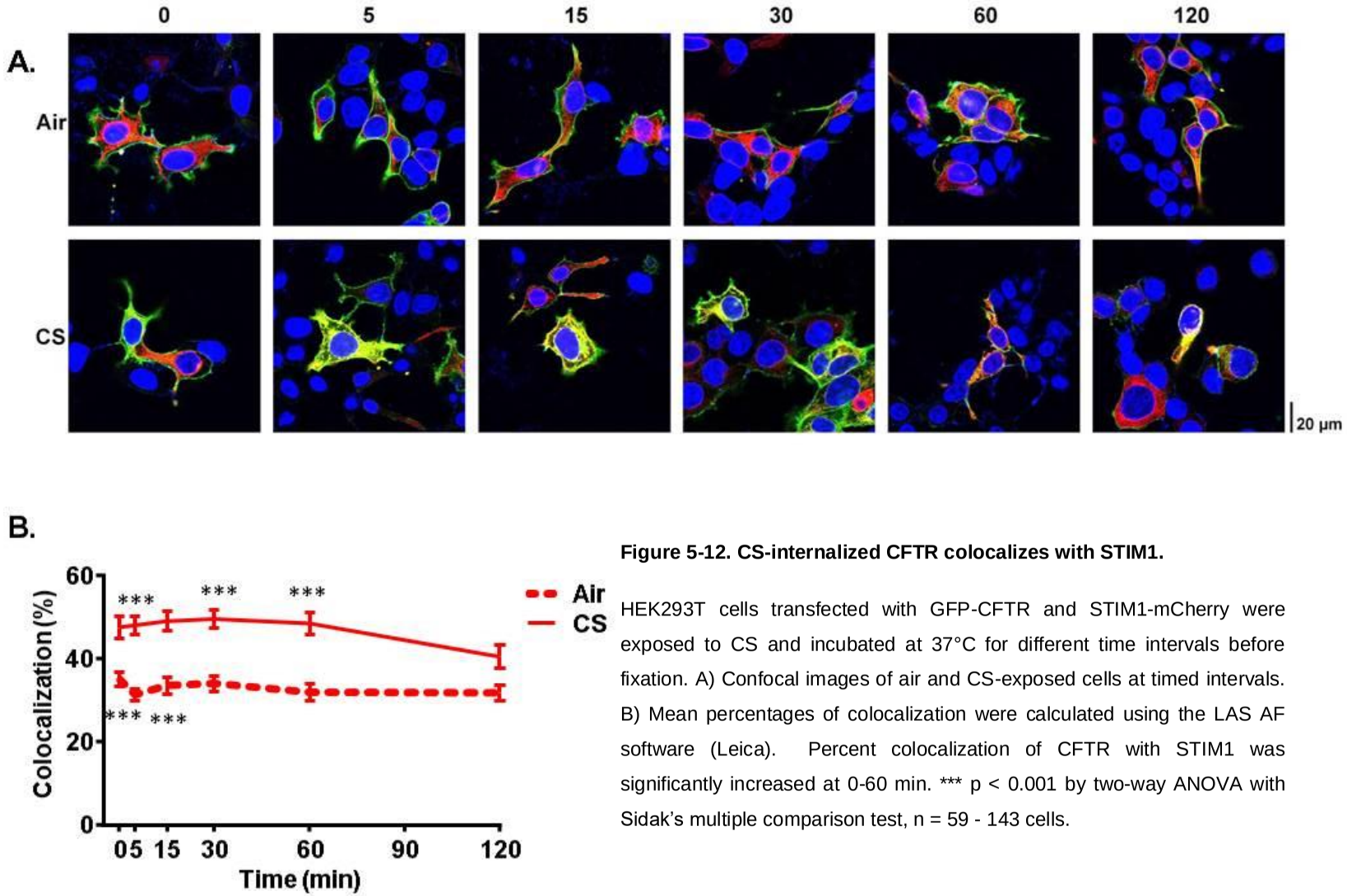

Figure 5-12. CS-internalized CFTR colocalizes with STIM1.

HEK293T cells transfected with GFP-CFTR and STIM1-mCherry were exposed to CS and incubated at 37°C for different time intervals before fixation. A) Confocal images of air and CS-exposed cells at timed intervals. B) Mean percentages of colocalization were calculated using the LAS AF software (Leica). Percent colocalization of CFTR with STIM1 was significantly increased at 0-60 min. *** $p < 0.001$ by two-way ANOVA with Sidak's multiple comparison test, n = 59 - 143 cells.

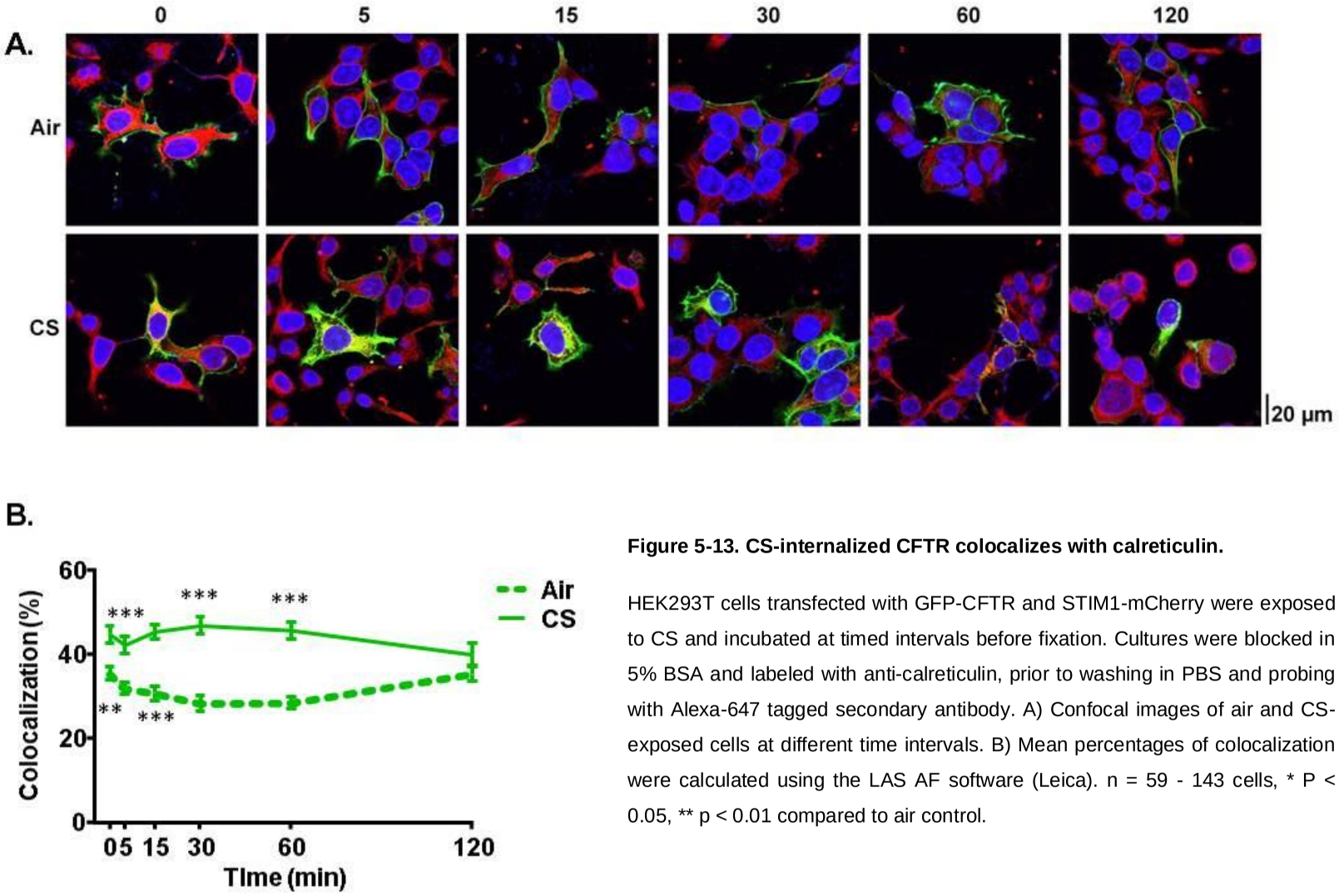

Figure 5-13. CS-internalized CFTR colocalizes with calreticulin.

HEK293T cells transfected with GFP-CFTR and STIM1-mCherry were exposed to CS and incubated at timed intervals before fixation. Cultures were blocked in 5% BSA and labeled with anti-calreticulin, prior to washing in PBS and probing with Alexa-647 tagged secondary antibody. A) Confocal images of air and CS-exposed cells at different time intervals. B) Mean percentages of colocalization were calculated using the LAS AF software (Leica). n = 59 - 143 cells, * $P < 0.05$, ** $p < 0.01$ compared to air control.

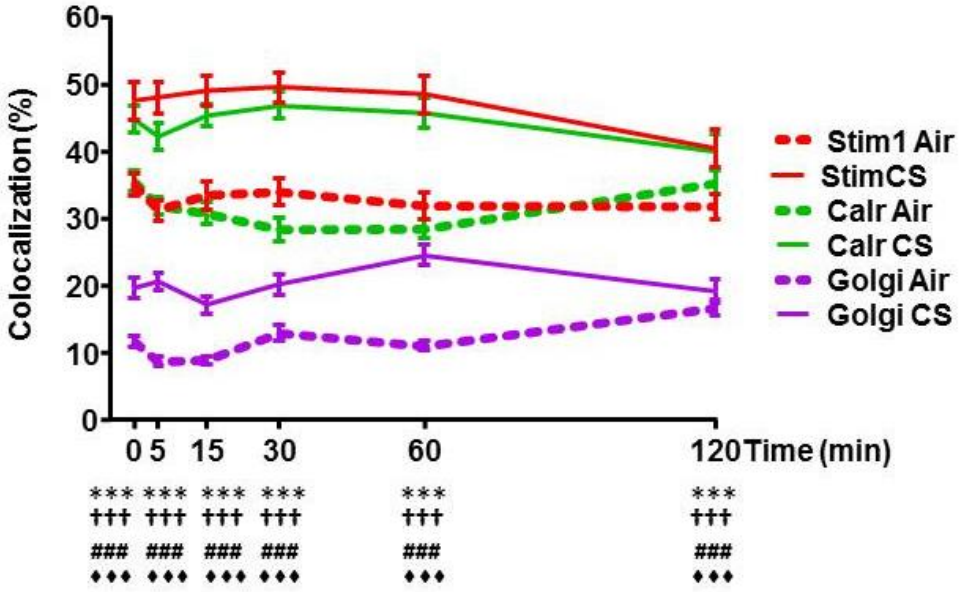

Figure 5-14. CFTR colocalizes significantly more with markers of the endoplasmic reticulum than the Golgi apparatus.

Compiled data from Figure 5-7, Figure 5-8, and Figure 5-9 demonstrates significantly more GFP-CFTR colocalization with rab5A-DsRed than rab7-DsRed or rab11-DsRed. *** = $p < 0.001$ of EE CS compared to EE air, * = $p < 0.05$ of EE CS compared to EE air, † = $p < 0.05$ of LE CS compared to air, ### = $p < 0.001$ of EE CS compared to LE CS, ♦♦♦ = $p < 0.001$ EE CS compared to RE CS two-way ANOVA with Sidak's multiple comparison test. n = 25 - 108 cells.

5.3 Discussion

Substantial research has been carried out into the endocytic pathway of CFTR as described in section 1.4.3. However, the endocytic machinery required for the rapid internalization of CFTR by CS has yet to be determined. Thus, in this chapter the abnormal endocytic pathway of GFP-CFTR following CS exposure was investigated.

Pre-treatment of HEK293T cells expressing GFP-CFTR with hypertonic sucrose had no effect on the cellular distribution of CFTR in air exposed control cells, but did blunt the CS-induced internalization of CFTR. Although hypertonic sucrose has been shown to disrupt the formation of clathrin lattices, it is also known to prevent endocytosis by other pathways including calveolae-mediated endocytosis and pinocytosis. Thus, the role of clathrin in CS-mediated CFTR internalization was assessed using colocalization studies. Colocalization of overexpressed fluorescently tagged CFTR and clathrin light chain increased significantly following CS exposure. Furthermore, inhibition of dynamin, a GTPase involved in the scission of clathrin coated-vesicles from the plasma membrane, ablated the internalization of CFTR by CS. These data were complemented by the use of dominant negative K44A-dynamin. Although these data provide clear evidence that CS-induced CFTR internalization is mediated by clathrin and dynamin, the data was limited by the fact that no inhibitors specific to calveolae-mediated endocytosis were utilized. Thus, whilst clathrin and dynamin are necessary for clathrin-mediated endocytosis, other endocytic pathways such as calveolae-mediated endocytosis cannot be ruled out.

CFTR plasma membrane stability, activity, endocytosis and recycling is sensitive to changes in both microfilament and microtubule regulation. Although nocodazole was unable to prevent the removal of CFTR from the plasma membrane by CS, the internalized portion of CFTR was significantly reduced, and internal CFTR displayed a different pattern of expression to that of vehicle exposed CFTR. While it is obvious that CFTR can still be internalized by CS when the microtubule network is disrupted, the pathway taken by the internalized CFTR is altered, and may be explained by the reliance of endosomal trafficking on the microtubule cytoskeleton. When HEK293T cells expressing GFP-CFTR, were pre-treated with cytochalasin D, an inhibitor of actin polymerization, GFP-CFTR was located internally. This data is consistent with published data by the Ganeshan group (2007), showing that CFTR is not trafficked correctly after disruption of the

actin cytoskeleton. Firstly, like microtubules, the actin cytoskeleton is involved in the function and trafficking of the endosomal pathway (Gauthier et al., 2007, Tanabe et al., 2011). Thus, disruption of the actin cytoskeleton may prevent movement of CS-exposed CFTR through the CS specific endocytic pathway. Secondly, the presence of large amounts of intracellular CFTR in the presence of cytochalasin D alone may overload the internalization pathway, and thus prevent further internalization of CFTR by CS.

Internalized CFTR has been shown to localize in early, late and recycling endosomes (Gentzsch et al., 2004). Here, significantly more CFTR accumulated in the early endosomes compared to the late and recycling endosomes following CS exposure, suggesting that CS may cause disruption of the normal maturation of early endosomes, leading to abnormal intracellular accumulation of CFTR. Interestingly, upon overexpression of Rab11, the images of CFTR following CS exposure appear to show increased localization of CFTR to the plasma membrane, suggesting that the presence of increased levels of Rab11 may assist in the recycling of CS-internalized CFTR to the plasma membrane. This thesis has specifically focused on underpinning the mechanisms behind internalization of CFTR through endocytosis. However, these data suggest that normal levels of recycling are not enough to return CS-internalized CFTR to the plasma membrane. There are a number of hypothesis that could explain this recycling effect. Firstly, the recycling pathway may be dysfunctional after CS exposure, preventing CFTR from reaching the recycling endosomes, but the function is restored upon overexpression of rab11. Secondly, since a large accumulation of CFTR in the early endosomes is observed, the defect could be further upstream in the endocytic pathway, i.e. at the early endosomes, preventing CFTR from leaving the early endosomes in its typical manner. Lastly, simply the large volume and rate of CFTR internalized by CS may overwhelm the recycling system, preventing efficient recycling of CFTR back to the plasma membrane. Further investigations into the effect of CS on recycling may reveal important information regarding the intracellular accumulation of CFTR and reduced potential Cl^- secretion by smoke.

Unexpectedly, CFTR dramatically increased colocalization with two different markers of the endoplasmic reticulum following CS exposure, suggesting that CS causes internalized CFTR to reside in the endoplasmic reticulum. Transport of plasma membrane proteins to the ER, termed retrograde transport, can occur via three different pathways. At the early endosome, the secretory and endocytic routes of plasma membrane proteins converge. A large body of evidence suggests

that endosomes form contact sites with the ER to exchange cholesterol and to allow the endocytic cargo to be modified by proteins located in the plasma membrane of the ER (Friedman et al., 2013). Furthermore, contact between early endosomes and the ER can be maintained as the organelles are trafficked along microtubules (Friedman et al., 2010). These direct contact sites may also allow the transport of plasma membrane CFTR to the ER to allow the modification of any CS-mediated structural changes. However, despite the documented contact sites between the early endosomes and the ER, transfer of mammalian proteins from the plasma membrane *directly* to the ER has not been recorded. Further experiments, including immunolocalization by confocal and super resolution microscopy, would determine whether CS increases endosomal-ER contact sites and give more insight into this phenomenon.

The second potential pathway of retrograde transport from the plasma membrane to the ER may be explained by the observed colocalization of CFTR with the *cis*-Golgi marker GM130 following CS exposure. Retrograde transport between the endosomes (early and late) and the Golgi apparatus has been well documented, primarily in the context of bacterial toxins, transmembrane enzymes and cargo proteins. The *trans*-Golgi network receives approximately 5% of glycoproteins from the plasma membrane (Duncan and Kornfeld, 1988). In mammalian cells, transmembrane enzymes and cargo proteins such as furin and the mannose-6-phosphate receptor are shuttled bi-directionally between early and late endosomes and the Golgi apparatus. Furthermore, in *S. cerevisiae*, chitin synthase-III has been shown to cycle between the plasma membrane, the endosomes and the Golgi apparatus, allowing regulated expression of the enzyme. Not only does retrograde trafficking occur between the plasma membrane, the endosomes and the Golgi, bidirectional trafficking between the Golgi and the ER is also well documented, and is thought to be dependent on COPI and COPII vesicles. Thus, a prospective pathway of CFTR internalization by CS may begin by clathrin-mediated endocytosis at the plasma membrane, followed by trafficking to the early endosomes. From here, CFTR can either be trafficked through the late endosomes or directly to the Golgi apparatus, and finally to the endoplasmic reticulum.

Either of the two pathways of retrograde transport, through early endosome-endoplasmic reticulum contacts, or through the Golgi apparatus are plausible hypotheses for the deposition of plasma membrane internalized CFTR at the endoplasmic reticulum. There are two theories as to how CS could cause such an

abnormal endocytic response. Firstly, in addition to the dephosphorylation of CFTR by CS identified in Chapter 4.0, CS may further modulate the structure of CFTR in such a way that leads to the retrieval of CFTR to the endoplasmic reticulum for correction. Secondly, as discussed previously, overloading of internalized CFTR at the early endosomes and/or dysfunction of the early or recycling endosomes may prevent CFTR from being cleared in its normal manner by recycling to the plasma membrane, or degradation at the lysosomes. We have previously shown that CS causes release of calcium from lysosomes (Rasmussen et al., 2014) as well as an increase in lysosomal pH (unpublished data). These phenomena may be responsible for dysfunction of the lysosomes which could prevent CFTR delivery to the lysosomes for degradation, and subsequently cause upstream dysfunction of endosomal trafficking.

Despite the clear colocalization of CFTR at the endoplasmic reticulum following CS exposure, the data presented here is limited in that it is assumed that the intracellular accumulation of CFTR has been internalized from the plasma membrane. This is likely correct due to the thorough work of Clunes *et al.* (2012), who demonstrated by tracking plasma membrane CFTR through surface labelling, that CFTR is rapidly internalized by smoke. Surface labelled internalized CFTR in BHK^{CFTR} cells by Clunes and colleagues presented an identical expression pattern to that seen here of smoke exposed GFP-CFTR transfected HEK293T cells, thus allowing the conclusion that the internal CFTR present in HEK293T transfected cells is internalized. This is further confirmed by a reduction in cell surface biotinylated CFTR in CS exposed HBECs in section 4.2.5.

Further experiments must therefore be performed in order to confirm the retrograde trafficking of CFTR to the endoplasmic reticulum by CS. For example, if CFTR is internalized from the plasma membrane to the endoplasmic reticulum, the presence of mature, fully glycosylated CFTR in the endoplasmic reticulum would provide a clear indication that retrograde trafficking had occurred. In fact, mature, fully glycosylated CFTR is found in the sarcoplasmic reticulum of airway smooth muscle, and is reported to play a role in the regulation of airway smooth muscle tone (Cook et al., 2016). However, they did no determine the pathway of mature CFTR into the sarcoplasmic reticulum. Ultimately, pulse chase experiments to allow the tracking of CFTR through the cellular compartments after smoke exposure would provide the clearest indication of the retrograde pathway undertaken by smoke exposed CFTR.

The major findings of this chapter are summarised below and in Figure 5-15.

- Inhibition of CS-induced CFTR internalization by hypertonic sucrose and increased colocalization of CFTR with clathrin light chain following smoke exposure suggest that CS-internalized CFTR is taken up by clathrin coated vesicles.

- CS-induced CFTR internalization was blunted by dynasore and overexpression of a dominant negative dynamin plasmid, suggesting that CFTR internalization by CS is dynamin-dependent.

- Nocodazole and cytochalasin D did not ablate CS-induced CFTR internalization but did result in an altered pathway of internalization.

- CS-internalized CFTR colocalized predominantly in the early and late endosomes, the Golgi apparatus, and the endoplasmic reticulum, but not in recycling endosomes.

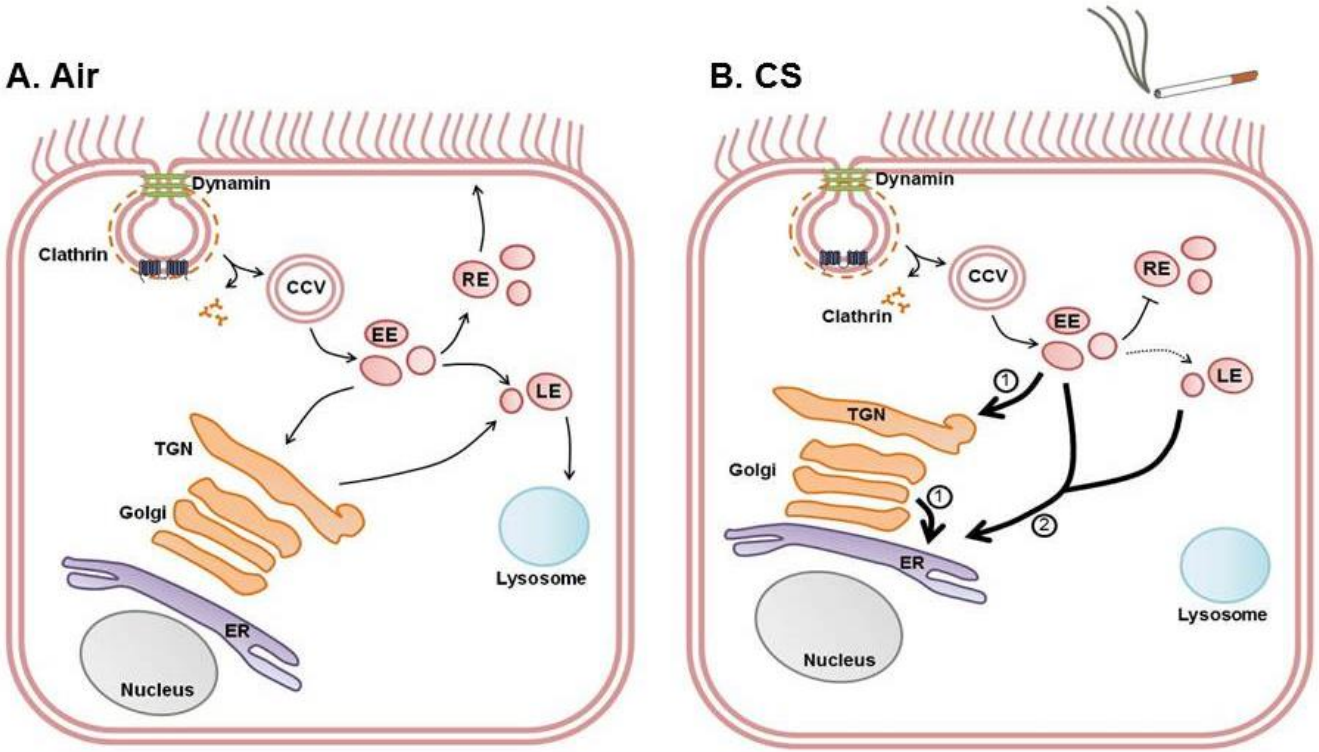

Figure 5-15. A proposed model for the endocytic pathway of CS exposed CFTR.

In normal cells, CFTR is taken up in clathrin coated vesicles (CCV), which are cleaved off the plasma membrane by dynamin. CFTR is then trafficked to the early endosomes and sorted for either recycling to the plasma membrane or trafficking to the late endosomes and onto the lysosomes for degradation. In CS exposed cells, CFTR is taken up by clathrin coated vesicles, cleaved off by dynamin and trafficked to the early endosomes. From here, no CFTR is sent to the recycling endosomes, or to the lysosomes, rather CFTR is trafficked in a retrograde manner back to the ER. There are too proposed pathways for CS-induced retrograde trafficking of CFTR. (1) Direct ER-EE contacts allow the passage of CFTR to the ER. (2) CFTR from the EEs and/or LEs is trafficked to the TGN, through the golgi to the ER.

6.0 General discussion

6.1 Summary of main findings

In this thesis, I sought to investigate the cellular mechanisms behind CS-induced CFTR internalization. The majority of the experiments used in this study were performed using transfected HEK293T cells to observe the effect of CS on CFTR trafficking. I found that not only is CS-induced CFTR internalization traceable over time, but it can also be manipulated by mutation of CFTR, and by a series of pharmacological inhibitors. The data provided in this thesis contributes to the growing knowledgebase centred on understanding the diminution of Cl^- secretion by CS in a variety of cell types, patients with COPD, and smokers (Kreindler et al., 2005, Welsh, 1983, Cantin et al., 2006b, Sloane et al., 2012, Clunes et al., 2012).

Previous work from our laboratory has demonstrated that CS caused a rapid internalization of CFTR in BHK cells stably expressing CFTR, HEK293T cells, Calu-3 cells and in polarised HBECs. The reduction of plasma membrane CFTR leads to a decrease in Cl^- secretion and ASL depth (Clunes et al., 2012). Here, the internalization of GFP-tagged CFTR was followed over time, and quantified by taking measurements of both plasma membrane, and intracellular fluorescence intensities. CFTR indeed internalized rapidly, plasma membrane fluorescence intensity decreased with a half-life of 10.5 min, and intracellular fluorescence intensity increased with a half-life of 27.7 min. In an effort to define the cellular processes that were necessary for CS-induced internalization, FRET was utilized to determine the importance of CFTR-CFTR interactions. Since CFTR is thought to become insoluble inside the cell following smoke exposure (Clunes et al., 2012), it was hypothesized that CFTR-CFTR FRET efficiency would increase post-CS exposure, like that of other aggregated proteins such as nocodazole-treated P23H-rhodopsin (Rajan et al., 2001). Interestingly, intracellular FRET efficiency was decreased compared to that of plasma membrane FRET efficiency in both air and CS exposed conditions, indicating that the CFTR molecules actually decrease in proximity upon internalization or change their orientation. However, whether a decrease in CFTR-CFTR interactions upon internalization is specific to the smoke response, or if it is a function of normal endocytosis remains to be seen.

To determine the domains of CFTR required for CS-induced internalization, two truncation mutants of CFTR were produced to remove the endocytic motifs, and to additionally remove NBD2 from the structure of CFTR. Interestingly, these

mutations had no effect on the CS-induced removal of CFTR from the plasma membrane, or the intracellular deposition of the mutants compared to wt-CFTR, suggesting that NBD2, and the C-terminal endocytic motifs in this region of CFTR are not required for CS-induced internalization. This data is interesting in that the tyrosine-based motif has been identified as a necessary signal on the C-terminus of CFTR for AP2 recruitment of clathrin coated vesicles (Weixel and Bradbury, 2000). As the data in Chapter 5 identify clathrin coated vesicles as the main form of vesicle for the uptake of CS-internalized CFTR into the cell, the fact that the typical endocytic motifs are not required leads to the speculation that another form of signalling, specific to CS-induced CFTR internalization, may be required for the uptake of CFTR into clathrin coated vesicles. Interestingly, in Chapter 4, CS caused dephosphorylation of CFTR. Furthermore, phosphorylation of CFTR by PKA prevented CS-induced internalization. As discussed in section 4.3, forskolin-induced PKA activity has been previously been identified as an antagonist of endocytosis in CFTR expressing T84 cells (Bradbury et al., 1992). Thus, these data suggest that dephosphorylation of CFTR may in fact be a signal for CS-induced internalization by clathrin-mediated endocytosis.

The data indicating that CFTR is dephosphorylated by smoke was verified by the use of a CFTR mutant with 15 consensus sites removed from the R domain and NBD1 and is not phosphorylated by PKA. Interestingly, immunostaining of these cells with a CFTR specific antibody after air exposure (control) demonstrated a large amount of intracellular $CFTR^{15SA}$ present within the cytosol. Furthermore, internalization of $CFTR^{15SA}$ was actually reduced compared to that of wt-CFTR. These data provide further evidence that dephosphorylation may be an important signalling factor for internalization, and lead to the speculation that dephosphorylation of CFTR may be a signal for internalization

The effects of CS on the trafficking of other plasma membrane ion channels was also investigated. Interestingly, Ano1 remained at the plasma membrane upon smoke exposure, while Orai1 was internalized. Given that dephosphorylation of CFTR may be an important signalling event leading to the internalization of CFTR by smoke, and that Orai1 has putative phosphorylation sites for both PKA (Howe, 2011) and PKC (Kawasaki et al., 2010), whilst Ano1 inhibitors of PKA and PKC had no effect on Ano1-mediated Cl^- secretion (Tian et al., 2011), it is convenient to speculate that CS may cause changes to the phosphorylation status of Orai1, but not Ano1.

As mentioned previously, inhibition of CS-induced CFTR internalization with hypertonic sucrose, and colocalization with clathrin light chain identified clathrin-mediated endocytosis as a potential major pathway for CS-induced CFTR internalization. Internalization was also dependent on dynamin. Once taken up by the cell, colocalization assays with endosomal markers revealed that a large amount of CFTR accumulated in the early endosomes compared to the late and recycling endosomes. Furthermore, CFTR colocalization with markers of the endoplasmic reticulum, STIM1 and calreticulin, dramatically increased following CS exposure leading to the speculation that internalized CFTR is trafficked retrograde from the plasma membrane to the endoplasmic reticulum. As discussed in section 5.3, presence of CFTR in the late endosomes and Golgi apparatus give some indication that the retrograde pathway of internalization may be from the early endosomes, and either directly to the Golgi, or through the late endosomes from the Golgi, and finally from the Golgi to the endoplasmic reticulum. Although the concept of CFTR retrograde trafficking through direct contact points between the early endosomes and the endoplasmic reticulum cannot be ruled out. Data from our laboratory demonstrates that CS causes lysosomal calcium release (Rasmussen et al., 2014) and an increase in lysosomal pH (unpublished data). These data provide first insights into the concept that dysregulation of the lysosomal and endosomal pathway may play a role in the abnormal endocytic route of CFTR to the endoplasmic reticulum following CS exposure. Additionally, both the microtubule and the actin cytoskeleton are important for the movement and function of the endosomal pathway. Inhibition of both of these components caused disruption of CS-induced CFTR internalization pathway, further implicating the importance of endosomal function in CS-induced CFTR internalization.

6.2 Clinical relevance of findings for patients with cigarette smoke related airway disease

CS exposure leads to diminished CFTR-mediated Cl^- secretion in smokers and patients with COPD alike. This decrease in Cl^- secretion is associated with ASL dehydration, an increase in mucus percent solids content, mucus accumulation, and reduced mucocilliary clearance. This phenotype, as described in section 1.5.2, closely resembled that of patients with CF. Given the recent success of CFTR specific correctors and potentiators in the treatment of CF patients, and the identification of dysregulated CFTR as a potential cause for COPD, the use of CFTR potentiators and correctors in patients with COPD may improve Cl^- secretion

and improve the mucus defects observed in these patients. To this effect, Sloane and colleagues have demonstrated that the use of ivacaftor, a CFTR potentiator, increases CFTR currents in both vehicle control and CS extract treated cells. Furthermore, ivacaftor increases the CS extract-induced reduction in ASL height and improves mucocilliary transport rates measured by assessing the mobility of fluorescent beads on primary epithelial cells. These data provide robust primary evidence for the use of therapeutics to improve Cl^- transport and mucocilliary clearance in patients with Cl^- secretion compromised by smoke. However, studies by Martina Gentzsch's group demonstrated that while ivacaftor improved function in G551D cells, ivacaftor reduced wt-CFTR levels and function (Cholon et al., 2014). Furthermore, ivacaftor is an extremely expensive drug, with per patient costs of almost $300,000 per year (Condren and Bradshaw, 2013). Thus, the search for cheaper and more potent treatments to improve CFTR function in patients with COPD continues. As such, several compounds in this thesis function to reduce CFTR internalization by CS, and would therefore provide potential therapies of smoking related disease. For example, in section 4.2.3, forskolin blunted intracellular accumulation of CFTR by approximately 48%. Forskolin is an FDA approved compound used in the treatment of asthma (Gonzalez-Sanchez et al., 2006). Thus, the use of forskolin in patients with CS diminished Cl^- may provide a novel treatment for improved ASL hydration and mucocilliary clearance.

6.3 Future experiments

Inevitably, there are a wide range of future experiments that could be performed that would provide further insight into the effects of CS on CFTR trafficking, and strengthen the conclusions made in this thesis. A large majority of experiments in this thesis were performed using overexpression of CFTR in HEK293T cells. While this cell line provides a convenient model for the genetic and pharmacological manipulation of overexpressed proteins, there are a number of limitations that stem from the interpretation of data from immortalized cell lines. For instance, even within the same cell type, differing protocols can produce variability in results. For example, $CFTR_{inh}172$ is able to fully abolish FSK-mediated CFTR currents in transiently transfected HEK293 cells (Mondini et al., 2012). However, in stably transfected HEK293 cells, $CFTR_{inh}172$ is able to blunt forskolin-mediated CFTR currents but not fully abolish it (Domingue et al., 2014). Furthermore, HEK293T cells provide a reductionist model for the study of CFTR. That is, many endogenous proteins that found *in vivo* in airway epithelial cells are not expressed in HEK293T

cells. While HEK293T cells provide an excellent platform for studying the effects of CS on CFTR in isolation, the lack of endogenous secretory and absorptive ion channels, as well as differential expression of regulatory proteins may induce a dissimilar response to that of native epithelia. Thus, reproduction of these data on a fully differentiated airway epithelial cell line would provide robust validation that the mechanisms of CFTR internalization identified in this thesis are recapitulated in native cells. Furthermore, measurement of ASL depth to test the effects of pharmacological inhibitors used in this study, such as dynasore, forskolin, and hypertonic sucrose, on CS-induced ASL dehydration would provide a first step to understanding the functional effects of inhibiting CS-induced CFTR internalization in secretory airway epithelial cells. Additionally, testing the inhibition of CS-induced CFTR internalization *in vivo* would provide valuable insight into whether the use of these inhibitors would prevent CS-induced reduction in Cl^- secretion, and subsequently a relief from symptoms associated with this response including mucus accumulation and inflammation.

Much of the work in this thesis was obtained by confocal microscopy. Previous studies of CFTR internalization performed using cell surface biotinylation demonstrated that normal endocytic rates of CFTR internalization are between 5-7% per minute (Lukacs et al., 1997, Prince et al., 1994, Silvis et al., 2003). A time course of CS-induced CFTR internalization by cell surface biotinylation would thus allow the comparison of native and CS-induced endocytosis. In a study in Furthermore, direct comparison between the rate of CS-induced internalization in HEK293T cells versus polarized airway epithelial cells would provide further evidence to confirm that HEK293T cells are an appropriate model for monitoring the CS effects on CFTR.

Confocal imaging of fluorescently tagged proteins is limited in that it is difficult to track a particular pool of CFTR over time. Moreover, the CS-induced decrease of CFTR from the plasma membrane measured during confocal imaging of GFP-tagged CFTR was substantially smaller than the increase in intracellular accumulation of CS exposed CFTR. These data lead to the speculation that the removal of CFTR from the plasma membrane may be masked by recycling of subapical CFTR back to the plasma membrane, and/or by the delivery of nascent CFTR to the plasma membrane. There are a number of experiments that could be performed to dissect the CS effects on CFTR trafficking. Firstly, the use of cyclohexamide to inhibit protein synthesis of nascent CFTR would reveal whether the removal of CS-exposed CFTR from the plasma membrane is masked by

exocytosis. Secondly, an interesting study by Gergley Lukacs group utilized the pH-sensitive fluorophore FITC conjugated to anti-mouse F_{ab} and anti-HA primary antibody to label surface CFTR. The internalization of CFTR at real time in live cells was imaged. The presence of pH sensitive FITC allowed for the differentiation of the endocytic compartments by their specific internal pH (Barriere et al., 2009). This technique would be extremely useful to further analyze the internalization pathway of CS exposed CFTR in real time. Furthermore, monitoring the internal pH would provide critical information towards the function of these vesicles following CS. Since our laboratory has demonstrated that lysosomal pH is increased following CS exposure (unpublished data), determining pH changes in other endocytic vesicles would be extremely informative. Colocalization of CFTR with markers of the endoplasmic reticulum following CS exposure suggest that CFTR may be trafficked in retrograde manner from the plasma membrane to the endoplasmic reticulum. Surface labeling CFTR in this manner would also allow the visualization of retrograde trafficking of CFTR to the endoplasmic reticulum.

Additionally, the presence of mature CFTR in the endoplasmic reticulum could be investigated by isolating the endoplasmic reticulum by differential centrifugation. Only immature, core glycosylated CFTR is typically found in the endoplasmic reticulum, so identification of mature, fully glycosylated CFTR here would be indicative of retrograde transport. However, it cannot be ruled out that CS may cause the removal of complex glycans from the extracellular face of CFTR, which would prevent the differentiation of nascent CFTR, and CFTR that has been trafficked to the plasma membrane and affected by smoke. Thus, control experiments, testing for the effects of CS on complex glycosylation must additionally be performed.

Data in this thesis demonstrated that both CFTR and Orai1 are internalized by smoke, whilst Ano1 remains at the plasma membrane. Reproducing the data presented with Orai1 would allow determination of the cellular mechanisms behind Orai1 internalization and would determine whether Orai1 is internalized by the same mechanisms as CFTR, or whether the CS response of different plasma membrane proteins is more complex. Furthermore, although it has been determined previously that CS exposure does not affect SOCE (Rasmussen et al., 2014). Functional experiments to determine the effects of Orai1 internalization on primary airway epithelial cells and *in vivo* may reveal pathologic effects of Orai1 dysregulation in smokers and patients with COPD.

The constituents of CS are extremely complex with over 7000 compounds present in CS (USDHHS, 2010). It is therefore not surprising that the results presented in this study regarding the effects of CS on CFTR are themselves complex. Individual components of CS have been shown to have differing effects on CFTR and other CS-mediated responses (Alexander et al., 2012, Rennolds et al., 2010). For example, exposure of primary murine nasal septal epithelial cultures to concentrations of acrolein representative of concentrations of acrolein in the airways of smokers (~100 μM) surprisingly caused a significant increase in apical chloride secretion. However higher concentrations of acrolein (300 μM) actually inhibited FSK-mediated CFTR current (Alexander et al., 2012). Furthermore, cadmium decreases both total CFTR protein expression and biotinylated surface levels of CFTR in Calu-3 cells (Rennolds et al., 2010). CS is highly oxidizing (Cantin et al., 2006b), and oxidative stress decreases CFTR function (Cantin et al., 2006a). Thus, screening other compounds found in CS should be performed to determine which constituents of CS are responsible for CS-induced internalization. Particularly since the mechanisms of CFTR internalization in response to smoke are extremely complex, as highlighted in this thesis, differing responses of CFTR to individual components of CS may provide further elucidation of the different cellular and endocytic components of CS-induced CFTR internalization. In addition to traditional cigarettes, new and emerging tobacco products are being produced at an extremely fast rate. E-cigarettes are becoming an extremely common form of smoking. They are promoted as safer than generic traditional cigarettes, and are even used as a tool to quit smoking in some countries (Rowell and Tarran, 2015). Investigation into the effect of e-cigarette smoke on CS-induced internalization would provide important predictions for the effects of e-cigarettes on lung function and mucus accumulation.

6.4 Final conclusions

The present work has focused on assessing of the cellular mechanisms leading to internalization of CFTR by CS. Thus, we conclude that CS-induced internalization of CFTR is rapid, with a half-life of intracellular accumulation of 27.7 min. Furthermore, internalization of CFTR by CS does not require C-terminal endocytic motifs. However, an alternative signal by dephosphorylation of the protein leads to its internalization, which is preventable by forskolin-mediated phosphorylation. Much like native CFTR, CS-induced CFTR internalization occurs through a clathrin- and dynamin-dependent pathway, but once internalized, CFTR is trafficked in a retrograde manner, through the early and late endosomes and the Golgi apparatus to the endoplasmic reticulum. Further investigation of these mechanisms on the function of CFTR in a primary airway epithelial cell line or in mammalian tissue would provide useful insight into the role of these pathways in a more system which is more representative of CFTR pathophysiology *in vivo,* and provide a platform for the production of therapeutics to allow treatment CFTR dysfunction in smoking related airway disease.

7.0 References

AGIUS, A. M., SMALLMAN, L. A. & PAHOR, A. L. 1998. Age, smoking and nasal ciliary beat frequency. *Clin Otolaryngol Allied Sci,* 23**,** 227-30.

ALEXANDER, N. S., BLOUNT, A., ZHANG, S., SKINNER, D., HICKS, S. B., CHESTNUT, M., KEBBEL, F. A., SORSCHER, E. J. & WOODWORTH, B. A. 2012. Cystic fibrosis transmembrane conductance regulator modulation by the tobacco smoke toxin acrolein. *Laryngoscope,* 122**,** 1193-7.

AMEEN, N., SILVIS, M. & BRADBURY, N. A. 2007. Endocytic trafficking of CFTR in health and disease. *J Cyst Fibros,* 6**,** 1-14.

AMEEN, N. A., MARINO, C. & SALAS, P. J. 2003. cAMP-dependent exocytosis and vesicle traffic regulate CFTR and fluid transport in rat jejunum in vivo. *Am J Physiol Cell Physiol,* 284**,** C429-38.

ANDERSON, M. P., BERGER, H. A., RICH, D. P., GREGORY, R. J., SMITH, A. E. & WELSH, M. J. 1991a. Nucleoside triphosphates are required to open the CFTR chloride channel. *Cell,* 67**,** 775-84.

ANDERSON, M. P., GREGORY, R. J., THOMPSON, S., SOUZA, D. W., PAUL, S., MULLIGAN, R. C., SMITH, A. E. & WELSH, M. J. 1991b. Demonstration that CFTR is a chloride channel by alteration of its anion selectivity. *Science,* 253**,** 202-5.

BAI, A., EIDELMAN, D. H., HOGG, J. C., JAMES, A. L., LAMBERT, R. K., LUDWIG, M. S., MARTIN, J., MCDONALD, D. M., MITZNER, W. A. & OKAZAWA, M. 1994. Proposed nomenclature for quantifying subdivisions of the bronchial wall. *J Appl Physiol (1985),* 77**,** 1011-4.

BALGHI, H., ROBERT, R., RAPPAZ, B., ZHANG, X., WOHLHUTER-HADDAD, A., EVAGELIDIS, A., LUO, Y., GOEPP, J., FERRARO, P., ROMEO, P., TREBAK, M., WISEMAN, P. W., THOMAS, D. Y. & HANRAHAN, J. W. 2011. Enhanced Ca2+ entry due to Orai1 plasma membrane insertion increases IL-8 secretion by cystic fibrosis airways. *FASEB J,* 25**,** 4274-91.

BARNES, P. J. 2000. Mechanisms in COPD: differences from asthma. *Chest,* 117**,** 10S-4S.

BARNES, P. J. 2004. Small airways in COPD. *N Engl J Med,* 350**,** 2635-7.

BARNES, P. J. 2009. Asthma and COPD basic mechanisms and clinical management. 2nd ed. Amsterdam ; Boston: Elsevier/Academic Press,.

BARRIERE, H., BAGDANY, M., BOSSARD, F., OKIYONEDA, T., WOJEWODKA, G., GRUENERT, D., RADZIOCH, D. & LUKACS, G. L. 2009. Revisiting the role of cystic fibrosis transmembrane conductance regulator and counterion permeability in the pH regulation of endocytic organelles. *Mol Biol Cell,* 20**,** 3125-41.

BERDIEV, B. K., TOUSSON, A., OOSTERVELD-HUT, H.M.J., QADRI, Y. J., CORMET-BOYAKA, E., HONG, J.S., FULLER, C. M., SORSCHER, E. J., LUKACS, G. L. AND BENOS, D. J. 2008. FRET assessment of CFTR molecular assembly. *FASEB J,* 22.

BILLET, A. & HANRAHAN, J. W. 2013. The secret life of CFTR as a calcium-activated chloride channel. *J Physiol,* 591**,** 5273-8.

BILLET, A., JIA, Y., JENSEN, T., RIORDAN, J. R. & HANRAHAN, J. W. 2015. Regulation of the cystic fibrosis transmembrane conductance regulator anion channel by tyrosine phosphorylation. *FASEB J,* 29**,** 3945-53.

BILLET, A., LUO, Y., BALGHI, H. & HANRAHAN, J. W. 2013. Role of tyrosine phosphorylation in the muscarinic activation of the cystic fibrosis transmembrane conductance regulator (CFTR). *J Biol Chem,* 288**,** 21815-23.

BOOTH, R. E. & STOCKAND, J. D. 2003. Targeted degradation of ENaC in response to PKC activation of the ERK1/2 cascade. *Am J Physiol Renal Physiol,* 284**,** F938-47.

BOUCHER, R. C. 1994. Human airway ion transport. Part one. *Am J Respir Crit Care Med,* 150**,** 271-81.

BOUCHER, R. C., STUTTS, M. J., KNOWLES, M. R., CANTLEY, L. & GATZY, J. T. 1986. Na+ transport in cystic fibrosis respiratory epithelia. Abnormal basal rate and response to adenylate cyclase activation. *J Clin Invest,* 78**,** 1245-52.

BOZOKY, Z., AHMADI, S., KELLER, J. P., MILMAN, T., BEAR, C. E. & FORMAN-KAY, J. 2015. The Role of Regulatory Region on Calcium-Induced Cftr Activation. *Pediatric Pulmonology,* 50**,** 195-195.

BRADBURY, N. A., JILLING, T., KIRK, K. L. & BRIDGES, R. J. 1992. Regulated endocytosis in a chloride secretory epithelial cell line. *Am J Physiol,* 262**,** C752-9.

BRODSKY, F. M., CHEN, C. Y., KNUEHL, C., TOWLER, M. C. & WAKEHAM, D. E. 2001. Biological basket weaving: formation and function of clathrin-coated vesicles. *Annu Rev Cell Dev Biol,* 17**,** 517-68.

BROWN, J. S., ZEMAN, K. L. & BENNETT, W. D. 2002. Ultrafine particle deposition and clearance in the healthy and obstructed lung. *Am J Respir Crit Care Med,* 166**,** 1240-7.

BROWN, M. B., HUNT, W. R., NOE, J. E., RUSH, N. I., SCHWEITZER, K. S., LEECE, T. C., MOLDOBAEVA, A., WAGNER, E. M., DUDEK, S. M., POIRIER, C., PRESSON, R. G., GULBINS, E. & PETRACHE, I. 2014. Loss of cystic fibrosis transmembrane conductance regulator impairs lung endothelial cell barrier function and increases susceptibility to microvascular damage from cigarette smoke. *Pulm Circ,* 4**,** 260-8.

BUTTON, B., CAI, L. H., EHRE, C., KESIMER, M., HILL, D. B., SHEEHAN, J. K., BOUCHER, R. C. & RUBINSTEIN, M. 2012. A periciliary brush promotes the lung health by separating the mucus layer from airway epithelia. *Science,* 337**,** 937-41.

CALVERLEY, P. M., RABE, K. F., GOEHRING, U. M., KRISTIANSEN, S., FABBRI, L. M., MARTINEZ, F. J., M & GROUPS, M. S. 2009. Roflumilast in symptomatic chronic obstructive pulmonary disease: two randomised clinical trials. *Lancet,* 374**,** 685-94.

CALVERLEY, P. M., STOCKLEY, R. A., SEEMUNGAL, T. A., HAGAN, G., WILLITS, L. R., RILEY, J. H., WEDZICHA, J. A. & INVESTIGATING NEW STANDARDS FOR PROPHYLAXIS IN REDUCTION OF EXACERBATIONS, I. 2011. Reported pneumonia in patients with COPD: findings from the INSPIRE study. *Chest,* 139**,** 505-12.

CANTIN, A. M., BILODEAU, G., OUELLET, C., LIAO, J. & HANRAHAN, J. W. 2006a. Oxidant stress suppresses CFTR expression. *Am J Physiol Cell Physiol,* 290**,** C262-70.

CANTIN, A. M., HANRAHAN, J. W., BILODEAU, G., ELLIS, L., DUPUIS, A., LIAO, J., ZIELENSKI, J. & DURIE, P. 2006b. Cystic fibrosis

transmembrane conductance regulator function is suppressed in cigarette smokers. *Am J Respir Crit Care Med,* 173**,** 1139-44.

CAPUTO, A., CACI, E., FERRERA, L., PEDEMONTE, N., BARSANTI, C., SONDO, E., PFEFFER, U., RAVAZZOLO, R., ZEGARRA-MORAN, O. & GALIETTA, L. J. 2008. TMEM16A, a membrane protein associated with calcium-dependent chloride channel activity. *Science,* 322**,** 590-4.

CARAMORI, G., CASOLARI, P., DI GREGORIO, C., SAETTA, M., BARALDO, S., BOSCHETTO, P., ITO, K., FABBRI, L. M., BARNES, P. J., ADCOCK, I. M., CAVALLESCO, G., CHUNG, K. F. & PAPI, A. 2009. MUC5AC expression is increased in bronchial submucosal glands of stable COPD patients. *Histopathology,* 55**,** 321-31.

CAZZOLA, M., PAGE, C 2014. Long-acting bronchodilators in COPD: where are we now and where are we going? *Breathe,* 10**,** 9.

CFF. 2015. *About Cystic Fibrosis* [Online]. Available: https://www.cff.org/What-is-CF/About-Cystic-Fibrosis/ [Accessed 10 Dec 2015].

CHANG, X. B., TABCHARANI, J. A., HOU, Y. X., JENSEN, T. J., KARTNER, N., ALON, N., HANRAHAN, J. W. & RIORDAN, J. R. 1993. Protein kinase A (PKA) still activates CFTR chloride channel after mutagenesis of all 10 PKA consensus phosphorylation sites. *J Biol Chem,* 268**,** 11304-11.

CHENG, J., MOYER, B. D., MILEWSKI, M., LOFFING, J., IKEDA, M., MICKLE, J. E., CUTTING, G. R., LI, M., STANTON, B. A. & GUGGINO, W. B. 2002. A Golgi-associated PDZ domain protein modulates cystic fibrosis transmembrane regulator plasma membrane expression. *J Biol Chem,* 277**,** 3520-9.

CHENG, S. H., GREGORY, R. J., MARSHALL, J., PAUL, S., SOUZA, D. W., WHITE, G. A., O'RIORDAN, C. R. & SMITH, A. E. 1990. Defective intracellular transport and processing of CFTR is the molecular basis of most cystic fibrosis. *Cell,* 63**,** 827-34.

CHENG, S. H., RICH, D. P., MARSHALL, J., GREGORY, R. J., WELSH, M. J. & SMITH, A. E. 1991. Phosphorylation of the R domain by cAMP-dependent protein kinase regulates the CFTR chloride channel. *Cell,* 66**,** 1027-36.

CHOLON, D. M., QUINNEY, N. L., FULCHER, M. L., ESTHER, C. R., JR., DAS, J., DOKHOLYAN, N. V., RANDELL, S. H., BOUCHER, R. C. & GENTZSCH, M. 2014. Potentiator ivacaftor abrogates pharmacological correction of DeltaF508 CFTR in cystic fibrosis. *Sci Transl Med,* 6**,** 246ra96.

CHURCH, D. F. & PRYOR, W. A. 1985. Free-radical chemistry of cigarette smoke and its toxicological implications. *Environ Health Perspect,* 64**,** 111-26.

CLANCY, J. P., ROWE, S. M., ACCURSO, F. J., AITKEN, M. L., AMIN, R. S., ASHLOCK, M. A., BALLMANN, M., BOYLE, M. P., BRONSVELD, I., CAMPBELL, P. W., DE BOECK, K., DONALDSON, S. H., DORKIN, H. L., DUNITZ, J. M., DURIE, P. R., JAIN, M., LEONARD, A., MCCOY, K. S., MOSS, R. B., PILEWSKI, J. M., ROSENBLUTH, D. B., RUBENSTEIN, R. C., SCHECHTER, M. S., BOTFIELD, M., ORDONEZ, C. L., SPENCER-GREEN, G. T., VERNILLET, L., WISSEH, S., YEN, K. & KONSTAN, M. W. 2012. Results of a phase IIa study of VX-809, an

investigational CFTR corrector compound, in subjects with cystic fibrosis homozygous for the F508del-CFTR mutation. *Thorax,* 67**,** 12-8.

CLUNES, L. A., BRIDGES, A., ALEXIS, N. & TARRAN, R. 2008. In vivo versus in vitro airway surface liquid nicotine levels following cigarette smoke exposure. *J Anal Toxicol,* 32**,** 201-7.

CLUNES, L. A., DAVIES, C. M., COAKLEY, R. D., ALEKSANDROV, A. A., HENDERSON, A. G., ZEMAN, K. L., WORTHINGTON, E. N., GENTZSCH, M., KREDA, S. M., CHOLON, D., BENNETT, W. D., RIORDAN, J. R., BOUCHER, R. C. & TARRAN, R. 2012. Cigarette smoke exposure induces CFTR internalization and insolubility, leading to airway surface liquid dehydration. *FASEB J,* 26**,** 533-45.

COHEN, N. A., ZHANG, S., SHARP, D. B., TAMASHIRO, E., CHEN, B., SORSCHER, E. J. & WOODWORTH, B. A. 2009. Cigarette smoke condensate inhibits transepithelial chloride transport and ciliary beat frequency. *Laryngoscope,* 119**,** 2269-74.

COLLACO, A., MARATHE, J., KOHNKE, H., KRAVSTOV, D. & AMEEN, N. 2010. Syntaxin 3 is necessary for cAMP- and cGMP-regulated exocytosis of CFTR: implications for enterotoxigenic diarrhea. *Am J Physiol Cell Physiol,* 299**,** C1450-60.

CONDREN, M. E. & BRADSHAW, M. D. 2013. Ivacaftor: a novel gene-based therapeutic approach for cystic fibrosis. *J Pediatr Pharmacol Ther,* 18**,** 8-13.

CONE, R. A. 2009. Barrier properties of mucus. *Adv Drug Deliv Rev,* 61**,** 75-85.

COOK, D. P., RECTOR, M. V., BOUZEK, D. C., MICHALSKI, A. S., GANSEMER, N. D., REZNIKOV, L. R., LI, X. P., STROIK, M. R., OSTEDGAARD, L. S., ABOU ALAIWA, M. H., THOMPSON, M. A., PRAKASH, Y. S., KRISHNAN, R., MEYERHOLZ, D. K., SEOW, C. Y. & STOLTZ, D. A. 2016. Cystic Fibrosis Transmembrane Conductance Regulator in Sarcoplasmic Reticulum of Airway Smooth Muscle Implications for Airway Contractility. *American Journal of Respiratory and Critical Care Medicine,* 193**,** 417-426.

CORRADI, V., VERGANI, P. & TIELEMAN, D. P. 2015. Cystic Fibrosis Transmembrane Conductance Regulator (CFTR): CLOSED AND OPEN STATE CHANNEL MODELS. *J Biol Chem,* 290**,** 22891-906.

CRUMP, R. G., ASKEW, G. R., WERT, S. E., LINGREL, J. B. & JOINER, C. H. 1995. In situ localization of sodium-potassium ATPase mRNA in developing mouse lung epithelium. *Am J Physiol,* 269**,** L299-308.

CSANADY, L., VERGANI, P. & GADSBY, D. C. 2010. Strict coupling between CFTR's catalytic cycle and gating of its Cl- ion pore revealed by distributions of open channel burst durations. *Proc Natl Acad Sci U S A,* 107**,** 1241-6.

DALEMANS, W., BARBRY, P., CHAMPIGNY, G., JALLAT, S., DOTT, K., DREYER, D., CRYSTAL, R. G., PAVIRANI, A., LECOCQ, J. P. & LAZDUNSKI, M. 1991. Altered chloride ion channel kinetics associated with the delta F508 cystic fibrosis mutation. *Nature,* 354**,** 526-8.

DAVENPORT, S. E., MERGEY, M., CHERQUI, G., BOUCHER, R. C., GESPACH, C. & GABRIEL, S. E. 1996. Deregulated expression and function of CFTR and Cl- secretion after activation of the Ras and Src/PyMT pathways in Caco-2 cells. *Biochem Biophys Res Commun,* 229**,** 663-72.

DECRAMER, M., RUTTEN-VAN MOLKEN, M., DEKHUIJZEN, P. N., TROOSTERS, T., VAN HERWAARDEN, C., PELLEGRINO, R., VAN SCHAYCK, C. P., OLIVIERI, D., DEL DONNO, M., DE BACKER, W., LANKHORST, I. & ARDIA, A. 2005. Effects of N-acetylcysteine on outcomes in chronic obstructive pulmonary disease (Bronchitis Randomized on NAC Cost-Utility Study, BRONCUS): a randomised placebo-controlled trial. *Lancet,* 365**,** 1552-60.

DENNING, G. M., ANDERSON, M. P., AMARA, J. F., MARSHALL, J., SMITH, A. E. & WELSH, M. J. 1992. Processing of mutant cystic fibrosis transmembrane conductance regulator is temperature-sensitive. *Nature,* 358**,** 761-4.

DHARMSATHAPHORN, K., MCROBERTS, J. A., MANDEL, K. G., TISDALE, L. D. & MASUI, H. 1984. A human colonic tumor cell line that maintains vectorial electrolyte transport. *Am J Physiol,* 246**,** G204-8.

DOMINGUE, J. C., AO, M., SARATHY, J., GEORGE, A., ALREFAI, W. A., NELSON, D. J. & RAO, M. C. 2014. HEK-293 cells expressing the cystic fibrosis transmembrane conductance regulator (CFTR): a model for studying regulation of Cl- transport. *Physiol Rep,* 2.

DONALDSON, S. H. & BOUCHER, R. C. 2007. Sodium channels and cystic fibrosis. *Chest,* 132**,** 1631-6.

DUDEZ, T., BOROT, F., HUANG, S., KWAK, B. R., BACCHETTA, M., OLLERO, M., STANTON, B. A. & CHANSON, M. 2008. CFTR in a lipid raft-TNFR1 complex modulates gap junctional intercellular communication and IL-8 secretion. *Biochim Biophys Acta,* 1783**,** 779-88.

DUNCAN, J. R. & KORNFELD, S. 1988. Intracellular movement of two mannose 6-phosphate receptors: return to the Golgi apparatus. *J Cell Biol,* 106**,** 617-28.

ERLE, D. J. & SHEPPARD, D. 2014. The cell biology of asthma. *J Cell Biol,* 205**,** 621-31.

EVANS, M. G. & MARTY, A. 1986. Calcium-dependent chloride currents in isolated cells from rat lacrimal glands. *J Physiol,* 378**,** 437-60.

FABBRI, L. M., CALVERLEY, P. M., IZQUIERDO-ALONSO, J. L., BUNDSCHUH, D. S., BROSE, M., MARTINEZ, F. J., RABE, K. F., M & GROUPS, M. S. 2009. Roflumilast in moderate-to-severe chronic obstructive pulmonary disease treated with longacting bronchodilators: two randomised clinical trials. *Lancet,* 374**,** 695-703.

FALIN, R. A. & COTTON, C. U. 2007. Acute downregulation of ENaC by EGF involves the PY motif and putative ERK phosphorylation site. *J Gen Physiol,* 130**,** 313-28.

FILOSTO, S., BASTON, D. S., CHUNG, S., BECKER, C. R. & GOLDKORN, T. 2013. Src mediates cigarette smoke-induced resistance to tyrosine kinase inhibitors in NSCLC cells. *Mol Cancer Ther,* 12**,** 1579-90.

FILOSTO, S., BECKER, C. R. & GOLDKORN, T. 2012. Cigarette smoke induces aberrant EGF receptor activation that mediates lung cancer development and resistance to tyrosine kinase inhibitors. *Mol Cancer Ther,* 11**,** 795-804.

FISCHER, H., ILLEK, B. & MACHEN, T. E. 1998. Regulation of CFTR by protein phosphatase 2B and protein kinase C. *Pflugers Arch,* 436**,** 175-81.

FOTIN, A., CHENG, Y., SLIZ, P., GRIGORIEFF, N., HARRISON, S. C., KIRCHHAUSEN, T. & WALZ, T. 2004. Molecular model for a complete clathrin lattice from electron cryomicroscopy. *Nature,* 432**,** 573-9.

FRIEDMAN, J. R., DIBENEDETTO, J. R., WEST, M., ROWLAND, A. A. & VOELTZ, G. K. 2013. Endoplasmic reticulum-endosome contact increases as endosomes traffic and mature. *Mol Biol Cell,* 24**,** 1030-40.

FRIEDMAN, J. R., WEBSTER, B. M., MASTRONARDE, D. N., VERHEY, K. J. & VOELTZ, G. K. 2010. ER sliding dynamics and ER-mitochondrial contacts occur on acetylated microtubules. *J Cell Biol,* 190**,** 363-75.

FULCHER, M. L., GABRIEL, S., BURNS, K. A., YANKASKAS, J. R. & RANDELL, S. H. 2005. Well-differentiated human airway epithelial cell cultures. *Methods Mol Med,* 107**,** 183-206.

GAILLARD, E. A., KOTA, P., GENTZSCH, M., DOKHOLYAN, N. V., STUTTS, M. J. & TARRAN, R. 2010. Regulation of the epithelial Na+ channel and airway surface liquid volume by serine proteases. *Pflugers Arch,* 460**,** 1-17.

GANESHAN, R., NOWOTARSKI, K., DI, A., NELSON, D. J. & KIRK, K. L. 2007. CFTR surface expression and chloride currents are decreased by inhibitors of N-WASP and actin polymerization. *Biochim Biophys Acta,* 1773**,** 192-200.

GAUTHIER, N. C., MONZO, P., GONZALEZ, T., DOYE, A., OLDANI, A., GOUNON, P., RICCI, V., CORMONT, M. & BOQUET, P. 2007. Early endosomes associated with dynamic F-actin structures are required for late trafficking of H. pylori VacA toxin. *J Cell Biol,* 177**,** 343-54.

GENTZSCH, M., CHANG, X. B., CUI, L., WU, Y., OZOLS, V. V., CHOUDHURY, A., PAGANO, R. E. & RIORDAN, J. R. 2004. Endocytic trafficking routes of wild type and DeltaF508 cystic fibrosis transmembrane conductance regulator. *Mol Biol Cell,* 15**,** 2684-96.

GENTZSCH, M., DANG, H., DANG, Y., GARCIA-CABALLERO, A., SUCHINDRAN, H., BOUCHER, R. C. & STUTTS, M. J. 2010. The cystic fibrosis transmembrane conductance regulator impedes proteolytic stimulation of the epithelial Na+ channel. *J Biol Chem,* 285**,** 32227-32.

GERASIMENKO, J. V., TEPIKIN, A. V., PETERSEN, O. H. & GERASIMENKO, O. V. 1998. Calcium uptake via endocytosis with rapid release from acidifying endosomes. *Curr Biol,* 8**,** 1335-8.

GIRALDEZ, T., AFONSO-ORAMAS, D., CRUZ-MUROS, I., GARCIA-MARIN, V., PAGEL, P., GONZALEZ-HERNANDEZ, T. & ALVAREZ DE LA ROSA, D. 2007. Cloning and functional expression of a new epithelial sodium channel delta subunit isoform differentially expressed in neurons of the human and monkey telencephalon. *J Neurochem,* 102**,** 1304-15.

GLOZMAN, R., OKIYONEDA, T., MULVIHILL, C. M., RINI, J. M., BARRIERE, H. & LUKACS, G. L. 2009. N-glycans are direct determinants of CFTR folding and stability in secretory and endocytic membrane traffic. *J Cell Biol,* 184**,** 847-62.

GONZALEZ-SANCHEZ, R., TRUJILLO, X., TRUJILLO-HERNANDEZ, B., VASQUEZ, C., HUERTA, M. & ELIZALDE, A. 2006. Forskolin versus sodium cromoglycate for prevention of asthma attacks: a single-blinded clinical trial. *J Int Med Res,* 34**,** 200-7.

GRAY, M. A., GREENWELL, J. R. & ARGENT, B. E. 1988. Secretin-regulated chloride channel on the apical plasma membrane of pancreatic duct cells. *J Membr Biol,* 105**,** 131-42.

GUGGINO, W. B. & STANTON, B. A. 2006. New insights into cystic fibrosis: molecular switches that regulate CFTR. *Nat Rev Mol Cell Biol,* 7**,** 426-36.

HAERTEIS, S., KRUEGER, B., KORBMACHER, C. & RAUH, R. 2009. The delta-subunit of the epithelial sodium channel (ENaC) enhances channel activity and alters proteolytic ENaC activation. *J Biol Chem,* 284**,** 29024-40.

HALLOWS, K. R., RAGHURAM, V., KEMP, B. E., WITTERS, L. A. & FOSKETT, J. K. 2000. Inhibition of cystic fibrosis transmembrane conductance regulator by novel interaction with the metabolic sensor AMP-activated protein kinase. *J Clin Invest,* 105**,** 1711-21.

HASSAN, F., XU, X., NUOVO, G., KILLILEA, D. W., TYRRELL, J., DA TAN, C., TARRAN, R., DIAZ, P., JEE, J., KNOELL, D., BOYAKA, P. N. & CORMET-BOYAKA, E. 2014. Accumulation of metals in GOLD4 COPD lungs is associated with decreased CFTR levels. *Respir Res,* 15**,** 69.

HEGEDUS, T., ALEKSANDROV, A., MENGOS, A., CUI, L., JENSEN, T. J. & RIORDAN, J. R. 2009. Role of individual R domain phosphorylation sites in CFTR regulation by protein kinase A. *Biochim Biophys Acta,* 1788**,** 1341-9.

HEGEDUS, T., SEROHIJOS, A. W., DOKHOLYAN, N. V., HE, L. & RIORDAN, J. R. 2008. Computational studies reveal phosphorylation-dependent changes in the unstructured R domain of CFTR. *J Mol Biol,* 378**,** 1052-63.

HELENIUS, A., MELLMAN, I., WALL, D. & HUBBARD, A. 1983. Endosomes. *Trends in Biochemical Sciences,* 8**,** 245-250.

HEUSER, J. E. & ANDERSON, R. G. 1989. Hypertonic media inhibit receptor-mediated endocytosis by blocking clathrin-coated pit formation. *J Cell Biol,* 108**,** 389-400.

HO, M. W., KAETZEL, M. A., ARMSTRONG, D. L. & SHEARS, S. B. 2001. Regulation of a human chloride channel. a paradigm for integrating input from calcium, type ii calmodulin-dependent protein kinase, and inositol 3,4,5,6-tetrakisphosphate. *J Biol Chem,* 276**,** 18673-80.

HOGG, J. C. 2004. Pathophysiology of airflow limitation in chronic obstructive pulmonary disease. *Lancet,* 364**,** 709-21.

HOGG, J. C., CHU, F., UTOKAPARCH, S., WOODS, R., ELLIOTT, W. M., BUZATU, L., CHERNIACK, R. M., ROGERS, R. M., SCIURBA, F. C., COXSON, H. O. & PARÉ, P. D. 2004. The nature of small-airway obstruction in chronic obstructive pulmonary disease. *N Engl J Med,* 350**,** 2645-53.

HOOPER, R., ZHANG, X., WEBSTER, M., GO, C., KEDRA, J., MARCHBANK, K., GILL, D. L., WEERARATNA, A. T., TREBAK, M. & SOBOLOFF, J. 2015. Novel Protein Kinase C-Mediated Control of Orai1 Function in Invasive Melanoma. *Mol Cell Biol,* 35**,** 2790-8.

HOWE, A. K. 2011. Cross-talk between calcium and protein kinase A in the regulation of cell migration. *Curr Opin Cell Biol,* 23**,** 554-61.

HU, W., HOWARD, M. & LUKACS, G. L. 2001. Multiple endocytic signals in the C-terminal tail of the cystic fibrosis transmembrane conductance regulator. *Biochem J,* 354**,** 561-72.

HUOTARI, J. & HELENIUS, A. 2011. Endosome maturation. *EMBO J,* 30**,** 3481-500.

HURST, J. R., VESTBO, J., ANZUETO, A., LOCANTORE, N., MULLEROVA, H., TAL-SINGER, R., MILLER, B., LOMAS, D. A., AGUSTI, A., MACNEE, W., CALVERLEY, P., RENNARD, S., WOUTERS, E. F., WEDZICHA, J. A. & EVALUATION OF, C. L. T. I. P. S. E. I. 2010. Susceptibility to exacerbation in chronic obstructive pulmonary disease. *N Engl J Med,* 363**,** 1128-38.

HWANG, T. C. & SHEPPARD, D. N. 2009. Gating of the CFTR Cl- channel by ATP-driven nucleotide-binding domain dimerisation. *J Physiol,* 587**,** 2151-61.

ISO, I. S. O. 2000. *Cigarettes - determination of total and nicotine-free dry particulate matter using a routine analytical smoking machine ISO 4387* [Online]. Geneva, Switzerland. Available: https://www.iso.org/obp/ui/#iso:std:28323:en.

JIA, Y., MATHEWS, C. J. & HANRAHAN, J. W. 1997. Phosphorylation by protein kinase C is required for acute activation of cystic fibrosis transmembrane conductance regulator by protein kinase A. *J Biol Chem,* 272**,** 4978-84.

KANELIS, V., HUDSON, R. P., THIBODEAU, P. H., THOMAS, P. J. & FORMAN-KAY, J. D. 2010. NMR evidence for differential phosphorylation-dependent interactions in WT and DeltaF508 CFTR. *EMBO J,* 29**,** 263-77.

KAWASAKI, T., UEYAMA, T., LANGE, I., FESKE, S. & SAITO, N. 2010. Protein kinase C-induced phosphorylation of Orai1 regulates the intracellular Ca2+ level via the store-operated Ca2+ channel. *J Biol Chem,* 285**,** 25720-30.

KEITH, C. H. T., P.G. 1965. Measurement of the total smoke issuing from a burning cigarette. *Tobacco Science,* 9**,** 61-64.

KENTUCKY, U. O. 2016. *Center for Tobacco Reference Products* [Online]. Available: https://ctrp.uky.edu/ [Accessed May 5 2016].

KIM, V. & CRINER, G. J. 2013. Chronic bronchitis and chronic obstructive pulmonary disease. *Am J Respir Crit Care Med,* 187**,** 228-37.

KNOWLES, M. R. & BOUCHER, R. C. 2002. Mucus clearance as a primary innate defense mechanism for mammalian airways. *J Clin Invest,* 109**,** 571-7.

KNOWLES, M. R., CLARKE, L. L. & BOUCHER, R. C. 1991. Activation by extracellular nucleotides of chloride secretion in the airway epithelia of patients with cystic fibrosis. *N Engl J Med,* 325**,** 533-8.

KREDA, S. M., GYNN, M. C., FENSTERMACHER, D. A., BOUCHER, R. C. & GABRIEL, S. E. 2001. Expression and localization of epithelial aquaporins in the adult human lung. *Am J Respir Cell Mol Biol,* 24**,** 224-34.

KREINDLER, J. L., JACKSON, A. D., KEMP, P. A., BRIDGES, R. J. & DANAHAY, H. 2005. Inhibition of chloride secretion in human bronchial epithelial cells by cigarette smoke extract. *Am J Physiol Lung Cell Mol Physiol,* 288**,** L894-902.

KULKA, M., DERY, R., NAHIRNEY, D., DUSZYK, M. & BEFUS, A. D. 2005. Differential regulation of cystic fibrosis transmembrane conductance

regulator by interferon gamma in mast cells and epithelial cells. *J Pharmacol Exp Ther,* 315**,** 563-70.

LE ROY, C. & WRANA, J. L. 2005. Clathrin- and non-clathrin-mediated endocytic regulation of cell signalling. *Nat Rev Mol Cell Biol,* 6**,** 112-26.

LEE, S. J., LI, Z., LITAN, A., YOO, S. & LANGHANS, S. A. 2015. EGF-induced sodium influx regulates EGFR trafficking through HDAC6 and tubulin acetylation. *BMC Cell Biol,* 16**,** 24.

LEPPLE-WIENHUES, A., WIELAND, U., LAUN, T., HEIL, L., STERN, M. & LANG, F. 2001. A src-like kinase activates outwardly rectifying chloride channels in CFTR-defective lymphocytes. *FASEB J,* 15**,** 927-31.

LI, C. & NAREN, A. P. 2005. Macromolecular complexes of cystic fibrosis transmembrane conductance regulator and its interacting partners. *Pharmacol Ther,* 108**,** 208-23.

LI, J., POULIKAKOS, P. I., DAI, Z., TESTA, J. R., CALLAWAY, D. J. & BU, Z. 2007. Protein kinase C phosphorylation disrupts Na+/H+ exchanger regulatory factor 1 autoinhibition and promotes cystic fibrosis transmembrane conductance regulator macromolecular assembly. *J Biol Chem,* 282**,** 27086-99.

LIEDTKE, C. M. & COLE, T. S. 1998. Antisense oligonucleotide to PKC-epsilon alters cAMP-dependent stimulation of CFTR in Calu-3 cells. *Am J Physiol,* 275**,** C1357-64.

LINSDELL, P., ZHENG, S. X. & HANRAHAN, J. W. 1998. Non-pore lining amino acid side chains influence anion selectivity of the human CFTR Cl- channel expressed in mammalian cell lines. *J Physiol,* 512 (Pt 1)**,** 1-16.

LOFFING, J., MOYER, B. D., MCCOY, D. & STANTON, B. A. 1998. Exocytosis is not involved in activation of Cl- secretion via CFTR in Calu-3 airway epithelial cells. *Am J Physiol,* 275**,** C913-20.

LUKACS, G. L., CHANG, X. B., BEAR, C., KARTNER, N., MOHAMED, A., RIORDAN, J. R. & GRINSTEIN, S. 1993. The delta F508 mutation decreases the stability of cystic fibrosis transmembrane conductance regulator in the plasma membrane. Determination of functional half-lives on transfected cells. *J Biol Chem,* 268**,** 21592-8.

LUKACS, G. L., MOHAMED, A., KARTNER, N., CHANG, X. B., RIORDAN, J. R. & GRINSTEIN, S. 1994. Conformational maturation of CFTR but not its mutant counterpart (delta F508) occurs in the endoplasmic reticulum and requires ATP. *EMBO J,* 13**,** 6076-86.

LUKACS, G. L., SEGAL, G., KARTNER, N., GRINSTEIN, S. & ZHANG, F. 1997. Constitutive internalization of cystic fibrosis transmembrane conductance regulator occurs via clathrin-dependent endocytosis and is regulated by protein phosphorylation. *Biochem J,* 328 (Pt 2)**,** 353-61.

LUO, J., PATO, M. D., RIORDAN, J. R. & HANRAHAN, J. W. 1998. Differential regulation of single CFTR channels by PP2C, PP2A, and other phosphatases. *Am J Physiol,* 274**,** C1397-410.

LUZ, S., KONGSUPHOL, P., MENDES, A. I., ROMEIRAS, F., SOUSA, M., SCHREIBER, R., MATOS, P., JORDAN, P., MEHTA, A., AMARAL, M. D., KUNZELMANN, K. & FARINHA, C. M. 2011. Contribution of casein kinase 2 and spleen tyrosine kinase to CFTR trafficking and protein kinase A-induced activity. *Mol Cell Biol,* 31**,** 4392-404.

MAEGAWA, M., ARAO, T., YOKOTE, H., MATSUMOTO, K., KUDO, K., TANAKA, K., KANEDA, H., FUJITA, Y., ITO, F. & NISHIO, K. 2009.

Epidermal growth factor receptor lacking C-terminal autophosphorylation sites retains signal transduction and high sensitivity to epidermal growth factor receptor tyrosine kinase inhibitor. *Cancer Sci,* 100**,** 552-7.

MAIER, T., GUELL, M. & SERRANO, L. 2009. Correlation of mRNA and protein in complex biological samples. *FEBS Lett,* 583**,** 3966-73.

MALL, M., GRUBB, B. R., HARKEMA, J. R., O'NEAL, W. K. & BOUCHER, R. C. 2004. Increased airway epithelial Na+ absorption produces cystic fibrosis-like lung disease in mice. *Nat Med,* 10**,** 487-93.

MANNINO, D. M., HOMA, D. M., AKINBAMI, L. J., FORD, E. S. & REDD, S. C. 2002. Chronic obstructive pulmonary disease surveillance--United States, 1971-2000. *Respir Care,* 47**,** 1184-99.

MARTINEZ, F. J., CALVERLEY, P. M., GOEHRING, U. M., BROSE, M., FABBRI, L. M. & RABE, K. F. 2015. Effect of roflumilast on exacerbations in patients with severe chronic obstructive pulmonary disease uncontrolled by combination therapy (REACT): a multicentre randomised controlled trial. *Lancet,* 385**,** 857-66.

MASON, S. J., PARADISO, A. M. & BOUCHER, R. C. 1991. Regulation of transepithelial ion transport and intracellular calcium by extracellular ATP in human normal and cystic fibrosis airway epithelium. *Br J Pharmacol,* 103**,** 1649-56.

MATHEWS, C. J., TABCHARANI, J. A., CHANG, X. B., JENSEN, T. J., RIORDAN, J. R. & HANRAHAN, J. W. 1998. Dibasic protein kinase A sites regulate bursting rate and nucleotide sensitivity of the cystic fibrosis transmembrane conductance regulator chloride channel. *J Physiol,* 508 (Pt 2)**,** 365-77.

MAXFIELD, F. R. & YAMASHIRO, D. J. 1987. Endosome acidification and the pathways of receptor-mediated endocytosis. *Adv Exp Med Biol,* 225**,** 189-98.

MCCUBREY, J. A., STEELMAN, L. S., CHAPPELL, W. H., ABRAMS, S. L., WONG, E. W., CHANG, F., LEHMANN, B., TERRIAN, D. M., MILELLA, M., TAFURI, A., STIVALA, F., LIBRA, M., BASECKE, J., EVANGELISTI, C., MARTELLI, A. M. & FRANKLIN, R. A. 2007. Roles of the Raf/MEK/ERK pathway in cell growth, malignant transformation and drug resistance. *Biochim Biophys Acta,* 1773**,** 1263-84.

MENSE, M., VERGANI, P., WHITE, D. M., ALTBERG, G., NAIRN, A. C. & GADSBY, D. C. 2006. In vivo phosphorylation of CFTR promotes formation of a nucleotide-binding domain heterodimer. *EMBO J,* 25**,** 4728-39.

MERCER, B. A. & D'ARMIENTO, J. M. 2006. Emerging role of MAP kinase pathways as therapeutic targets in COPD. *Int J Chron Obstruct Pulmon Dis,* 1**,** 137-50.

MERCER, R. R., RUSSELL, M. L., ROGGLI, V. L. & CRAPO, J. D. 1994. Cell number and distribution in human and rat airways. *Am J Respir Cell Mol Biol,* 10**,** 613-24.

MIDDLETON, L. M. & HARVEY, R. D. 1998. PKC regulation of cardiac CFTR Cl- channel function in guinea pig ventricular myocytes. *Am J Physiol,* 275**,** C293-302.

MOLLER, W., FELTEN, K., SOMMERER, K., SCHEUCH, G., MEYER, G., MEYER, P., HAUSSINGER, K. & KREYLING, W. G. 2008. Deposition,

retention, and translocation of ultrafine particles from the central airways and lung periphery. *Am J Respir Crit Care Med,* 177**,** 426-32.

MONDINI, A., SASSONE, F., CIVELLO, D. A., GARAVAGLIA, M. L., BAZZINI, C., RODIGHIERO, S., VEZZOLI, V., CONTI, F., TORIELLI, L., CAPASSO, G., PAULMICHL, M. & MEYER, G. 2012. Hypertension-linked mutation of alpha-adducin increases CFTR surface expression and activity in HEK and cultured rat distal convoluted tubule cells. *PLoS One,* 7**,** e52014.

MONTERISI, S., FAVIA, M., GUERRA, L., CARDONE, R. A., MARZULLI, D., RESHKIN, S. J., CASAVOLA, V. & ZACCOLO, M. 2012. CFTR regulation in human airway epithelial cells requires integrity of the actin cytoskeleton and compartmentalized cAMP and PKA activity. *J Cell Sci,* 125**,** 1106-17.

MORAN, A. R., NORIMATSU, Y., DAWSON, D. C. & MACDONALD, K. D. 2014. Aqueous cigarette smoke extract induces a voltage-dependent inhibition of CFTR expressed in Xenopus oocytes. *Am J Physiol Lung Cell Mol Physiol,* 306**,** L284-91.

MORGAN, L., PEARSON, M., DE IONGH, R., MACKEY, D., VAN DER WALL, H., PETERS, M. & RUTLAND, J. 2004. Scintigraphic measurement of tracheal mucus velocity in vivo. *Eur Respir J,* 23**,** 518-22.

MOYER, B. D., LOFFING, J., SCHWIEBERT, E. M., LOFFING-CUENI, D., HALPIN, P. A., KARLSON, K. H., ISMAILOV, I. I., GUGGINO, W. B., LANGFORD, G. M. & STANTON, B. A. 1998. Membrane trafficking of the cystic fibrosis gene product, cystic fibrosis transmembrane conductance regulator, tagged with green fluorescent protein in madin-darby canine kidney cells. *J Biol Chem,* 273**,** 21759-68.

NAMKUNG, W., PHUAN, P. W. & VERKMAN, A. S. 2011. TMEM16A inhibitors reveal TMEM16A as a minor component of calcium-activated chloride channel conductance in airway and intestinal epithelial cells. *J Biol Chem,* 286**,** 2365-74.

OKIYONEDA, T. & LUKACS, G. L. 2007. Cell surface dynamics of CFTR: the ins and outs. *Biochim Biophys Acta,* 1773**,** 476-9.

OUSINGSAWAT, J., MARTINS, J. R., SCHREIBER, R., ROCK, J. R., HARFE, B. D. & KUNZELMANN, K. 2009. Loss of TMEM16A causes a defect in epithelial Ca2+-dependent chloride transport. *J Biol Chem,* 284**,** 28698-703.

PARK, C. Y., HOOVER, P. J., MULLINS, F. M., BACHHAWAT, P., COVINGTON, E. D., RAUNSER, S., WALZ, T., GARCIA, K. C., DOLMETSCH, R. E. & LEWIS, R. S. 2009. STIM1 clusters and activates CRAC channels via direct binding of a cytosolic domain to Orai1. *Cell,* 136**,** 876-90.

PEARSE, B. M. 1976. Clathrin: a unique protein associated with intracellular transfer of membrane by coated vesicles. *Proc Natl Acad Sci U S A,* 73**,** 1255-9.

PEDEMONTE, N., LUKACS, G. L., DU, K., CACI, E., ZEGARRA-MORAN, O., GALIETTA, L. J. & VERKMAN, A. S. 2005. Small-molecule correctors of defective DeltaF508-CFTR cellular processing identified by high-throughput screening. *J Clin Invest,* 115**,** 2564-71.

PETERS, K. W., QI, J., JOHNSON, J. P., WATKINS, S. C. & FRIZZELL, R. A. 2001. Role of snare proteins in CFTR and ENaC trafficking. *Pflugers Arch,* 443 Suppl 1**,** S65-9.

PHILLIPS, J., KLUSS, B., RICHTER, A. & MASSEY, E. 2005. Exposure of bronchial epithelial cells to whole cigarette smoke: assessment of cellular responses. *Altern Lab Anim,* 33**,** 239-48.

PICCIOTTO, M. R., COHN, J. A., BERTUZZI, G., GREENGARD, P. & NAIRN, A. C. 1992. Phosphorylation of the cystic fibrosis transmembrane conductance regulator. *J Biol Chem,* 267**,** 12742-52.

POOLE, P. J. & BLACK, P. N. 2006. Mucolytic agents for chronic bronchitis or chronic obstructive pulmonary disease. *Cochrane Database Syst Rev***,** CD001287.

POPATIA, R., HAVER, K. & CASEY, A. 2014. Primary Ciliary Dyskinesia: An Update on New Diagnostic Modalities and Review of the Literature. *Pediatr Allergy Immunol Pulmonol,* 27**,** 51-59.

PRAT, A. G., XIAO, Y. F., AUSIELLO, D. A. & CANTIELLO, H. F. 1995. cAMP-independent regulation of CFTR by the actin cytoskeleton. *Am J Physiol,* 268**,** C1552-61.

PRINCE, L. S., WORKMAN, R. B., JR. & MARCHASE, R. B. 1994. Rapid endocytosis of the cystic fibrosis transmembrane conductance regulator chloride channel. *Proc Natl Acad Sci U S A,* 91**,** 5192-6.

QUON, B. S. & ROWE, S. M. 2016. New and emerging targeted therapies for cystic fibrosis. *BMJ,* 352**,** i859.

RAB, A., ROWE, S. M., RAJU, S. V., BEBOK, Z., MATALON, S. & COLLAWN, J. F. 2013. Cigarette smoke and CFTR: implications in the pathogenesis of COPD. *Am J Physiol Lung Cell Mol Physiol,* 305**,** L530-41.

RAJAN, R. S., ILLING, M. E., BENCE, N. F. & KOPITO, R. R. 2001. Specificity in intracellular protein aggregation and inclusion body formation. *Proc Natl Acad Sci U S A,* 98**,** 13060-5.

RAMSEY, B. W., DAVIES, J., MCELVANEY, N. G., TULLIS, E., BELL, S. C., DREVINEK, P., GRIESE, M., MCKONE, E. F., WAINWRIGHT, C. E., KONSTAN, M. W., MOSS, R., RATJEN, F., SERMET-GAUDELUS, I., ROWE, S. M., DONG, Q., RODRIGUEZ, S., YEN, K., ORDONEZ, C., ELBORN, J. S. & GROUP, V. X. S. 2011. A CFTR potentiator in patients with cystic fibrosis and the G551D mutation. *N Engl J Med,* 365**,** 1663-72.

RANDELL, S. H., BOUCHER, R. C. & UNIVERSITY OF NORTH CAROLINA VIRTUAL LUNG, G. 2006. Effective mucus clearance is essential for respiratory health. *Am J Respir Cell Mol Biol,* 35**,** 20-8.

RASMUSSEN, J. E., SHERIDAN, J. T., POLK, W., DAVIES, C. M. & TARRAN, R. 2014. Cigarette smoke-induced Ca2+ release leads to cystic fibrosis transmembrane conductance regulator (CFTR) dysfunction. *J Biol Chem,* 289**,** 7671-81.

REID, L. 1960. Measurement of the bronchial mucous gland layer: a diagnostic yardstick in chronic bronchitis. *Thorax,* 15**,** 132-41.

RENNARD, S. I., CALVERLEY, P. M., GOEHRING, U. M., BREDENBROKER, D. & MARTINEZ, F. J. 2011. Reduction of exacerbations by the PDE4 inhibitor roflumilast--the importance of defining different subsets of patients with COPD. *Respir Res,* 12**,** 18.

RENNARD, S. I. & VESTBO, J. 2006. COPD: the dangerous underestimate of 15%. *Lancet,* 367**,** 1216-9.

RENNOLDS, J., BUTLER, S., MALONEY, K., BOYAKA, P. N., DAVIS, I. C., KNOELL, D. L., PARINANDI, N. L. & CORMET-BOYAKA, E. 2010. Cadmium regulates the expression of the CFTR chloride channel in human airway epithelial cells. *Toxicol Sci,* 116**,** 349-58.

ROBERTS, R. L., BARBIERI, M. A., PRYSE, K. M., CHUA, M., MORISAKI, J. H. & STAHL, P. D. 1999. Endosome fusion in living cells overexpressing GFP-rab5. *J Cell Sci,* 112 (Pt 21)**,** 3667-75.

ROCK, J. R., O'NEAL, W. K., GABRIEL, S. E., RANDELL, S. H., HARFE, B. D., BOUCHER, R. C. & GRUBB, B. R. 2009. Transmembrane protein 16A (TMEM16A) is a Ca2+-regulated Cl- secretory channel in mouse airways. *J Biol Chem,* 284**,** 14875-80.

ROGAN, M. P., STOLTZ, D. A. & HORNICK, D. B. 2011. Cystic fibrosis transmembrane conductance regulator intracellular processing, trafficking, and opportunities for mutation-specific treatment. *Chest,* 139**,** 1480-90.

ROWELL, T. R. & TARRAN, R. 2015. Will chronic e-cigarette use cause lung disease? *Am J Physiol Lung Cell Mol Physiol,* 309**,** L1398-409.

RUBIN, B. K., RAMIREZ, O., ZAYAS, J. G., FINEGAN, B. & KING, M. 1992. Respiratory mucus from asymptomatic smokers is better hydrated and more easily cleared by mucociliary action. *Am Rev Respir Dis,* 145**,** 545-7.

SAETTA, M., TURATO, G., BARALDO, S., ZANIN, A., BRACCIONI, F., MAPP, C. E., MAESTRELLI, P., CAVALLESCO, G., PAPI, A. & FABBRI, L. M. 2000. Goblet cell hyperplasia and epithelial inflammation in peripheral airways of smokers with both symptoms of chronic bronchitis and chronic airflow limitation. *Am J Respir Crit Care Med,* 161**,** 1016-21.

SCHREIBER, R., HOPF, A., MALL, M., GREGER, R. & KUNZELMANN, K. 1999. The first-nucleotide binding domain of the cystic-fibrosis transmembrane conductance regulator is important for inhibition of the epithelial Na+ channel. *Proc Natl Acad Sci U S A,* 96**,** 5310-5.

SCHROEDER, B. C., CHENG, T., JAN, Y. N. & JAN, L. Y. 2008. Expression cloning of TMEM16A as a calcium-activated chloride channel subunit. *Cell,* 134**,** 1019-29.

SCHWIEBERT, E. M., GESEK, F., ERCOLANI, L., WJASOW, C., GRUENERT, D. C., KARLSON, K. & STANTON, B. A. 1994. Heterotrimeric G proteins, vesicle trafficking, and CFTR Cl- channels. *Am J Physiol,* 267**,** C272-81.

SEKAR, R. B. & PERIASAMY, A. 2003. Fluorescence resonance energy transfer (FRET) microscopy imaging of live cell protein localizations. *J Cell Biol,* 160**,** 629-33.

SETHI, S., MALONEY, J., GROVE, L., WRONA, C. & BERENSON, C. S. 2006. Airway inflammation and bronchial bacterial colonization in chronic obstructive pulmonary disease. *Am J Respir Crit Care Med,* 173**,** 991-8.

SHEPPARD, D. N. & WELSH, M. J. 1999. Structure and function of the CFTR chloride channel. *Physiol Rev,* 79**,** S23-45.

SHORT, D. B., TROTTER, K. W., RECZEK, D., KREDA, S. M., BRETSCHER, A., BOUCHER, R. C., STUTTS, M. J. & MILGRAM, S. L. 1998. An apical PDZ protein anchors the cystic fibrosis transmembrane conductance regulator to the cytoskeleton. *J Biol Chem,* 273**,** 19797-801.

SILVIS, M. R., PICCIANO, J. A., BERTRAND, C., WEIXEL, K., BRIDGES, R. J. & BRADBURY, N. A. 2003. A mutation in the cystic fibrosis transmembrane conductance regulator generates a novel internalization sequence and enhances endocytic rates. *J Biol Chem,* 278**,** 11554-60.

SLOANE, P. A., SHASTRY, S., WILHELM, A., COURVILLE, C., TANG, L. P., BACKER, K., LEVIN, E., RAJU, S. V., LI, Y., MAZUR, M., BYAN-PARKER, S., GRIZZLE, W., SORSCHER, E. J., DRANSFIELD, M. T. & ROWE, S. M. 2012. A pharmacologic approach to acquired cystic fibrosis transmembrane conductance regulator dysfunction in smoking related lung disease. *PLoS One,* 7**,** e39809.

SMYTH, J. T., HWANG, S. Y., TOMITA, T., DEHAVEN, W. I., MERCER, J. C. & PUTNEY, J. W. 2010. Activation and regulation of store-operated calcium entry. *J Cell Mol Med,* 14**,** 2337-49.

SOLDATI, T. & SCHLIWA, M. 2006. Powering membrane traffic in endocytosis and recycling. *Nat Rev Mol Cell Biol,* 7**,** 897-908.

ST-LAURENT, J., PROULX, L. I., BOULET, L. P. & BISSONNETTE, E. 2009. Comparison of two in vitro models of cigarette smoke exposure. *Inhal Toxicol,* 21**,** 1148-53.

STENMARK, H., PARTON, R. G., STEELE-MORTIMER, O., LUTCKE, A., GRUENBERG, J. & ZERIAL, M. 1994. Inhibition of rab5 GTPase activity stimulates membrane fusion in endocytosis. *EMBO J,* 13**,** 1287-96.

STUTTS, M. J., CHINET, T. C., MASON, S. J., FULLTON, J. M., CLARKE, L. L. & BOUCHER, R. C. 1992. Regulation of Cl- channels in normal and cystic fibrosis airway epithelial cells by extracellular ATP. *Proc Natl Acad Sci U S A,* 89**,** 1621-5.

SWIATECKA-URBAN, A., DUHAIME, M., COUTERMARSH, B., KARLSON, K. H., COLLAWN, J., MILEWSKI, M., CUTTING, G. R., GUGGINO, W. B., LANGFORD, G. & STANTON, B. A. 2002. PDZ domain interaction controls the endocytic recycling of the cystic fibrosis transmembrane conductance regulator. *J Biol Chem,* 277**,** 40099-105.

TABCHARANI, J. A., CHANG, X. B., RIORDAN, J. R. & HANRAHAN, J. W. 1991. Phosphorylation-regulated Cl- channel in CHO cells stably expressing the cystic fibrosis gene. *Nature,* 352**,** 628-31.

TAMASHIRO, E., XIONG, G., ANSELMO-LIMA, W. T., KREINDLER, J. L., PALMER, J. N. & COHEN, N. A. 2009. Cigarette smoke exposure impairs respiratory epithelial ciliogenesis. *Am J Rhinol Allergy,* 23**,** 117-22.

TANABE, K., OHASHI, E., HENMI, Y. & TAKEI, K. 2011. Receptor sorting and actin dynamics at early endosomes. *Commun Integr Biol,* 4**,** 742-4.

TARRAN, R. 2004. Regulation of airway surface liquid volume and mucus transport by active ion transport. *Proc Am Thorac Soc,* 1**,** 42-6.

TARRAN, R., BUTTON, B. & BOUCHER, R. C. 2006. Regulation of normal and cystic fibrosis airway surface liquid volume by phasic shear stress. *Annu Rev Physiol,* 68**,** 543-61.

TARRAN, R., BUTTON, B., PICHER, M., PARADISO, A. M., RIBEIRO, C. M., LAZAROWSKI, E. R., ZHANG, L., COLLINS, P. L., PICKLES, R. J., FREDBERG, J. J. & BOUCHER, R. C. 2005. Normal and cystic fibrosis airway surface liquid homeostasis. The effects of phasic shear stress and viral infections. *J Biol Chem,* 280**,** 35751-9.

TARRAN, R., GRUBB, B. R., GATZY, J. T., DAVIS, C. W. & BOUCHER, R. C. 2001a. The relative roles of passive surface forces and active ion transport in the modulation of airway surface liquid volume and composition. *J Gen Physiol,* 118**,** 223-36.

TARRAN, R., GRUBB, B. R., PARSONS, D., PICHER, M., HIRSH, A. J., DAVIS, C. W. & BOUCHER, R. C. 2001b. The CF salt controversy: in vivo observations and therapeutic approaches. *Mol Cell,* 8**,** 149-58.

TAYLOR, S. S., BUECHLER, J. A. & YONEMOTO, W. 1990. cAMP-dependent protein kinase: framework for a diverse family of regulatory enzymes. *Annu Rev Biochem,* 59**,** 971-1005.

THELIN, W. R., KESIMER, M., TARRAN, R., KREDA, S. M., GRUBB, B. R., SHEEHAN, J. K., STUTTS, M. J. & MILGRAM, S. L. 2005. The cystic fibrosis transmembrane conductance regulator is regulated by a direct interaction with the protein phosphatase 2A. *J Biol Chem,* 280**,** 41512-20.

THERMOFISHER. 2015. *Peirce BCA protein assay kit* [Online]. Available: https://tools.thermofisher.com/content/sfs/manuals/MAN0011430_Pierce_BCA_Protein_Asy_UG.pdf [Accessed May 2 2016].

THIAGARAJAH, J. R. & VERKMAN, A. S. 2003. CFTR pharmacology and its role in intestinal fluid secretion. *Curr Opin Pharmacol,* 3**,** 594-9.

THURLBECK, W. M. & ANGUS, G. E. 1964. A Distribution Curve for Chronic Bronchitis. *Thorax,* 19**,** 436-42.

TIAN, Y., KONGSUPHOL, P., HUG, M., OUSINGSAWAT, J., WITZGALL, R., SCHREIBER, R. & KUNZELMANN, K. 2011. Calmodulin-dependent activation of the epithelial calcium-dependent chloride channel TMEM16A. *FASEB J,* 25**,** 1058-68.

TOUSSON, A., FULLER, C. M. & BENOS, D. J. 1996. Apical recruitment of CFTR in T-84 cells is dependent on cAMP and microtubules but not Ca2+ or microfilaments. *J Cell Sci,* 109 (Pt 6)**,** 1325-34.

TREHARNE, K. J., XU, Z., CHEN, J. H., BEST, O. G., CASSIDY, D. M., GRUENERT, D. C., HEGYI, P., GRAY, M. A., SHEPPARD, D. N., KUNZELMANN, K. & MEHTA, A. 2009. Inhibition of protein kinase CK2 closes the CFTR Cl channel, but has no effect on the cystic fibrosis mutant deltaF508-CFTR. *Cell Physiol Biochem,* 24**,** 347-60.

ULLRICH, A. & SCHLESSINGER, J. 1990. Signal transduction by receptors with tyrosine kinase activity. *Cell,* 61**,** 203-12.

US CF FOUNDATION, J. H. U., HOSPITAL FOR SICK CHILDREN. 2015. *The Clinical and Functional TRanslation of CFTR (CFTR2)* [Online]. Available: http://www.cftr2.org/files/CFTR2_13August2015.pdf [Accessed April 29 2016].

USDHHS, U. S. D. O. H. A. H. S. 2010. *How Tobacco Smoke Causes Disease: The Biology and Behavioral Basis for Smoking-Attributable Disease: A Report of the Surgeon General.* Atlanta (GA).

VAN GOOR, F., HADIDA, S., GROOTENHUIS, P. D., BURTON, B., STACK, J. H., STRALEY, K. S., DECKER, C. J., MILLER, M., MCCARTNEY, J., OLSON, E. R., WINE, J. J., FRIZZELL, R. A., ASHLOCK, M. & NEGULESCU, P. A. 2011. Correction of the F508del-CFTR protein processing defect in vitro by the investigational drug VX-809. *Proc Natl Acad Sci U S A,* 108**,** 18843-8.

VERGANI, P., LOCKLESS, S. W., NAIRN, A. C. & GADSBY, D. C. 2005. CFTR channel opening by ATP-driven tight dimerization of its nucleotide-binding domains. *Nature,* 433**,** 876-80.

VIGNOLA, A. M., CHANEZ, P., CHIAPPARA, G., MERENDINO, A., PACE, E., RIZZO, A., LA ROCCA, A. M., BELLIA, V., BONSIGNORE, G. & BOUSQUET, J. 1997. Transforming growth factor-beta expression in mucosal biopsies in asthma and chronic bronchitis. *Am J Respir Crit Care Med,* 156**,** 591-9.

WAINWRIGHT, C. E., ELBORN, J. S., RAMSEY, B. W., MARIGOWDA, G., HUANG, X., CIPOLLI, M., COLOMBO, C., DAVIES, J. C., DE BOECK, K., FLUME, P. A., KONSTAN, M. W., MCCOLLEY, S. A., MCCOY, K., MCKONE, E. F., MUNCK, A., RATJEN, F., ROWE, S. M., WALTZ, D., BOYLE, M. P., GROUP, T. S. & GROUP, T. S. 2015. Lumacaftor-Ivacaftor in Patients with Cystic Fibrosis Homozygous for Phe508del CFTR. *N Engl J Med,* 373**,** 220-31.

WALDMANN, R., CHAMPIGNY, G., BASSILANA, F., VOILLEY, N. & LAZDUNSKI, M. 1995. Molecular cloning and functional expression of a novel amiloride-sensitive Na+ channel. *J Biol Chem,* 270**,** 27411-4.

WALLACE, A. M., HARDIGAN, A., GERAGHTY, P., SALIM, S., GAFFNEY, A., THANKACHEN, J., ARELLANOS, L., D'ARMIENTO, J. M. & FORONJY, R. F. 2012. Protein phosphatase 2A regulates innate immune and proteolytic responses to cigarette smoke exposure in the lung. *Toxicol Sci,* 126**,** 589-99.

WANG, F., ZELTWANGER, S., HU, S. & HWANG, T. C. 2000. Deletion of phenylalanine 508 causes attenuated phosphorylation-dependent activation of CFTR chloride channels. *J Physiol,* 524 Pt 3**,** 637-48.

WANG, X., MATTESON, J., AN, Y., MOYER, B., YOO, J. S., BANNYKH, S., WILSON, I. A., RIORDAN, J. R. & BALCH, W. E. 2004. COPII-dependent export of cystic fibrosis transmembrane conductance regulator from the ER uses a di-acidic exit code. *J Cell Biol,* 167**,** 65-74.

WARD, C. L. & KOPITO, R. R. 1994. Intracellular turnover of cystic fibrosis transmembrane conductance regulator. Inefficient processing and rapid degradation of wild-type and mutant proteins. *J Biol Chem,* 269**,** 25710-8.

WEBER, W. M., SEGAL, A., SIMAELS, J., VANKEERBERGHEN, A., CASSIMAN, J. J. & VAN DRIESSCHE, W. 2001. Functional integrity of the vesicle transporting machinery is required for complete activation of cFTR expressed in xenopus laevis oocytes. *Pflugers Arch,* 441**,** 850-9.

WEIXEL, K. & BRADBURY, N. A. 2002. Analysis of CFTR endocytosis by cell surface biotinylation. *Methods Mol Med,* 70**,** 323-40.

WEIXEL, K. M. & BRADBURY, N. A. 2000. The carboxyl terminus of the cystic fibrosis transmembrane conductance regulator binds to AP-2 clathrin adaptors. *J Biol Chem,* 275**,** 3655-60.

WELSH, M. J. 1983. Cigarette smoke inhibition of ion transport in canine tracheal epithelium. *J Clin Invest,* 71**,** 1614-23.

WHITSETT, J. A. & ALENGHAT, T. 2015. Respiratory epithelial cells orchestrate pulmonary innate immunity. *Nat Immunol,* 16**,** 27-35.

WHO. 2015. *Tobacco* [Online]. Available: http://www.who.int/mediacentre/factsheets/fs339/en/ [Accessed 10 Dec 2015].

XIE, W., KAETZEL, M. A., BRUZIK, K. S., DEDMAN, J. R., SHEARS, S. B. & NELSON, D. J. 1996. Inositol 3,4,5,6-tetrakisphosphate inhibits the calmodulin-dependent protein kinase II-activated chloride conductance in T84 colonic epithelial cells. *J Biol Chem,* 271**,** 14092-7.

XU, X., BALSIGER, R., TYRRELL, J., BOYAKA, P. N., TARRAN, R. & CORMET-BOYAKA, E. 2015. Cigarette smoke exposure reveals a novel role for the MEK/ERK1/2 MAPK pathway in regulation of CFTR. *Biochim Biophys Acta,* 1850**,** 1224-32.

YAGHI, A., ZAMAN, A., COX, G. & DOLOVICH, M. B. 2012. Ciliary beating is depressed in nasal cilia from chronic obstructive pulmonary disease subjects. *Respir Med,* 106**,** 1139-47.

YANG, Y. D., CHO, H., KOO, J. Y., TAK, M. H., CHO, Y., SHIM, W. S., PARK, S. P., LEE, J., LEE, B., KIM, B. M., RAOUF, R., SHIN, Y. K. & OH, U. 2008. TMEM16A confers receptor-activated calcium-dependent chloride conductance. *Nature,* 455**,** 1210-5.

ZHANG, L., ALEKSANDROV, L. A., RIORDAN, J. R. & FORD, R. C. 2011. Domain location within the cystic fibrosis transmembrane conductance regulator protein investigated by electron microscopy and gold labelling. *Biochim Biophys Acta,* 1808**,** 399-404.

ZHENG, J. P., KANG, J., HUANG, S. G., CHEN, P., YAO, W. Z., YANG, L., BAI, C. X., WANG, C. Z., WANG, C., CHEN, B. Y., SHI, Y., LIU, C. T., CHEN, P., LI, Q., WANG, Z. S., HUANG, Y. J., LUO, Z. Y., CHEN, F. P., YUAN, J. Z., YUAN, B. T., QIAN, H. P., ZHI, R. C. & ZHONG, N. S. 2008. Effect of carbocisteine on acute exacerbation of chronic obstructive pulmonary disease (PEACE Study): a randomised placebo-controlled study. *Lancet,* 371**,** 2013-8.

ZHU, T., DAHAN, D., EVAGELIDIS, A., ZHENG, S., LUO, J. & HANRAHAN, J. W. 1999. Association of cystic fibrosis transmembrane conductance regulator and protein phosphatase 2C. *J Biol Chem,* 274**,** 29102-7.